2004-35

Final Report

INVENTORY OF PROPERTIES OF MINNESOTA CERTIFIED ASPHALT BINDERS

Research

Technical Report Documentation Page

1. Report No. MN/RC-2004-35	2.	3. Recipients Accession No.	
4. Title and Subtitle Inventory of Properties of Minnesota Certified Asphalt Binders		5. Report Date April 2004	
		6.	
7. Author(s) Timothy R. Clyne, Mihai O. Marasteanu		8. Performing Organization Report No.	
9. Performing Organization Name and Address University of Minnesota Department of Civil Engineering 500 Pillsbury Dr. S.E. Minneapolis, MN 55455-0116		10. Project/Task/Work Unit No.	
		11. Contract (C) or Grant (G) No. (c)81655 (wo)64	
12. Sponsoring Organization Name and Address Minnesota Department of Transportation Research Services Section Mail Stop 330 395 John Ireland Boulevard St. Paul, Minnesota 55155		13. Type of Report and Period Covered Final Report	
		14. Sponsoring Agency Code	
15. Supplementary Notes www.lrrb.org/PDF/200435.pdf			

16. Abstract (Limit: 200 words)

The objective of this study was to create an inventory of the rheological properties of certified asphalt binders used in Minnesota. A literature search was performed to identify existing databases as well as more complex test methods for asphalt binder characterization that have been proposed recently.

Nine different asphalt binders were studied. The binders were aged according to standard aging procedures and subject to a number of tests. The Bending Beam Rheometer (BBR) and Direct Tension Tester (DTT) were used together to determine the critical cracking temperature of the binders at low temperatures. The Dynamic Shear Rheometer (DSR) was used to test frequency sweeps (to generate master curves and to calculate zero shear viscosity), strain sweeps (to verify linear viscoelasticity), repeated creep (to measure the permanent strain accumulated after 100 cycles), and fatigue tests (to test for fatigue cracking at intermediate temperatures).

A database was created in Microsoft Access®, which is easy to use and readily available to most users. Test results, along with some model parameters, were stored in tables inside the database. As more test results become available, the can easily be imported to the database.

17. Document Analysis/Descriptors		18. Availability Statement	
Performance graded asphalt binders	Superpave specifications Laboratory test methods	No restrictions. Document available from: National Technical Information Services, Springfield, Virginia 22161	
19. Security Class (this report) Unclassified	20. Security Class (this page) Unclassified	21. No. of Pages 102	22. Price

INVENTORY OF PROPERTIES OF MINNESOTA CERTIFIED ASPHALT BINDERS

Final Report

Prepared by:

Timothy R. Clyne

Mihai O. Marasteanu

University of Minnesota
Department of Civil Engineering

April 2004

Published by:

Minnesota Department of Transportation
Research Services Section
MS 330
395 John Ireland Boulevard
St. Paul, MN 55155

ACKNOWLEDGEMENTS

The authors would like to thank Jason Szondy, Paul Lohmann, John Olson, and Jim McGraw at the Minnesota Department of Transportation (Mn/DOT) for their technical assistance during the project. Their guidance and assistance in carrying out the laboratory tests are greatly appreciated. We would also like to thank Hussain Bahia at the University of Wisconsin for his assistance in data analysis techniques.

TABLE OF CONTENTS

LIST OF TABLES

LIST OF FIGURES

EXECUTIVE SUMMARY

In order to understand the complex behavior of asphalt pavements and their performance in the field, it is necessary to have immediate and easy access to information about selected pavements. This can be accomplished through the development of a comprehensive database that could be used for storing and disseminating various types of information for asphalt pavement construction projects around the state. The objective of this study was to create an inventory of the rheological properties of certified asphalt binders used in Minnesota. This inventory would include standard Superpave specification information as well as more advanced test results that may be used for specification purposes in the future.

A literature search was performed to identify existing databases and their structures and to select a format for a new database. The search also included a review of the more complex test methods for asphalt binder characterization that have been proposed in the past years and have been accepted by the research community.

Nine different asphalt binders, shown in the following table, were studied in this project.

U of M ID	PG Grade	Source
BI1	64-28 HFD Blend	Koch
BI2	64-28 Stylink	Koch
BI3	64-34 Stylink	Koch
BI4	64-34 Elvaloy	MIF
BI5	58-34 Elvaloy	Murphy
BI6	58-34 Oxidized	Husky
BI7	58-28 MnROAD	Koch
BI8	58-34 MnROAD	Koch
BI9	58-40 MnROAD	Koch

These asphalts were subject to standard aging procedures in the Rolling Thin Film Oven (RTFOT) and the Pressurized Aging Vessel (PAV). The residues, as well as the original (unaged) binder, were subject to a number of tests that have shown promise in perfecting the current PG grading specifications. The tests were performed on the Bending Beam Rheometer (BBR), Direct Tension Tester (DTT), and Dynamic Shear Rheometer (DSR). The list of tests include:

- Frequency Sweeps (DSR)
    - Master Curves
    - Zero Shear Viscosity
- Strain Sweeps (DSR)
- Repeated Creep (DSR)
- Time Sweeps – Fatigue (DSR)
- Creep Tests (BBR)
- Direct Tension Tests (DTT)
- Critical Cracking Temperature – using BBR and DTT data

A database was created in Microsoft Access®, which is easy to use and readily available to most users. Test results were stored in tables inside the database. Various model parameters, which describe the rheological properties of asphalt binders observed in numerous tests, were stored in additional tables. As more test results become available, they can be easily imported to the database.

The aim of this project was not so much to exhaustively analyze the binders in terms of their relative performance to one another, but to simply understand how to perform the tests and then catalogue the data in a database for future reference. This was accomplished successfully. Future work may include refinement of the testing and analysis methods, testing of additional binders, and adding newly developed tests to the existing database.

CHAPTER 1:
INTRODUCTION

Background

In order to understand the complex behavior of asphalt pavements and their performance in the field, it is necessary to have immediate and easy access to bits of information about selected pavements. This can be accomplished through the development of a comprehensive database that could be used for storing and disseminating various types of information for asphalt pavement construction projects around the state. One essential part of this database would be an inventory of the properties of certified performance grade (PG) asphalt binders in Minnesota. This inventory would provide a much broader representation of the rheological properties of asphalt binders commonly used in Minnesota. In addition to the traditional PG data, it will provide relevant information that can significantly improve the selection process of the binders used for different construction jobs.

Objectives

The objective of this study was to create an inventory of the rheological properties of certified asphalt binders used in Minnesota. This inventory would include standard Superpave specification information as well as more advanced test results that may be used for specifications in the future. The newly proposed test methods include zero shear viscosity, repeated creep, strain sweeps, time sweeps (fatigue), and critical cracking temperature.

Scope

Nine different asphalt binders were studied in this project. These asphalts were subject to standard aging procedures in the Rolling Thin Film Oven (RTFOT) and the Pressurized Aging Vessel (PAV). The residues as well as the original (unaged) binder were subject to a number of tests that have shown promise in perfecting the current PG grading specifications. The tests were performed on the Bending Beam Rheometer (BBR), Direct Tension Tester (DTT), and Dynamic Shear Rheometer (DSR). A database was created in Microsoft Access®. Test results along with some model parameters were stored in tables inside the database.

Report Organization

This report is arranged into six chapters: Introduction, Literature Review, Research Methodology, Results and Discussion, Database Description, and Conclusions and Recommendations. The Literature Review identifies existing databases and their structures in order to have a guide for creating a new database. It also includes a widespread review of the more complex test methods for asphalt binder characterization that have been proposed in the past years and have been accepted by the research community. Research Methodology gives details about the materials used, along with a description of the tests performed in the laboratory. Results and Discussion analyzes the experimental data obtained. The data analysis includes model fitting for some test results and presents the data in tables and charts. A description of the database, including its structure and basic table information, is included in chapter 5. The report closes with some final conclusions and recommendations. A number of appendices contain plots from the various test results.

CHAPTER 2:
LITERATURE REVIEW

Introduction

In order for researchers to continually monitor and improve pavement performance, it is essential to have immediate and easy access to field and laboratory data. This can be accomplished through the development of a comprehensive database that could be used for storing and disseminating various types of information for asphalt pavement construction projects in Minnesota. One essential component of this comprehensive database would be an inventory of the properties of certified asphalt binders in Minnesota. In order to accomplish this, one must first understand the design and implementation of an efficient database. It is also important to examine current test procedures for characterizing asphalt binders, as well as explore more complex test methods for asphalt binder characterization that have recently been proposed and accepted in the research community.

Data Inventory Efforts

Penn State University

As part of the Strategic Highway Research Program (SHRP), Pennsylvania State University was awarded contract SHRP A-002A. This project was a large effort to characterize the rheological properties of over 20 different asphalt binders. The goal was to perform a number of tests on asphalt binders and distribute the information to interested researchers around the country. A major part of this project was to develop a database that had the ability to insert a myriad of different files into the database in a timely and efficient manner. More than 2,000 raw data files were used, each with multiple fields. The major effort in this task was the development of a method for automatically parsing and preparing files so that they could be appended to the database. The files, being produced by different types of testing equipment, were typically in ASCII format but also contained mixed header and data information. These files were parsed into a consistent format in two separate tables for efficient use in the database [1].

In order to make the database as user-friendly as possible for a number of outside organizations, a parsing program was developed to generate ASCII files. Visual Basic™ was

used to write the parsing and file handling programs. The parsed files were then appended to the database created for that project. These files easily can be transferred into SAS®, dBase®, and most other database formats.

After extensive study, Microsoft Access®, a Windows-based relational database, was chosen as the database tool for this study. The advantages of this program include robustness, ease of use, file compatibility and linking, and database management and linking. The database created with Access® has the ability to add more tables in the future as the need arises. Table 2.1 lists the various Access tables that were contained in the database.

Table 2.1 List of Tables in PSU Database

- MRL data for tested asphalt binders
- Model parameters
- RMS parallel plate test results
- RMS parallel plate header information
- RMS torsion bar test results
- RMS torsion bar header information
- BBR prototype test results
- BBR Cannon test results
- BBR Cannon header information
- Direct tension test results
- Direct tension header information
- Asphalt mixture flexural beam fatigue test results
- Asphalt mixture fracture strength data
- Asphalt mixture fracture temperature data
- Asphalt mixture wheel-tracking rutting data

Minnesota Department of Transportation

The Minnesota Department of Transportation (Mn/DOT) Office of Materials currently employs three databases covering the following data: Mn/ROAD materials and test results, materials and test results from other state highways, and pavement management data including distresses and pavement conditions. Currently, the three databases are separate entities. However, efforts are being made to link them together in some form. The database developed in this project will attempt to fit within the framework of existing database structures at Mn/DOT.

The Mn/ROAD database contains a wealth of information about each of the materials used in the various cells at Mn/ROAD. The database contains tables relating to MAT (materials), DISTRESS (Distress monitoring), CELL (Cell information), WIM (weigh in

motion), KWIM (kistler weigh in motion), WEATHER (weather), FWD (falling weight), FORENSIC (forensic related), but the sensors and many other tables are not in this form yet and are named individually (example TC_1995 is the thermal couple data from 1995. It is organized by individual tables noted with "MAT_%%%%". The oracle tables that exist have very little documentation at this time. The MAT_SAMPLES table is the primary table of concern in the database; it describes the location and time that samples are collected in the field. All the other tables relate back to the MAT_SAMPLES table and are tied by a field named MNROAD_ID. Many of the testing tables can be modified, since the data is entered by spreadsheets, text files, or access databases. Mn/DOT tries to limit the number of tables and fits similar testing data in one table for simplicity. They generally have the flexibility to add new tables and modify existing tables as needed.

Superpave Binder Specifications

Introduction

The Superpave binder specification was developed during the Strategic Highway Research Program (SHRP) that was conducted from 1988 through 1994. In the late 1970's and early 1980's, transportation officials were concerned that the properties of paving-grade asphalt cement had changed and that the asphalt cements that were produced at that time were of inferior quality. This led to the development of SHRP in the mid 1980's. One of the primary objectives of SHRP was to develop specifications for asphalt cement that were more directly related to pavement performance than the specifications that had existed prior to SHRP. The specifications that resulted from the SHRP research are part of a new and comprehensive system for selecting and specifying aggregates, binders, and mixtures. Collectively, these specifications are known as Superpave.

The traditional penetration- or viscosity-graded specifications that were in use before SHRP were based on measurements of viscosity, penetration, ductility, and softening point temperature. These measurements are not adequate to properly describe the properties of paving-grade asphalt cement that are needed to predict pavement performance. The new Superpave binder specification is designed to provide specification properties that can be related to pavement performance. The binders specified within Superpave are often referred to as performance-graded asphalt binders, or simply as PGAB.

Superpave Conditioning Procedures and Test Methods

The Superpave binder specification is based on the following test methods:

- ***Rotational Viscometer*** *(RV)*: A test method used to determine the (rotational) viscosity at pumping, mixing and compaction temperatures. (*AASHTO T 316*)
- ***Rolling Thin-Film Oven Test*** *(RTFOT):* A method of practice used to simulate the short-term aging that occurs during mixing, storage, transportation, lay down, and compaction. (*AASHTO T 240*)
- ***Pressurized Aging Vessel*** *(PAV):* A method of practice, based on a pressurized and heated aging vessel, to simulate the long-term aging that occurs in the field. (*AASHTO R 28*)
- ***Dynamic Shear Rheometer*** *(DSR):* A test method used to determine the shear resistance of asphalt binders at temperatures at which rutting and fatigue occur. (*AASHTO T 315*)
- ***Bending Beam Rheometer*** *(BBR):* A test method used to determine the low-temperature stiffness of asphalt binders at temperatures at which thermal cracking occurs. (*AASHTO T 313*)
- ***Direct Tension Test*** *(DTT):* A test method used to determine the tensile strength of asphalt binders at low temperature. The strength data is used in the determination of the critical cracking temperature. (*AASHTO T 314)*

The Superpave binder specification results in a series of PGAB grades that are designated according to the upper and lower pavement service temperatures. The specification tolerance limits are the same for all the grades, but the limits are obtained at different temperatures for different materials, in accordance to the climatic region served. For example, in the PGAB specification, one of the criteria for rutting is that $|G^*|/\sin\delta$ be greater than 2.20 kPa after RTFOT aging. This requirement must be obtained at 46, 52, 58, 64, 70, 76 or 82°C for each corresponding PGAB grade. In a similar manner, a series of low temperatures are specified, ranging in 6°C increments from -46°C to -10°C.

Superpave PGAB Specification Criteria

The Superpave specification requirements are given in AASHTO M 320, "Standard Specification for Performance-Graded Asphalt Binder." Note that SI units are used throughout the Superpave specification. Units for viscosity in the SI system are Pascal-seconds (Pa-s).

Stress, stiffness, and strength are reported in Pascals (Pa). The prefixes k and M are used to indicate thousands and millions, respectively. Thus, 1.00 kPa is 10^3 Pascals, and 1.00 MPa is 10^6 Pascals. Temperatures are always measured or reported in degrees Celsius (°C).

Each specification criteria listed in M 320 is associated with a different form of pavement distress. Although the specification criteria are often associated on a one-on-one basis with particular forms of pavement distress, it should be emphasized that the tests and the associated properties represent a suite of complimentary requirements, all of which are needed in order to properly characterize or specify a binder. Specific associations with distress types are as follows:

- Rutting - unaged binder with a minimum value of $|G^*|/\sin\delta$ measured at the maximum pavement temperature using the dynamic shear rheometer (DSR).
- Rutting - RTFOT-aged binder with a minimum value of $|G^*|/\sin\delta$ measured at the maximum pavement temperature using the dynamic shear rheometer (DSR).
- Fatigue - PAV-aged binder with a maximum value of $|G^*|\sin\delta$ measured at the intermediate pavement temperature using the dynamic shear rheometer (DSR).
- Thermal cracking - PAV-aged binder with a maximum value of stiffness (S) and a minimum value for the m-value measured at the minimum pavement design temperature plus 10°C using the bending beam rheometer (BBR).

A summary of the steps required to grade an asphalt cement is listed below.

<u>Safety, Handling, and Loss on Heating</u>

- Flash Point Temperature ≥ 230°C
- Viscosity at 135°C ≤ 3 Pa-s
- Mass loss < 1%

<u>Performance Criteria - High Temperature</u> (select lowest of the two values)

- Highest temperature (original material) where:

  $|G^*|/\sin\delta \geq 1.00$ kPa

- Highest temperature (RTFOT residue) where:

  $|G^*|/\sin\delta \geq 2.20$ kPa

Performance Criteria - Low Temperature (select highest of the two values)

- Lowest temperature (PAV residue) where:

$$S(60\text{s}) \leq 300\text{MPa}$$

- Lowest temperature (PAV residue) where:

$$m(60\text{s}) \geq 0.300$$

Performance Criteria - Intermediate Temperature

- Lowest temperature (PAV residue) where:

$$|G^*| \sin\delta \leq 5.00 \text{ MPa}$$

Note that the DSR data used for the high and intermediate temperatures criteria are obtained at a frequency of 10 rad/s, which simulates an approximate speed of 97 km/hr (60 mph). The BBR data used for the low temperature criterion are obtained at 60 seconds.

Critical Cracking Temperature

The recent AASHTO MP1a standard (and corresponding standard AASHTO PP42) involves the calculation of low-temperature binder properties using data from the bending beam rheometer (BBR) and the direct tension tester (DTT). This method uses a thermo-viscoelastic model to calculate the relaxation modulus master curve and subsequently the thermally induced stress curve based on BBR data. The analysis method presented in this section is described in detail by references [2] and [3].

The stiffness master curves are generated by fitting the Christensen-Anderson-Marasteanu (CAM) model to the BBR stiffness data obtained at two temperatures:

$$S(\xi) = S_{glassy}\left[1+\left(\frac{\xi}{\xi_c}\right)^v\right]^{-\frac{w}{v}} \quad (1)$$

where

$S(\xi)$ = Stiffness at a reduced time ξ (MPa)

S_{glassy} = 3 GPa, assumed constant

ξ_c, w, v = model parameters

The stiffness master curve is then converted to the creep compliance curve by taking its inverse:

$$D(\xi) = \frac{1}{S(\xi)} \tag{2}$$

where

$D(\xi)$ = Creep compliance at reduced time ξ

A convolution integral is required to convert BBR creep stiffness (actually compliance, $D(\xi)$) to relaxation modulus:

$$\int_{-\infty}^{t} E(\xi)D(t-\xi)d\xi = t \tag{3}$$

where

$E(\xi)$ = Relaxation modulus at reduced time ξ

$D(t)$ = Creep compliance at time t

An approximation to the relaxation modulus is calculated using the Hopkins and Hamming algorithm, which is fitted to the CAM model:

$$E(t_{n+1/2}) = \frac{t_{n+1} - \sum_{t=0}^{n-1} E(t_{i+1/2})[f(t_{n+1}-t_i) - f(t_1 - t_{i+1})]}{f(t_{n+1}-t_n)} \tag{4}$$

where

$E(t_{n+1/2})$ = Relaxation modulus at the midpoint of each time step

$f(t)$ = Creep at the midpoint of the data acquisition time step

The thermally induced stress is calculated by numerically solving the hereditary integral:

$$\sigma(\xi) = \int_{0}^{\xi} E_M(\xi - \xi') \frac{d(\alpha \Delta T)}{d\xi'} d\xi' \tag{5}$$

where

$\sigma(\xi)$ = Thermal stress built up in asphalt binder at reduced time ξ

E_M = Relaxation modulus in the form of a master curve at reference temperature T_M

α = Coefficient of linear thermal expansion/contraction

ΔT = Change in temperature

This integration is accomplished using a 24-point Gaussian numerical method to calculate the binder thermal stresses at each 0.5°C interval from 22°C to -40°C. The calculated thermally induced stress is then multiplied by the empirical pavement constant (PC = 18 or 24) to predict the thermal stress produced in the hot-mix asphalt pavement. Finally this thermal stress is

plotted together with the failure stress obtained with the DTT to determine the critical cracking temperature, T_{cr}, of the pavement.

Rheological Master Curves

The SHRP asphalt binder specification is based on the assumption that the performance of asphalt binders can be adequately represented by thermo-rheologically simple linear viscoelastic behavior [4]. This assumption requires that a material must obey two simultaneous conditions:

1. The homogeneity (proportionality) condition is obeyed.
2. The linear superposition principle holds.

Marasteanu and Anderson [4, 5] have proposed analysis procedures for verifying linear viscoelastic conditions and determining errors in asphalt binder test data. Providing conditions 1 and 2 hold, and that the data obtained from testing is free from errors, "master curves" can be constructed to describe the time-temperature dependency of asphalt binders. A quantitative mathematical model allows researchers to calculate the stiffness, phase angle, and other rheological properties for a wide range of loading times (or frequencies) and temperatures from measurements made over smaller ranges. Modulus values measured at different temperatures are often plotted as the logarithm of the modulus vs. the logarithm of time (or frequency), and the resulting data are "shifted" horizontally to form a master curve [6]. The shift factors may be fit by regression or made to fit a certain function like the Arrhenius function or the Williams-Landel-Ferry (WLF) equation. The parameters in the aforementioned equations are theoretically based and provide insight into the molecular structure of the asphalt binders.

The master curve model used to fit the test data must account for different regions of behavior observed in asphalt binders. At low temperatures, physical hardening is prominent and affects the temperature dependency of asphalt binders. The shear modulus approaches a limiting value, which is referred to as the glass modulus. The glass modulus physically represents the limiting stiffness attained at short loading times (or high frequencies) and low temperatures. It typically has a value of 1GPa. At high temperatures, binders behave as Newtonian fluids. The slope of the log-log plot of shear modulus vs. frequency approaches 1:1, signifying viscous flow has been reached. At intermediate temperatures, asphalt binders behave as thermo-rheologically simple linear viscoelastic materials at small strains [6, 7].

In some forms, the master curve can be described by two parameters: the rheological index, R, and the crossover frequency, ω_c [7]. The rheological index is the difference between the glass modulus, G_g, and the complex shear modulus at the crossover frequency, $|G^*(\omega_c)|$. R, which is asphalt specific, is directly proportional to the relaxation spectrum. It indicates the rheological type and shows the energy storage of the binder during deformation. The crossover frequency, ω_c, represents the frequency at which the phase angle, δ, is 45 degrees, or where the storage and the loss modulus are equal. The crossover frequency can be seen as a hardness parameter that indicates the general consistency of the asphalt at the selected temperature.

A number of models have been developed to represent both the time and temperature dependence of asphalt binders [6-9]. The most widely accepted of these is the Christensen-Anderson-Marasteanu (CAM) model. In the linear viscoelastic region, the CAM model is represented as follows [10]:

$$\left|G^*(\omega)\right| = G_g\left[1+\left(\frac{\omega_c}{\omega}\right)^{v}\right]^{-\frac{w}{v}} \tag{6}$$

where

$|G^*(\omega)|$ = absolute value of complex modulus as a function of frequency ω (GPa)

G_g = glassy modulus (log $[G_g]$ is considered fixed at 9.1)

ω_c, v, w = model parameters

Any commercial statistical software can be used to fit the CAM model to test data obtained from the Dynamic Shear Rheometer (DSR) at a chosen reference temperature (often 22°C).

Zero Shear Viscosity

Recent research has shown that the current high temperature specification ($|G^*|/\sin\delta$ from DSR tests) does not accurately predict rutting performance in asphalt pavements. This is especially true of polymer modified binders. Alternatively, the zero shear rate viscosity, ZSR, has shown promise as a better predictor of high temperature pavement performance. The name comes from the fact that, at very low frequencies (shear rates), the dynamic viscosity, η', of uncross-linked polymers approaches the ordinary steady flow viscosity [11]. The steady state viscosity is equivalent to zero shear viscosity, η_o, for shear experiments for a linear viscoelastic

material [12]. Researchers have shown that η_o correlates well with the number of cycles needed to obtain a certain rut depth in accelerated testing facilities [12, 13].

Marasteanu and Anderson [11] have documented several well-known methods for determining the zero shear viscosity of asphalt binders. Long term creep tests performed on a stress rheometer can directly measure η_o. ZSR can be calculated as the inverse of the slope of the steady-state part of the compliance curve [14]:

$$\eta_o = \lim_{t-creep\to\infty}\left[\frac{t}{J_{creep}(t)}\right] \tag{7}$$

Anderson et al [14] note that η_o can also be derived from the residual compliance obtained in the creep recovery test. The problem with this test is the time needed to reach the steady state. In particular, with many polymer modified binders, an extended time (several hours or even days, depending on test temperature) may be needed to reach a steady-state flow.

The zero shear viscosity can be derived from rotational viscosity tests [11]. Rotational data obtained at different temperatures and different shear rates can be extrapolated to zero shear rate to estimate η_o. This method can introduce large approximations, especially for test data that shows a distinct departure from steady state conditions.

Sybilski [13] describes a model in which rotational viscosity data can be used to calculate η_o. The Cross model describes a flow curve of a pseudoplastic fluid in the following form:

$$\frac{\eta_o - \eta(\dot{\gamma})}{\eta(\dot{\gamma})} = (K\dot{\gamma})^m \tag{8}$$

where

η_o = steady-state shear viscosity at vanishing shear rate (zero shear viscosity)

$\eta(\dot{\gamma})$ = viscosity as a function of shear rate $\dot{\gamma}$

K, m = material constants

The zero shear rate viscosity calculated from this model at 60°C was observed to correlate well with the number of wheel passes required to cause 10 mm of rutting, N_{10}, in an accelerated laboratory wheel-tracking device at 45°C.

Marasteanu and Anderson [11] proposed a method in which the zero shear rate viscosity can be determined from rheological master curves constructed from DSR test data. It has been shown that as the test frequency becomes very low (0.1 rad/s), η_o can be approximated by [11-12, 14]:

$$\eta_o \cong \eta' \cong \frac{G''}{\omega} \cong \frac{|G^*|}{\omega} \tag{9}$$

where

G'' = loss modulus

$|G^*|$ = complex shear modulus

η' = in-phase component of the complex viscosity

ω = angular frequency (rad/s)

This equation is valid as long as the phase angle, δ, is close to 90°. However, many polymer modified binders have a phase angle significantly less than 90°. The CAM model (equation 6) was proposed to obtain the modulus values corresponding to phase angles of 90°. After manipulating equation 6, the zero shear rate viscosity can be calculated as follows:

$$\eta_o = \frac{|G^*|_{90}}{\omega_{90}} = \frac{G_g}{\omega_c}\left[\frac{(w-1)^{w-1}}{w^w}\right]^{\frac{1}{v}} \tag{10}$$

Equation 10 has successfully been used to calculate η_o at any temperature by simply applying the corresponding time-temperature superposition shift factor to ω_c.

Rowe et al [12] have proposed a method for using the zero shear rate viscosity as a high-temperature specification parameter for asphalt binders. This method was based on the current Superpave specification in order to reach a controlling value for η_o. They also discuss a fundamental approach to grade "bumping" due to traffic loading and speed effects. However, Anderson et al [14] caution against endorsing the zero shear viscosity as a specification criterion at the moment. While η_o corresponds well to rut measurements made at laboratory accelerated loading facilities, there are no known field trials in which the zero shear viscosity of asphalt binders has been related to pavement performance.

Repeated Creep

As mentioned above, the current Superpave specification, $|G^*|/\sin\delta$, does not accurately predict the high-temperature performance of asphalt pavements. An alternative to measuring the zero shear rate viscosity is the repeated creep recovery test for binders (RCRB) [15]. This test has been used to evaluate the relative rut resistance, R, of asphalt binders. Bahia et al [16] suggest that rutting is a repeated creep mechanism developed under sinusoidal loading pulses. The pavement layer subject to traffic loading would recover some deformation due to elastic stored energy in the layer materials. The energy is dissipated in damping and in permanent flow. The damping energy is recoverable if given enough time, but the energy related to permanent flow is lost. The permanent portion of the dissipated energy is believed to be the main contributor to the rutting behavior of asphalt pavements.

Bahia et al [16] have developed a repeated creep test of asphalt binders using the DSR in stress-controlled mode. The RCRB test protocol consists of applying a creep load for 1 second followed by a recovery period of 9 seconds. The parallel plate test geometry (25-mm plate diameter) is used, and tests are carried out at several temperatures. Typical data obtained from the RCRB test is shown in Figure 2.1. The slope, γ', which is the accumulated strain of the binder, is constant throughout the test. This implies that the binder exhibits linear viscoelastic behavior. The viscous component of the creep stiffness, G_v, can be estimated from creep and recovery data measured with the DSR. G_v has been shown to be a good indicator of the rate of permanent strain accumulation for asphalt binders, and was therefore proposed by Bahia et al [16] as a better high-temperature specification parameter.

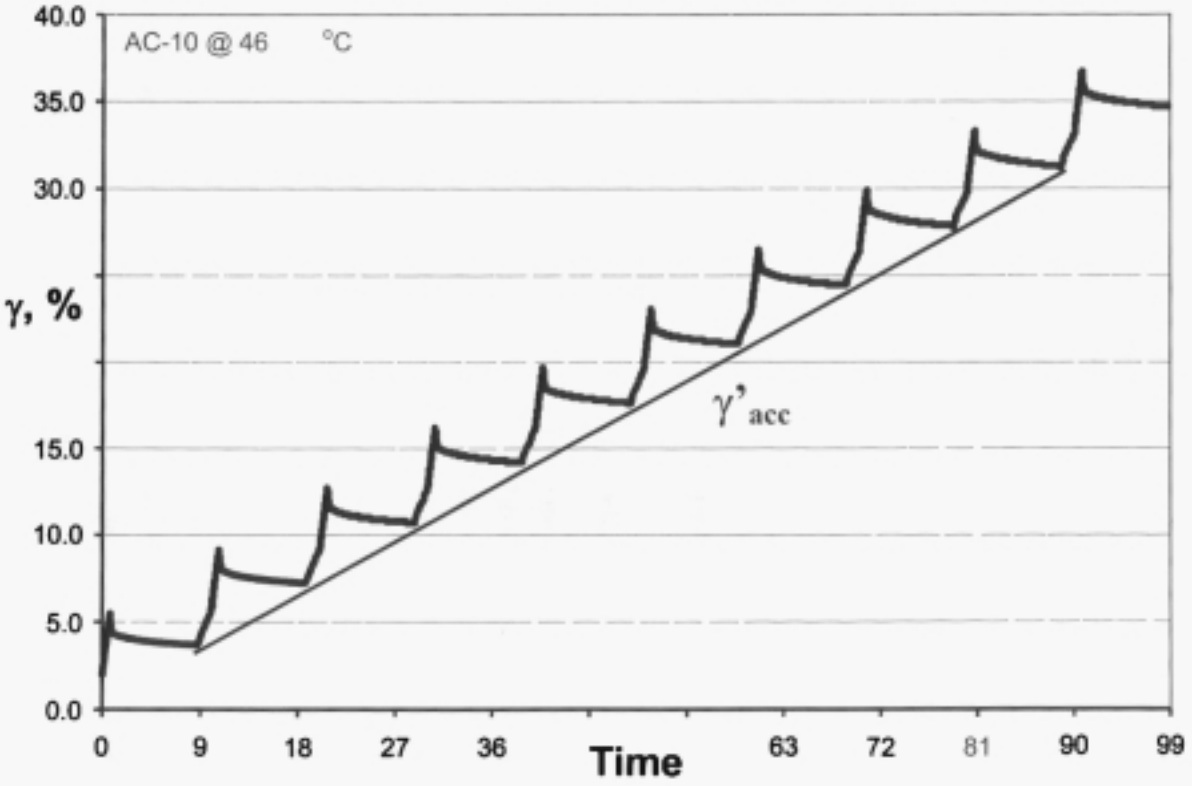

Figure 2.1 Typical Creep and Recovery Test Data

Bouldin et al [15] have proposed a different method to revise the Superpave high-temperature specification. The method uses a semi-empirical model that fits RCRB test data using data generated from conventional Superpave DSR tests. Conceptually, this approach is based on the assumptions that the strain accumulation rate depends on the binder stiffness and viscoelastic contribution and that these two contributions are independent. An empirically determined hyperbolic function predicts the accumulated shear strain in the asphalt binder:

$$\left(\gamma_{acc}\right)^{-1} = k \cdot \left|G^*\right| \cdot \left\{ Y_o + a \cdot \left[1 - e^{\left(\frac{-\left|\delta - X_o + b \cdot \ln(2)^{1/c}\right|}{b} \right)^c} \right] \right\} \tag{11}$$

where

γ_{acc} = accumulated shear strain

$|G^*|$ = complex shear modulus

δ = phase angle, degrees

k = a constant

Y_o, X_o, a, b, and c = empirical fitting parameters

Bouldin et al [15] have shown that the accumulated strain predicted using equation 11 correlates well with the measured accumulated strain from the RCRB test. They claim that this approach better accounts for the increased influence of the phase angle, δ, on the accumulated strain, γ_{acc}, without neglecting the significant effect of binder stiffness.

Time Sweep

As with high-temperature specifications, the intermediate temperature parameter $|G^*|\sin\delta$ does not relate well to the accumulation of fatigue damage in asphalt mixtures. The Superpave specification was developed assuming linear viscoelastic behavior, but asphalt pavements in fatigue demonstrate nonlinear damage behavior. This makes the analysis of fatigue damage quite complex.

Anderson et al [17] have observed two different failure modes when asphalt binders are tested with DSR time sweeps:

1. Internal microcracking appears to occur
2. Plastic flow at the sample edges occurs, a phenomenon known as edge fracture

They performed strain-controlled time sweep experiments with the DSR with 8-mm diameter parallel plates at a frequency of 10 Hz. True fatigue, as associated with internal microdamage, was observed to occur at temperatures in which the stiffness was greater than 15 MPa. In the region of 5 MPa, obtained at higher test temperatures, edge fracture or instability flow was prominent. Anderson et al [17] concluded that with its current limitations, the DSR is not a suitable method for characterizing the fatigue behavior of asphalt binders.

Bonnetti et al [18] and Bahia et al [16] have defined the fatigue failure of asphalts by three main damage stages. The first stage represents the stage during which the energy per cycle is dissipated in viscoelastic damping with negligible damage. The next stage is the crack

initiation stage, in which an additional amount of damage per cycle is observed, consuming added energy beyond viscoelastic damping. The last stage is the crack propagation stage, in which the material responds to changes very rapidly under constant stress or strain until complete fracture is reached. This is assumed to be the most critical stage during which damage per cycle is sufficiently high that healing and recovery from damage are unlikely to occur.

A suitable means of evaluating the fatigue response of asphalt binders is to use the cumulative dissipated energy ratio (DER) concept [18]:

$$DER = \frac{\sum_{i=1}^{n} W_i}{W_n} \tag{12}$$

where

W_i = dissipated energy per cycle

W_n = dissipated energy at cycle n

Research has shown that this method allows the determination of the fatigue life of asphalt mixtures as well as asphalt binders under both constant stress and constant strain modes. N_p, which is a parameter that represents the binder fatigue life, is the number of cycles of load applications to reach the crack propagation stage of the fatigue cracking process. Statistical analysis of the fatigue behavior has shown that the conventional power law model (equation 13), expressed as the number of cycles to failure in fatigue as a function of the initial dissipated energy, fits the data collected quite well. The two parameters, *K1* for slope and *K2* for intercept, could be used successfully to describe the fatigue behavior of binders [18].

$$N_f = K_2 \cdot \left(\frac{1}{W_i} \right)^{K_1} \tag{13}$$

Bonnetti et al [18] have observed different response behavior of the asphalt binder depending on the type of rheometer used to conduct time sweep tests. Under strain-controlled conditions, the asphalt tends to store energy because of the constrained deformation, whereas under stress-controlled conditions, the material freely dissipates the energy into permanent deformation. They also found that testing under high strain or stress conditions represented weak pavement conditions, while testing under low stress or strain conditions represented strong pavement conditions. It was hypothesized that pavements with thin asphalt layers operate under strain-controlled conditions, while pavements with thick layers operate under stress-controlled

conditions. However, it is recognized that the actual pavement characteristics in the field are highly variable and can rarely be accurately estimated.

Low-Temperature Fracture

During the SHRP program to develop performance-based specifications for asphalt binders, the researchers acknowledged that, "Ideally it is necessary to determine the fracture mechanics parameters for neat asphalt cement as well as for hot mix asphalt concrete" [19]. However, because of the sophisticated test methods required and a lack of resources, the direct tension test (DTT) was developed as a surrogate for a more fundamental fracture test [20]. Ongoing work by Hesp and his associates [19-22] has been focused on the development of a fracture mechanics based approach that will more accurately predict the low-temperature performance of asphalt pavements. Using linear elastic fracture mechanics (LEFM) theory, the stress level at which a crack propagates under plane-strain conditions is given by the following relationship [21]:

$$\sigma_f = \sqrt{\frac{E \cdot G_c}{\pi\left(1-\upsilon^2\right)a}} \tag{14}$$

where

σ_f = failure stress within the material far away from the crack

E = Young's modulus

G_c = fracture energy

υ = Poisson's ratio

a = crack length

In this theory, the critical stress intensity factor, or fracture toughness, in tension is defined as:

$$K_{Ic} = \sigma_f \sqrt{\pi a} = \sqrt{\frac{E \cdot G_{Ic}}{\left(1-\upsilon^2\right)}} \tag{15}$$

Using the Paris law relationship, which relates crack growth rate to more fundamental material properties such as the tensile strength and fracture energy of the material, single-event thermal cracking and thermal fatigue cracking can be defined by:

$$\Delta C = A \cdot \left(\Delta K\right)^n \tag{16}$$

where

ΔC = change in crack length caused by a single cooling cycle

ΔK = change in stress intensity factor caused by a single cycle

A, n = Paris law fracture parameters for asphalt concrete

Hesp and his colleagues [19-22] have developed a rather simple method for determining the fracture toughness, K_{Ic}, and fracture energy, G_{Ic}, of asphalt binders and mastics in the linear viscoelastic regime. Based on the fracture toughness determination of metals, ASTM E399, the test involves breaking a notched asphalt binder specimen in a three-point bend configuration inside a controlled environmental chamber. The beams are loaded at a constant rate until the fracture propagates. In this method, the fracture toughness of the binder can be determined by:

$$K_{Ic} = \frac{P_f \cdot S}{B \cdot W^{\frac{3}{2}}} \cdot \frac{3\left(\frac{a}{W}\right)^{\frac{1}{2}} \left\{1.99 - \frac{a}{W}\left(1 - \frac{a}{W}\right)\left[2.15 - 3.93\left(\frac{a}{W}\right) + 2.7\left(\frac{a}{W}\right)^2\right]\right\}}{2\left[1 + 2\left(\frac{a}{W}\right)\right]\left(1 - \frac{a}{W}\right)^{\frac{3}{2}}} \qquad (17)$$

where

K_{Ic} = fracture toughness under plane-strain conditions

P_f = applied failure load

S = load span, 100 mm

B = specimen thickness, 12.5 mm

W = specimen height, 25 mm

a = crack length

Hoare and Hesp [19] describe the use of the J-integral method, based on ASTM E813, for determining the fracture energy, J_{Ic}, of asphalt binders. This method is based on elastic-plastic fracture mechanics (EPFM), making it suitable for measuring the fracture energy in the brittle-to-tough transition region. The testing configuration is similar to that for measuring K_{Ic}, although the notch is deeper and more slender to begin with. J_{Ic} values can be calculated from the measured total energy to failure by solving the following differential equation:

$$J_{Ic} = -\frac{1}{B} \cdot \frac{dU_T}{da} \qquad (18)$$

where

J_{Ic} = elastic-plastic fracture energy

B = specimen thickness

U_T = total strain energy, which is equal to the area under the load-displacement plot in J

a = notch length

A major drawback of using the J-integral method is the complexity of the experimental and analysis procedures. It can be shown that J_{Ic} becomes equal to G_{Ic} at low temperatures in the linear-elastic regime. Therefore, the method used to determine fracture toughness described above can also be used to determine fracture energy:

$$G_{Ic} = \frac{K_{Ic}^2 \left(1 - \upsilon^2\right)}{E} \tag{19}$$

where

G_{Ic} = fracture energy or critical elastic energy release rate

E = Young's modulus (approximate value obtained from K_{Ic} test)

υ = Poisson's ratio (estimated to be 0.5)

If a notched fracture toughness test were to be used for specification purposes, it would greatly simplify matters if the stiffness modulus could be obtained directly from the force-displacement data (possibly replacing the BBR). This estimated stiffness value is the Young's modulus value used in equation 19. The failure strain for unnotched specimens can also be calculated from K_{Ic} test data according to the following standard three-point bending formula:

$$\varepsilon_f = \frac{6 \cdot d_f \cdot W}{S^2} \tag{20}$$

where

ε_f = failure strain

d_f = crosshead displacement at failure

S = load span

W = specimen height

Roy and Hesp [22] have determined that using a notched specimen can significantly affect the failure properties of asphalt binders. While the BBR and DTT appear to predict low-temperature performance rather well for unmodified binders, three-point bending tests on notched asphalt specimens may provide significant improvement of binder characterization. Such simple tests would allow the determination of the true performance-based material properties, E, K_{Ic}, and G_{Ic}, under realistic conditions of severe tensile constraint. Anderson et al [20] recommend further study before fracture energy can be recommended as a specification parameter. However, test results show that the critical cracking temperature, T_{cr}, generated by AASHTO M 320 and MP1a rank binders quite differently from the ranking determined by fracture energy.

Glass Transition Temperature

Another method used to predict the low-temperature performance of asphalt binders is to estimate the glass transition temperature, T_g. The glass transition temperature, originally described for polymeric materials, is defined as the temperature at which the molecular volume of a material undergoes a significant collapse in response to controlled cooling [23]. The typical procedure used to arrive at T_g has been to determine the temperature at which the thermal coefficient of expansion undergoes a discontinuity as the sample is slowly cooled.

Recently, other methods have been made available for measuring T_g, including differential scanning calometry (DSC), rheological behavior by observing values of the loss modulus or phase angle vs. temperature, and dilatometry [24]. The glass transition temperature may be obtained from DSC by observing changes in the base line as the temperature passes through T_g. Two types of DSC test procedure are in use: standard and modulated DSC. Researchers generally agree that the modulated DSC procedure gives better estimates of T_g than does standard DSC. Dilatometric (volumetric) methods for measuring the T_g of asphalt binders have been described by Anderson and Marasteanu [24]. Differences in test protocol between different researchers, such as sample size and cooling rate, have given different values for T_g. Torsion bar testing in the DSR provides another means to measure the glass transition temperature [23, 24]. When the loss modulus, G'', is plotted vs. temperature, the resulting curve most often exhibits a peak value. The temperature at which the peak value for G'' is reached is interpreted as T_g. Anderson and Marasteanu [24] concluded that DSC, dilatometry, and G'' peak

values all give estimates of T_g that are in relatively good agreement. Reinke and Engber [23] have shown that the glass transition temperature is usually very close to the limiting temperatures produced by BBR and DTT data.

Summary

A number of important points can be gleaned from the literature review and applied to the current study. First, drawing on the understanding of previous database projects, the University of Minnesota will construct a database for use at the Minnesota Department of Transportation (Mn/DOT). This database will collect and store asphalt binder data from a number of different tests performed in the laboratory. It will be easy to use and understand, and able to accommodate future data as it is collected.

Based on recent research cited in several sources above, the current Superpave specifications may not be adequate in characterizing the performance of asphalt binders. This is especially true as more and more polymer modified binders are being used in Minnesota and around the country. As a result, several new test procedures have been proposed to better characterize asphalt binders at high, low and intermediate temperatures. Several of these tests will be conducted by the University of Minnesota on typical binders used in Minnesota, both neat and modified. Among these methods are frequency sweep, master curves, and zero shear viscosity using the DSR at high temperatures, time sweep and dissipated energy ratio using the DSR at intermediate temperatures, and critical cracking temperature using the BBR and DTT at low temperatures. These test results will be incorporated into the database constructed for this project.

CHAPTER 3:
RESEARCH METHODOLOGY

Introduction

Nine different asphalt binders were provided to the University of Minnesota from various refineries around the area. Each of the binders was run through the same aging and testing procedures. The binders are listed in Table 3.1. The University of Minnesota was provided with approximately one gallon (4 L) of each binder from the various refineries. This ensured sufficient quantities for all of the aging and testing procedures in this project.

Table 3.1 Asphalt Binder Information

U of M ID	PG Grade	Source
BI1	64-28 HFD Blend	Koch
BI2	64-28 Stylink	Koch
BI3	64-34 Stylink	Koch
BI4	64-34 Elvaloy	MIF
BI5	58-34 Elvaloy	Murphy
BI6	58-34 Oxidized	Husky
BI7	58-28 MnROAD	Koch
BI8	58-34 MnROAD	Koch
BI9	58-40 MnROAD	Koch

Aging

The asphalt binders used in this project were all subject to the same aging procedures required in the Superpave program and referenced in AASHTO M 320: Performance Graded Asphalt Binder. Some asphalt was kept in the original (as-received) condition. Some additional asphalt binder was aged according to AASHTO T 240: Effect of Heat and Air on a Moving Film of Asphalt (Rolling Thin-Film Oven Test). A portion of the residue from the rolling thin-film oven was aged according to AASHTO R 28: Accelerated Aging of Asphalt Binder Using a Pressurized Aging Vessel (PAV). Asphalt binders in these three conditions (original, RTFOT, PAV) were then tested using various procedures described in the following sections and shown in Table 3.2.

Table 3.2 Laboratory Testing Matrix

Test Procedure	Aging Condition		
	Original	*RTFOT*	*PAV*
DSR Frequency Sweep	X	X	X
DSR Strain Sweep		X	X
DSR Repeated Creep		X	
DSR Fatigue			X
BBR		X	X
DTT		X	X

Dynamic Shear Rheometer (DSR) Testing

All of the dynamic shear rheometer (DSR) testing was performed on an AR 2000 with an environmental test chamber from TA Instruments.

Frequency Sweeps

Frequency sweep tests were performed on asphalt binders in all three conditions: original, RTFOT, and PAV. Unaged (original) binders were tested for grade verification only. These materials were tested at the high PG temperature and the PG temperature + 6°C. The samples were all poured and trimmed at the PG temperature. The tests were run on 25-mm parallel plates with a 1.0 mm gap. The sample was allowed to equilibrate for ten minutes at each temperature prior to testing. The University of Minnesota tested samples 1-6. Data from samples 7-9 were obtained from Mathy Technology & Engineering Services, Inc.

RTFOT aged samples were tested from 34°C to the PG temperature + 6°C. The samples were poured and trimmed at 52°C, which was the midpoint of testing temperatures. The tests were run on 25-mm parallel plates with a 1.0 mm gap. The sample was allowed to equilibrate for ten minutes at each temperature prior to testing.

PAV aged samples were tested over a range from 4°C to the PG temperature + 6°C. From 4°C to 34°C the tests were performed on 8-mm plates with a 2.0 mm gap. The samples were poured and trimmed at 45°C and then lowered to the test temperature. From 34°C to the PG temperature + 6°C the tests were performed on 25-mm plates with a 1.0 mm gap. The samples were poured and trimmed at 52°C. Tests on the PAV residue were run at 34°C on both the 8 mm and 25 mm plates.

All of the frequency sweep tests were performed from 1 to 100 rad/s. The frequencies increased in log mode with five points per decade. The controlled strain was adjusted at each

temperature so that the oscillating torque remained under 2 mN-m. This ensured that the tests were performed in the linear viscoelastic range. Table 3.3 shows the ranges of strain values used in each test. As a general rule, for every 6°C increase in temperature the input strain doubled.

Table 3.3 Input Strain Levels for Frequency Sweep Tests

Test Condition	Strain Range
Original, 25 mm plates	5 – 15%
RTFOT, 25 mm plates	0.1 – 8%
PAV, 25 mm plates	0.1 – 4%
PAV, 8 mm plates	0.02 – 3.5%

Strain Sweeps

Strain sweeps were performed on RTFOT and PAV material at the conclusion of frequency sweep tests. No strain sweeps were run on the original binder. For RTFOT aged asphalts, the strain sweeps were performed 6°C above the PG temperature. For example, a PG 64-28 binder was tested at 70°C. The samples were all poured and trimmed at 52°C, which was the midpoint of temperatures for frequency sweep tests. The tests were run on 25-mm parallel plates with a 1.0 mm gap. The sample was allowed to equilibrate temperature for ten minutes prior to testing. The initial strain was set at 2 percent, the final strain was set at 200 percent, and the strain increased in 2 percent increments. The test frequency was set at 10 rad/s. The complex modulus (|G*|) was monitored until it dropped at least 20 percent.

For PAV aged samples, strain sweeps were run at two different temperatures. The test was run exactly the same as described above at 6°C above the PG temperature. In addition, tests were run at 34°C at the conclusion of frequency sweep tests at low temperatures. The samples were poured and trimmed at 45°C and then lowered to the test temperature. These tests were run on 8-mm parallel plates with a 2.0 mm gap. The test frequency was set at 10 rad/s. The strains ran from 0.2 percent to 2.0 percent in 0.2 percent increments, and then from 2 percent to 200 percent in 2 percent increments. The complex modulus was monitored until it dropped at least 20 percent. The tests were stopped manually after 75 - 200 percent strain at high temperatures and 35 - 80 percent at 34°C.

Repeated Creep

Repeated creep tests were run on RTFOT aged material at the high PG temperature. The samples were poured and trimmed at either 58°C or 64°C, depending on the PG grade. The tests were performed on 25-mm plates with a 1.0 mm gap. The sample was allowed to equilibrate temperature for ten minutes prior to testing. The shear stress was set to 25 Pa. This allowed for a recovery strain in excess of 20 times the rheometer strain resolution. The loading and unloading times were set to be 1 s and 9 s, respectively. The test was run for a total of 100 repeated cycles. Time and strain data collected during the test was then fit to the Burgers or four-element model.

Fatigue

Fatigue tests were performed on PAV aged material at low temperatures. In order to test all of the binders for true fatigue (see discussion in [17]), the binders were tested at the temperature that gave an initial stiffness of 25 MPa at 10 rad/s. The temperature for each test was interpolated from frequency sweep test data conducted at different temperatures. The test temperatures are shown in Table 3.4.

Table 3.4 Fatigue Test Temperatures

Binder ID	Test Temperature, °C
BI1	9.2
BI2	9.2
BI3	1.5
BI4	2.1
BI5	1.8
BI6	3.1
BI7	8.8
BI8	2.5
BI9	-9.0

The fatigue tests were performed on 8-mm plates with a 2.0 mm gap. The samples were loaded at 45°C and then cooled down to trim at the test temperature. The sample was allowed to equilibrate temperature for ten minutes prior to testing. A time sweep was performed on each sample, in which an oscillating stress of 500 kPa was applied at 10 rad/s. The DSR performed a continuous oscillation procedure, and the complex modulus (|G*|) was monitored until it dropped

sharply. The fatigue test lasted anywhere from 15 minutes to 2.5 hours. On occasion it was necessary to increase the oscillating stress to 750 kPa to facilitate failure in the specimen.

Standard Performance Grade (PG) Tests

Dynamic Shear Rheometer (DSR)

The standard test method, AASHTO T 315: Determining the Rheological Properties of Asphalt Binder using a Dynamic Shear Rheometer (DSR), was not independently performed on the asphalt binders used in this project. However, the frequency sweeps described above did capture the relevant parameters for this test. The angular frequency of 10 rad/s was one of the frequencies tested. The temperature ranges covered the test temperatures required by the AASHTO method (PG temperature and PG + 6°C). The test data was checked against AASHTO T 315 to verify the binder PG grade.

Bending Beam Rheometer (BBR)

The test standard AASHTO T 313: Determining the Flexural Creep Stiffness of Asphalt Binder Using the Bending Beam Rheometer (BBR) was followed to test the asphalt binders at low temperatures. A simply supported beam of asphalt binder was subject to a constant load of 980 mN for a duration of four minutes. The deflection was measured over time, and the stiffness (S) and m-value were calculated from the raw data. The test temperatures were as specified in AASHTO T 313. For example, a PG 64-28 binder was tested at -18 °C and -24°C. All of the PAV and RTFOT residues were tested in this fashion. The testing was performed on a Cannon Thermoelectric BBR.

Direct Tension Test (DTT)

The asphalt binders were tested in direct tension according to AASHTO T 314: Determining the Fracture Properties of Asphalt Binder in Direct Tension (DT). A dog bone-shaped asphalt binder specimen was pulled in tension at a constant strain rate until it breaks. The test temperatures were the same as those for the BBR. Both RTFOT and PAV aged samples were tested in this fashion for binders 1-6. Mathy Technology & Engineering Services, Inc tested samples 7-9. The testing was performed on a Bohlin Direct Tension Tester.

CHAPTER 4:
RESULTS AND DISCUSSION

Master Curves

The CAM model (equation 6 in Chapter 2) was used to fit frequency sweep data to master curves. RTFOT and PAV aged binders were fit to master curves at a reference temperature of 34°C. The commercial software package SigmaStat was used to fit the test data to the model through nonlinear regression. Horizontal shift factors were applied at each temperature so that the complex modulus (|G*|) formed a smooth master curve. These same shift factors were also applied to the phase angle data to generate phase angle master curves. Figures 4.1 and 4.2 show the complex modulus and phase angle master curves for RTFOT aged binders, respectively. Figures 4.3 and 4.4 show the complex modulus and phase angle master curves for PAV aged binders, respectively. Appendix A contains complex modulus and phase angle master curves for each individual binder at a reference temperature of 34°C. Table 4.1 contains all of the model parameters for the master curves.

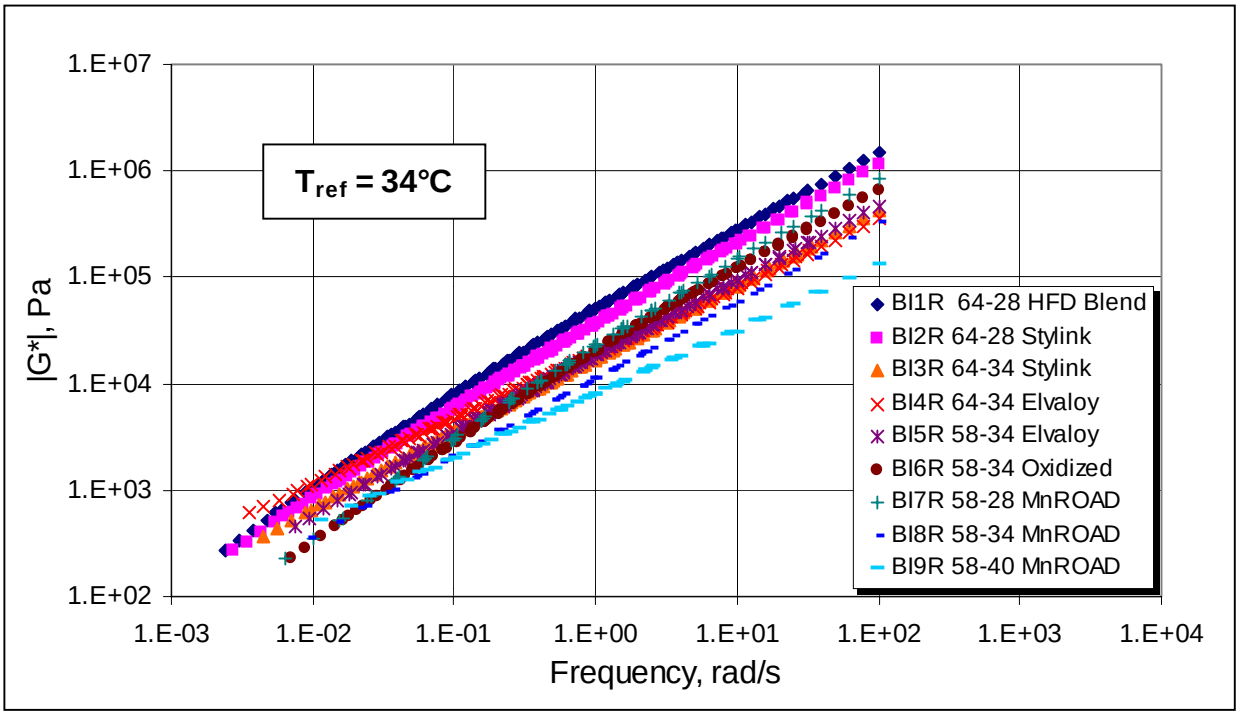

Figure 4.1 Complex Modulus Master Curves, RTFOT Aged Binders

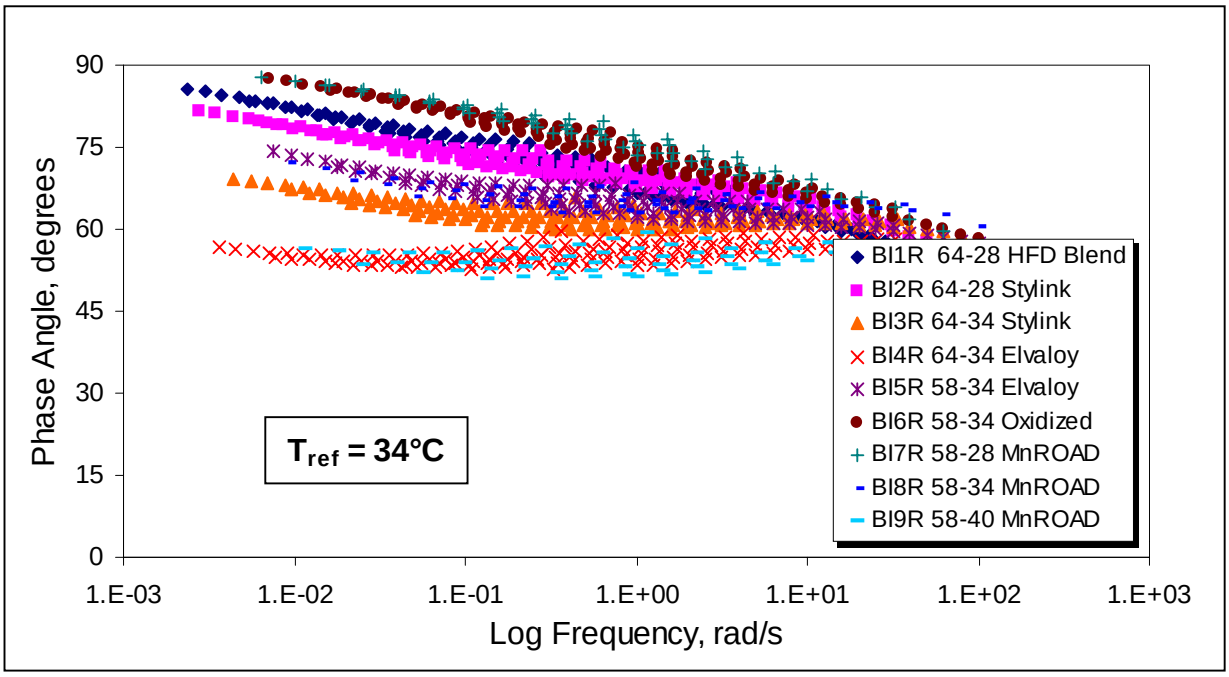

Figure 4.2 Phase Angle Master Curves, RTFOT Aged Binders

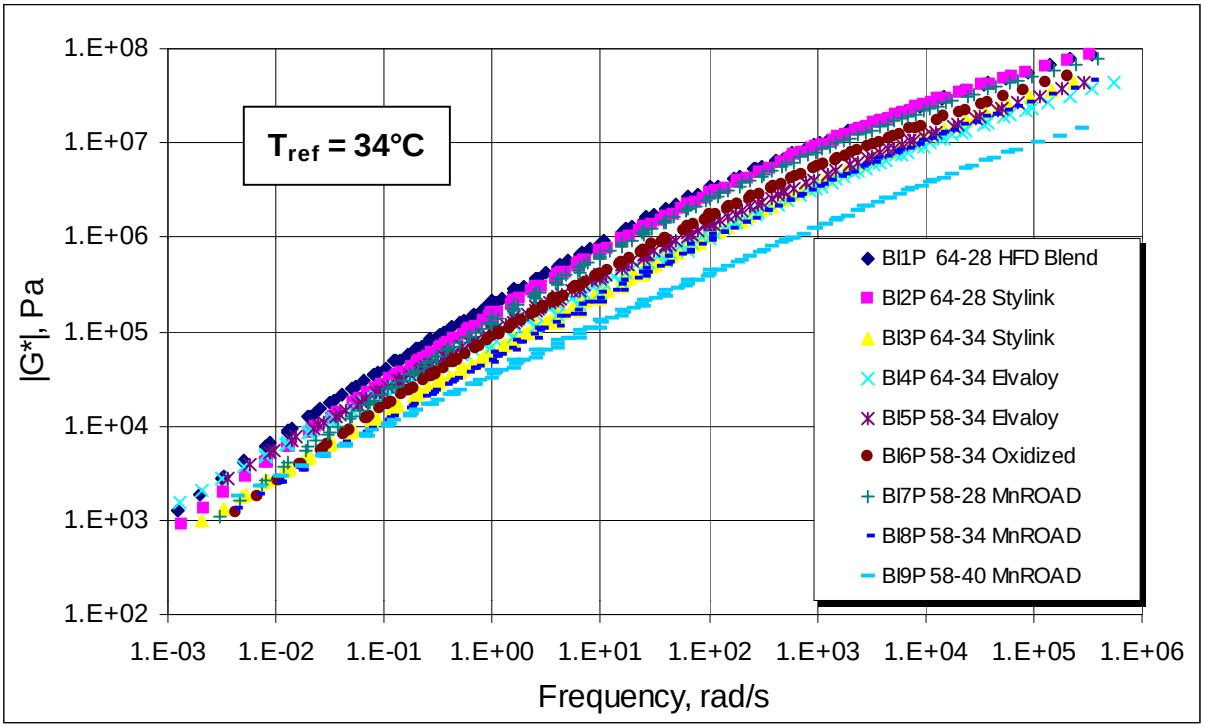

Figure 4.3 Complex Modulus Master Curves, PAV Aged Binders

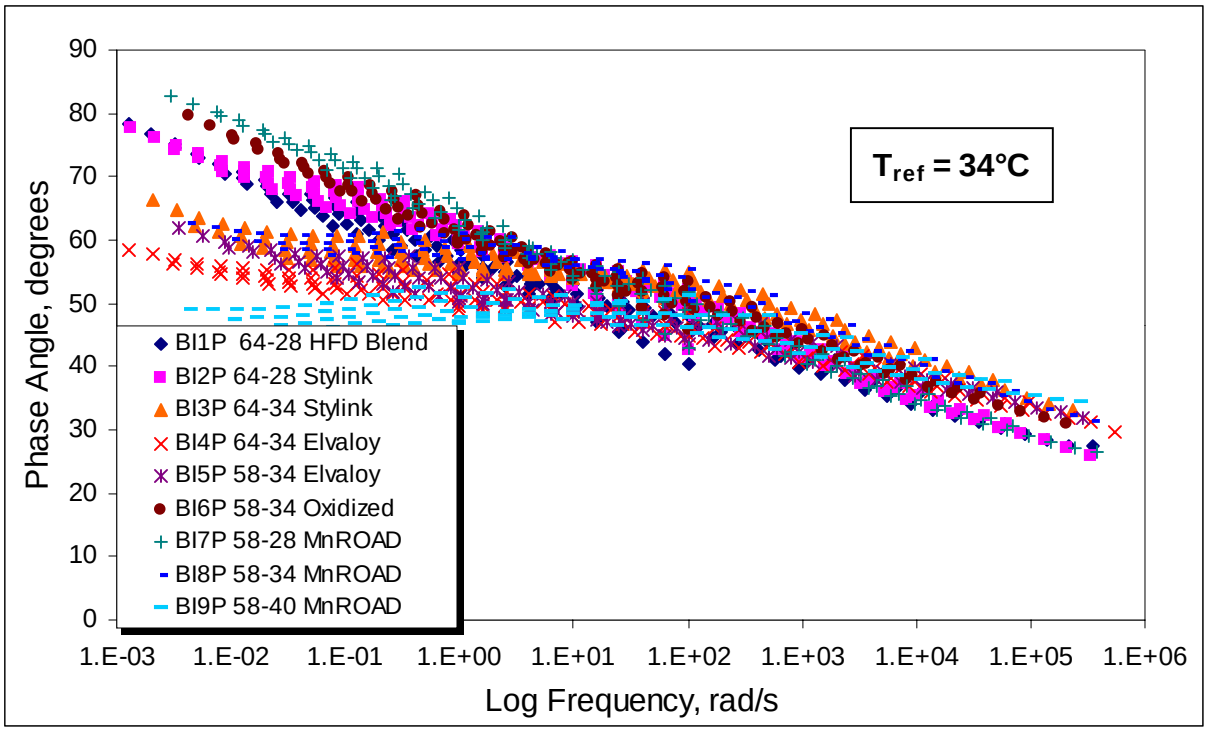

Figure 4.4 Phase Angle Master Curves, PAV Aged Binders

Table 4.1 Master Curve Model Parameters

RTFOT Aged Binders									
	BI1R	**BI2R**	**BI3R**	**BI4R**	**BI5R**	**BI6R**	**BI7R**	**BI8R**	**BI9R**
q	3.29	4.76	6.85	6.80	5.60	2.69	3.36	6.78	6.69
v	0.14	0.18	0.26	0.15	0.16	0.13	0.14	0.26	0.11
w	1.05	0.89	0.71	0.68	0.82	1.20	1.13	0.74	0.71
a34	0	0	0	0	0	0	0	0	0
a40	-0.54	-0.51	-0.48	-0.49	-0.49	-0.50	-0.48	-0.45	-0.44
a46	-1.02	-0.97	-0.91	-0.97	-0.94	-0.97	-0.98	-0.90	-0.87
a52	-1.45	-1.41	-1.30	-1.38	-1.35	-1.38	-1.41	-1.29	-1.24
a58	-1.87	-1.82	-1.67	-1.76	-1.75	-1.78	-1.81	-1.67	-1.60
a64	-2.26	-2.20	-2.01	-2.11	-2.12	-2.15	-2.19	-2.03	-1.93
a70	-2.62	-2.56	-2.35	-2.44	x	x	x	x	x

PAV Aged Binders									
	BI1P	**BI2P**	**BI3P**	**BI4P**	**BI5P**	**BI6P**	**BI7P**	**BI8P**	**BI9P**
q	2.54	3.10	5.85	5.80	5.21	2.67	1.35	5.47	7.47
v	0.13	0.14	0.17	0.14	0.14	0.12	0.12	0.16	0.14
w	0.98	0.96	0.71	0.67	0.71	1.04	1.23	0.75	0.59
a4	3.54	3.52	3.37	3.73	3.46	3.32	3.58	3.55	3.44
a10	2.77	2.79	2.67	2.98	2.70	2.57	2.85	2.84	2.77
a16	2.02	2.07	1.98	2.24	1.98	1.86	2.11	2.12	2.07
a22	1.29	1.36	1.31	1.53	1.30	1.20	1.38	1.41	1.38
a28	0.63	0.67	0.66	0.84	0.64	0.57	0.68	0.72	0.71
a34	0	0	0	0	0	0	0	0	0
a40	-0.58	-0.61	-0.59	-0.67	-0.59	-0.53	-0.61	-0.63	-0.59
a46	-1.11	-1.15	-1.07	-1.19	-1.07	-1.04	-1.16	-1.14	-1.11
a52	-1.59	-1.63	-1.51	-1.67	-1.56	-1.53	-1.63	-1.57	-1.56
a58	-2.06	-2.07	-1.92	-2.09	-2.01	-1.96	-2.10	-1.99	-1.97
a64	-2.49	-2.49	-2.31	-2.50	-2.45	-2.38	-2.53	-2.37	-2.35
a70	-2.90	-2.87	-2.68	-2.89	x	x	x	x	x

The complex modulus master curves show the same general behavior for RTFOT and PAV conditions. The PAV materials were obviously much stiffer than the RTFOT samples over the entire range of frequencies. The PAV materials also had a steeper slope than the RTFOT materials, which indicates that once an asphalt is aged sufficiently (PAV aged) the stiffness changes greatly with the frequency of loading (or temperature). Figure 4.3 also shows |G*| approaching a horizontal asymptote as the frequency increases (the temperature decreases). Figure 4.1 shows |G*| only in the linear range because the RTFOT samples were not tested at temperatures below 34°C.

The phase angle master curves are not particularly smooth like the complex modulus master curves. One explanation for this is that the polymer inside most of the binders

significantly changes the viscoelastic properties. Overall the phase angles for PAV materials were much lower than that of the RTFOT materials. As the asphalt is aged it becomes stiffer and more elastic. The PAV materials again had a steeper slope than the RTFOT materials. The asphalt binders that contained large amounts of polymers had lower phase angles than binders with little or no polymer. This is true for both RTFOT and PAV aged binders.

A number of observations can be made from examining the |G*| master curve for RTFOT aged binders (Figure 4.1). Binders 1 and 2 were the stiffest across the entire range of frequencies, and their curves were quite close to each other. These are the two PG 64-28 binders, which contain little if any polymer. Binders 6 (PG 58-34 Oxidized) and 7 (PG 58-28) had the steepest |G*| curves. The complex modulus for these two binders was the lowest at high temperatures, but at 34°C the modulus approached those of binders 1 and 2. Binder 9 (PG 58-40) had the lowest modulus over most of the frequency range. This is consistent with it being the softest binder by PG grading. Binders 3, 4, 5, and 8 were all modified and had the flattest slopes in |G*|. At high temperatures their complex modulus values were in the middle of the range of binders tested, but at lower temperatures the |G*| were among the lowest in the group of binders tested. Creating master curves from data over a range of temperatures and frequencies showed the differences between different binder grades, modification techniques, and sources.

One can also learn about the behavior of asphalt binders by plotting master curves of the complex modulus vs. temperature. Figures 4.5 and 4.6 plot |G*| vs. temperature at 10 rad/s for RTFOT and PAV aged binders, respectively. As the temperature increases, the modulus decreases significantly. Binders 1 and 2 were the stiffest over the entire range of temperatures, while binders 8 and 9 were the softest. Many of the modified asphalts (binders 3, 4, 8, and 9) had flatter curves than the other binders. The modulus for these binders does not change as dramatically as the temperature changes compared to the other binders. On the other hand, binders 6 and 7 had the steepest curves. They are the most susceptible to small temperature changes.

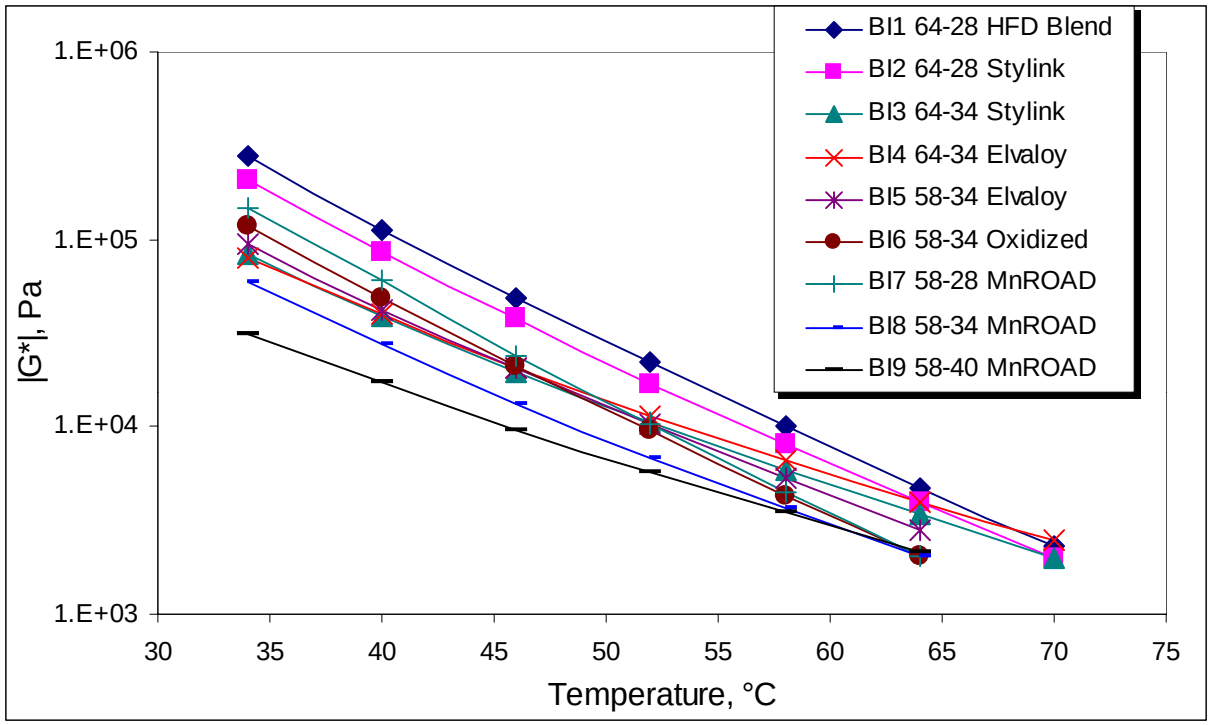

Figure 4.5 |G*| vs. Temperature @ 10 rad/s, RTFOT Aged Binders

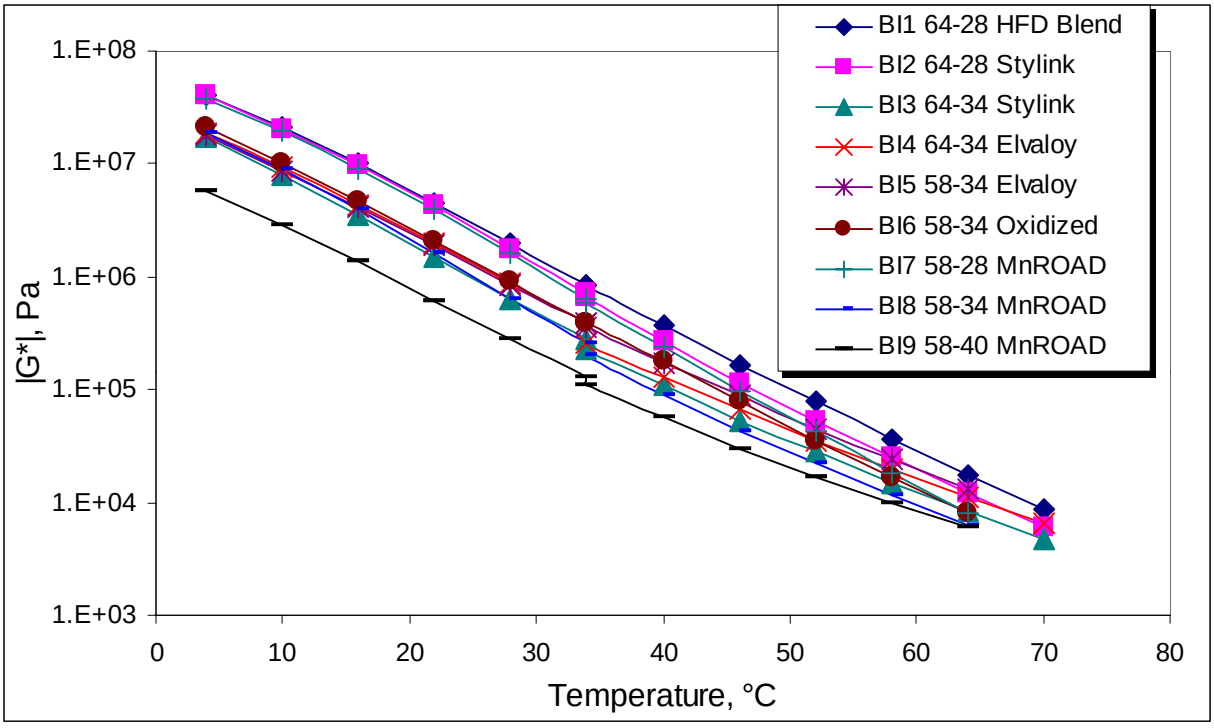

Figure 4.6 |G*| vs. Temperature @ 10 rad/s, PAV Aged Binders

Zero Shear Viscosity

It was reported in the Literature Review (Chapter 2) that there are a number of techniques to calculate the zero shear viscosity (ZSV) of asphalt binders. This research project examined four different ways to calculate ZSV based on data obtained from frequency sweep tests at several temperatures. The first two methods are the most simple. The zero shear viscosity, η_o, can be approximated by G"/ω or G*/ω. This method is acceptable as long as the phase angle is close to 90° and the frequency is sufficiently low. If these conditions are not met, the accuracy of the estimate decreases significantly. For an angular frequency of 1 rad/s (the lowest in the frequency sweeps that were performed) ZSV approximated by these two methods are shown in Tables 4.2 and 4.3.

Table 4.2 Zero Shear Viscosity (η_o = G"/ω)

	Zero Shear Viscosity, Pa-s								
Temp, °C	**BI1**	**BI2**	**BI3**	**BI4**	**BI5**	**BI6**	**BI7**	**BI8**	**BI9**
34	47070.0	33810.0	15020.0	15160.0	16850.0	18790.0	22480.0	10130.0	6240.0
40	18750.0	13870.0	7180.0	7748.0	7606.0	7554.0	8929.0	4869.0	3488.0
46	7512.0	5858.0	3656.0	4173.0	3567.0	3037.0	3266.0	2315.0	1970.0
52	3225.0	2583.0	1969.0	2320.0	1751.0	1228.0	1273.0	1193.0	1164.0
58	1387.0	1172.0	1079.0	1361.0	874.8	521.0	523.1	621.1	709.5
64	604.1	547.4	598.9	817.3	439.6	230.8	224.3	328.1	439.4
70	274.5	263.3	335.9	504.6					

Table 4.3 Zero Shear Viscosity (η_o = G*/ω)

	Zero Shear Viscosity, Pa-s								
Temp, °C	**BI1**	**BI2**	**BI3**	**BI4**	**BI5**	**BI6**	**BI7**	**BI8**	**BI9**
34	51350.0	36580.0	17360.0	18920.0	19070.0	19830.0	23420.0	11380.0	8020.0
40	19960.0	14820.0	8303.0	9723.0	8488.0	7803.0	9145.0	5466.0	4504.0
46	7826.0	6172.0	4190.0	5245.0	3911.0	3090.0	3306.0	2573.0	2535.0
52	3304.0	2683.0	2219.0	2902.0	1883.0	1238.0	1280.0	1305.0	1479.0
58	1405.0	1202.0	1192.0	1689.0	923.9	522.7	524.2	666.3	881.7
64	608.1	556.5	649.7	1001.0	457.0	231.0	224.4	344.6	527.4
70	275.2	266.1	359.3	603.8					

The CAM model is another method that was used to calculate zero shear viscosity. This method was shown in equation 10 in the Literature Review. It involves fitting the master curve to frequency sweep data and then manipulating the model to obtain η_o, applying the appropriate shift factor at different temperatures. One limitation in this method is that the model parameter

w needs to be greater than 1.0 for the equation to be meaningful. This was the case on only three of the binders used in this study. Interestingly enough, these three binders contained no polymer. Table 4.4 shows the zero shear viscosity estimated by the CAM model for the available binders.

Table 4.4 Zero Shear Viscosity (η_o by CAM Model)

	Zero Shear Viscosity, Pa-s		
Temp, °C	BI1	BI6	BI7
34	156069.2	33640.2	36050.8
40	45197.8	10574.5	11901.9
46	15049.3	3627.1	3759.4
52	5559.3	1395.0	1412.9
58	2120.4	559.3	554.0
64	862.2	240.4	232.4
70	372.2		

The final method that was used to calculate zero shear viscosity was to simply determine the slope of the master curve at very low frequencies. As the phase angle approaches 90° the master curve will approach an asymptote, the slope of which represents η_o. Table 4.5 includes the zero shear viscosity estimated by this method.

Table 4.5 Zero Shear Viscosity (η_o by slope)

	Zero Shear Viscosity, Pa-s								
Temp, °C	BI1	BI2	BI3	BI4	BI5	BI6	BI7	BI8	BI9
34	104367.3	81052.1	52550.9	81720.0	43177.1	30192.2	31800.7	21155.8	16829.2
40	30224.9	25059.0	17485.6	26633.5	13815.1	9490.6	10498.7	7451.2	6087.9
46	10063.9	8595.4	6487.5	8855.8	5012.5	3255.3	3316.2	2641.4	2287.5
52	3717.6	3125.8	2645.3	3438.2	1908.8	1252.0	1246.3	1072.8	960.6
58	1418.0	1213.0	1133.4	1433.9	775.6	502.0	488.7	451.6	425.8
64	576.6	507.3	508.7	629.8	326.2	215.7	205.0	198.3	196.6
70	248.9	222.8	233.1	294.7					

Figure 4.7 shows a typical plot of how the zero shear viscosity changes with temperature. As the temperature increases, ZSV decreases logarithmically, which means the resistance to flow becomes less. The first two methods (G"/ω or G*/ω) give almost the same value for ZSV. The CAM and slope methods have steeper slopes on the η_o – temperature plot than the estimates using the stiffness. Appendix B shows plots of zero shear viscosity vs. temperature for each of the nine asphalt binders.

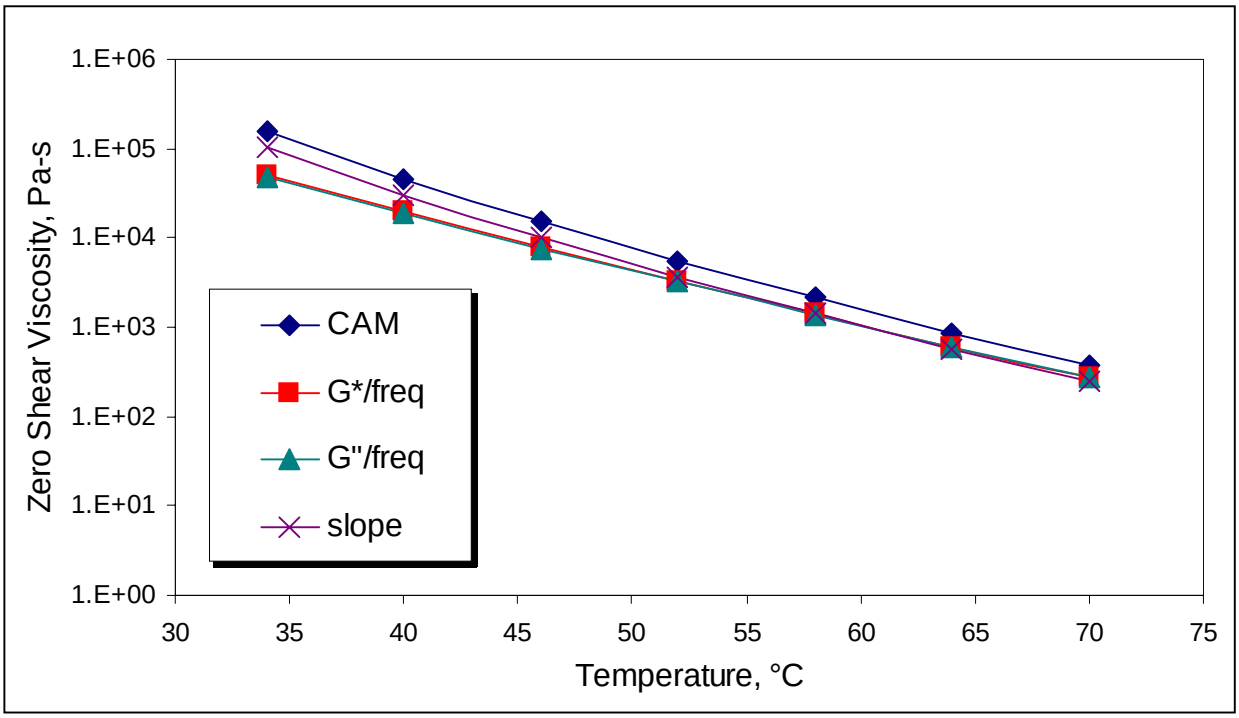

Figure 4.7 Typical Zero Shear Viscosity Plot

Figure 4.8 shows a plot of zero shear viscosity (slope method) vs. temperature for all nine binders. There are distinct differences between the binders as shown on this plot. Binders 1-4 had higher η_o values than binders 5-9. This would be expected, since binders 1-4 have a high temperature PG grade of 64, while binders 5-9 have a high temperature PG grade of 58 (by AASHTO M 320). A higher η_o value indicates greater resistance to rutting at high temperatures. The polymer-modified binders typically had flatter curves on the η_o – temperature plot. This indicates that as the temperature increases the polymer adds some resistance to flow that is not present in the unmodified binders.

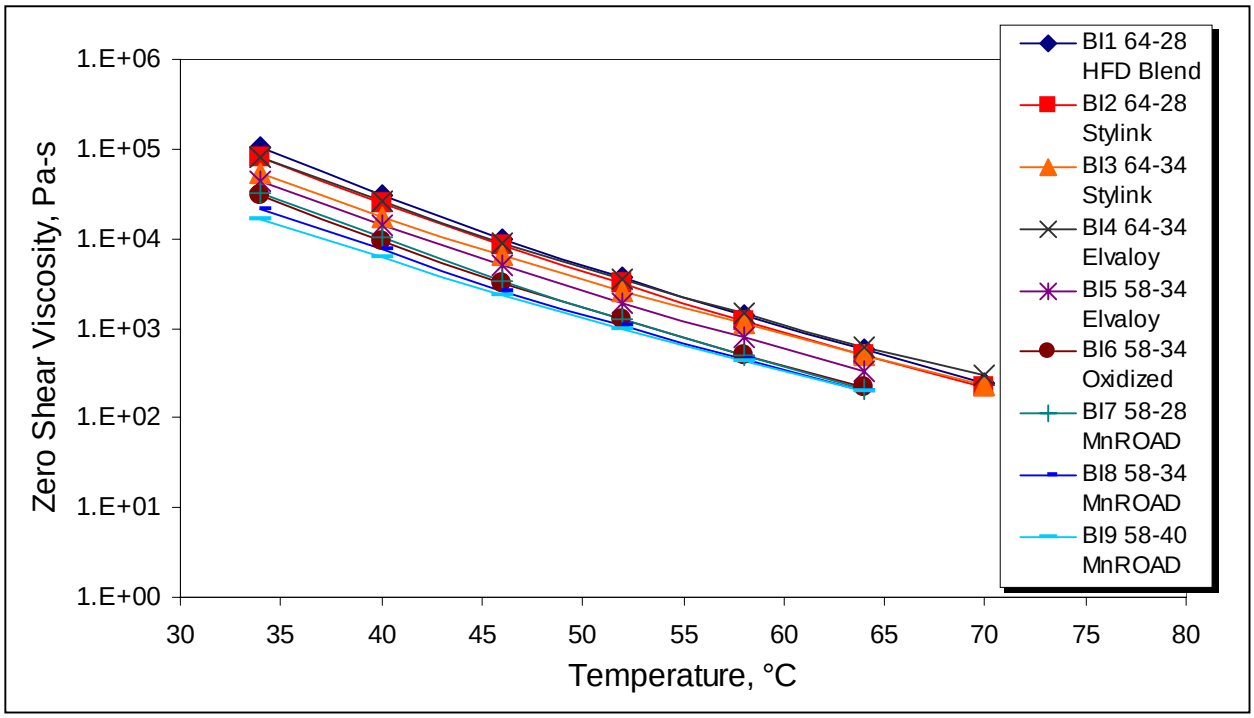

Figure 4.8 Zero Shear Viscosity (η_o by slope)

The above discussion demonstrates that the zero shear viscosity of asphalt binders can be determined by several different methods. All of the methods involve performing frequency sweep tests with the dynamic shear rheometer. The methods are straightforward and easy to apply. However, the CAM model has limitations in terms of the model parameter w. If η_o is proposed as a binder high temperature performance specification, one of these calculation methods can be easily used.

Repeated Creep

The repeated creep test measures the permanent strain (γ) accumulated in the binder after 100 cycles of shear loading and unloading. The higher the permanent shear strain, the lower the rut resistance of the pavement and likewise the viscosity of the asphalt binder. Three methods were used to determine the permanent strain of the binders. The first is simply from measuring the total strain during the repeated creep test. The second method involves using the time and strain data collected in cycles 50 and 51 to fit the following Burgers or four-element model [16]:

$$\gamma(t) = \frac{\tau_o}{G_o} + \frac{\tau_o}{G_1}\left(1 - e^{\frac{-t \cdot G_1}{\eta_1}}\right) + \frac{\tau_o}{\eta_o} t \qquad (1)$$

By normalizing the strain to the stress applied, the following equation, representing the creep compliance, J(t), in terms of its elastic component (J_e), the delayed-elastic (J_{de}), and the viscous component (J_v), could be defined [16]:

$$J(t) = J_e + J_{de} + J_v \tag{2}$$

The viscous component is inversely proportional to viscosity (η_o). A higher viscosity is indicative of higher resistance to permanent deformation of the material. Figure 4.9 shows an example of how equation 1 was fit to repeated creep test data. Plots of repeated creep results for each of the nine binders are shown in Appendix C.

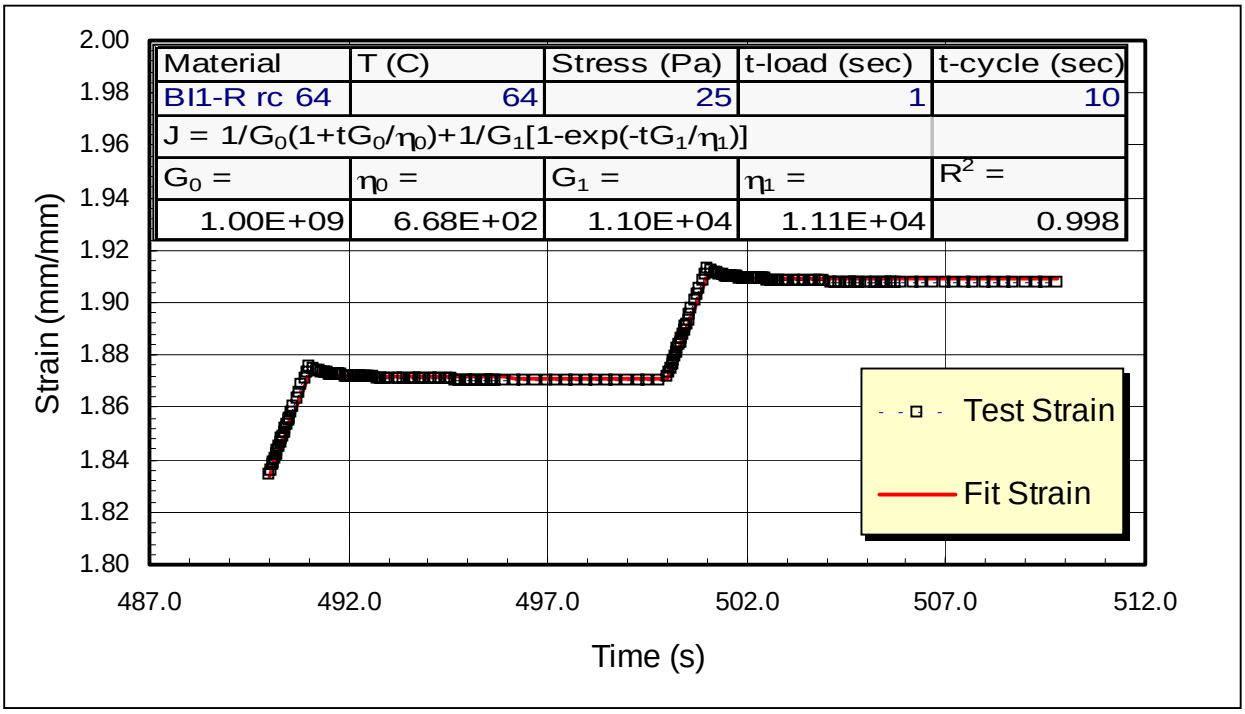

Figure 4.9 Typical Model Fit to Repeated Creep Test Data

The other method that was used to predict the permanent strain was proposed by Shenoy [25]. One can use frequency sweep data (|G*| and δ) in which the frequency corresponds to the loading time used in the repeated creep experiment, along with the applied stress (σ_o) in the creep experiment, to estimate the permanent strain. Shenoy's equation is:

$$\gamma_{max} = \frac{100 \cdot \sigma_o}{|G^*|}\left(1 - \frac{1}{\tan\delta \sin\delta}\right) \tag{3}$$

Equation 3 was used to estimate the permanent strain from the repeated creep tests.

Table 4.6 presents the total permanent strain (mm/mm) by each of the three above methods. Figure 4.10 presents this information graphically. The "Fit" and "Shenoy" methods predict γ quite well for all of the binders. The predictions are slightly less accurate for some of the modified binders (binders 3, 4, 8, and 9). Binders 1, 2, 6, and 7 show the highest permanent strain. One would assume that these binders would be more susceptible to rutting than those with lower permanent strain measures. Binders 4 and 9 have the lowest permanent strain after 100 cycles, which would indicate increased rut resistance.

Table 4.6 Permanent Strain from Repeated Creep Tests

	Maximum Permanent Strain (mm/mm)								
Method	**BI1**	**BI2**	**BI3**	**BI4**	**BI5**	**BI6**	**BI7**	**BI8**	**BI9**
Test	3.72	3.21	1.42	0.45	1.63	4.48	4.54	1.42	0.50
Fit	3.74	3.32	1.56	0.53	1.68	4.51	4.53	1.47	0.56
Shenoy	3.64	3.66	2.09	0.34	1.73	4.40	4.46	2.19	0.24

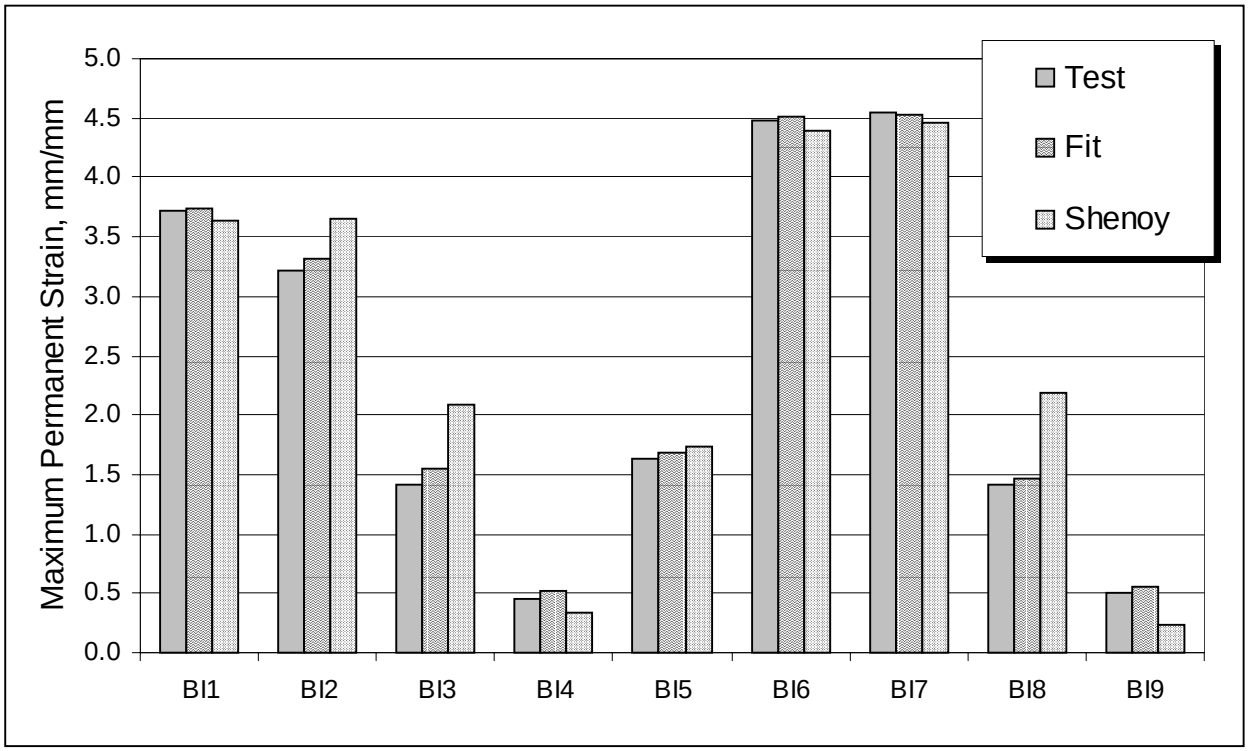

Figure 4.10 Permanent Strain Graph

Strain Sweeps

Figure 4.11 shows the result of strain sweep tests for RTFOT aged binders. The first thing to note is that in the strain range at which frequency sweep tests were performed (< 8% strain) the materials remained linear. This demonstrates that the master curve analysis, which assumed linear viscoelastic conditions, was valid. In fact, the binders reached about 100% strain before any of them showed a significant reduction in complex modulus (|G*|). Some of the more heavily polymered binders (binders 3, 5, and 9) showed the sharpest reduction in modulus with increasing strain. This indicates that under increased strain in the pavement, these materials may rut faster than those binders that do not lose stiffness as quickly.

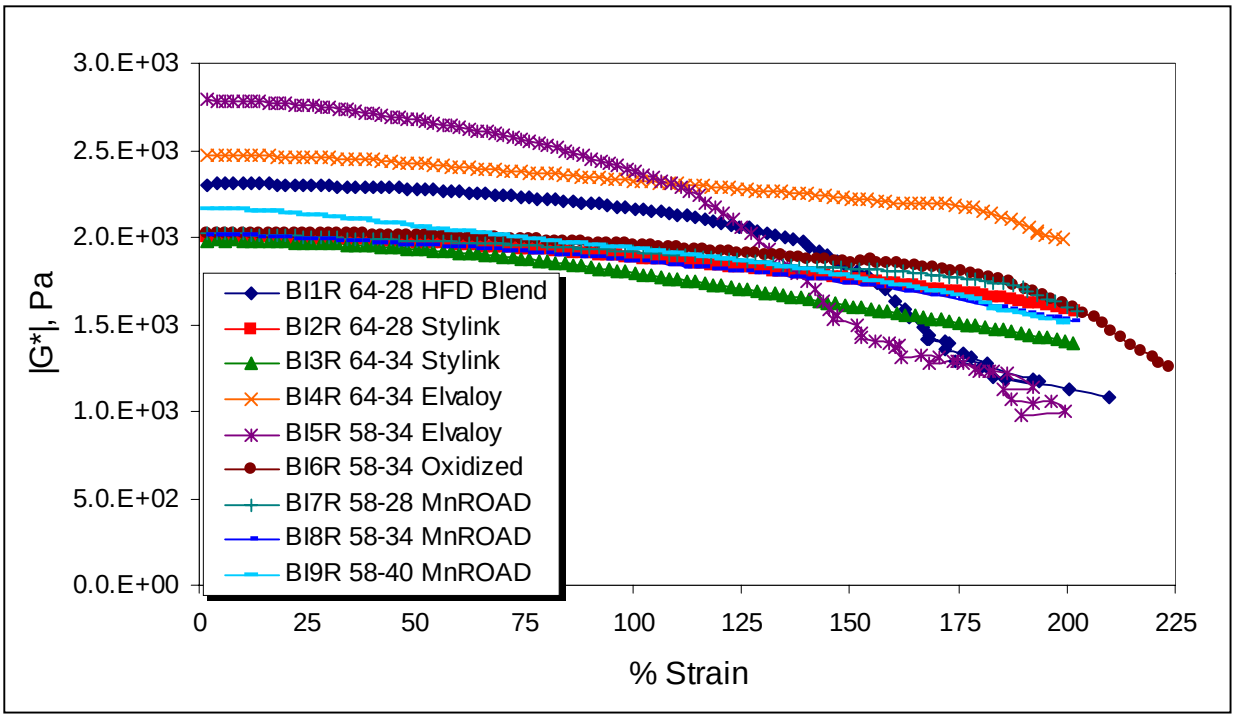

Figure 4.11 Strain Sweep Results (RTFOT, High Temperature)

Figures 4.12 and 4.13 show the strain results for PAV aged binders at high temperatures and 34°C, respectively. In both cases, the modulus drops off more sharply than that of the RTFOT aged binders. As the stiffness of the binders increase, they are less capable of resisting shear loads at high strains.

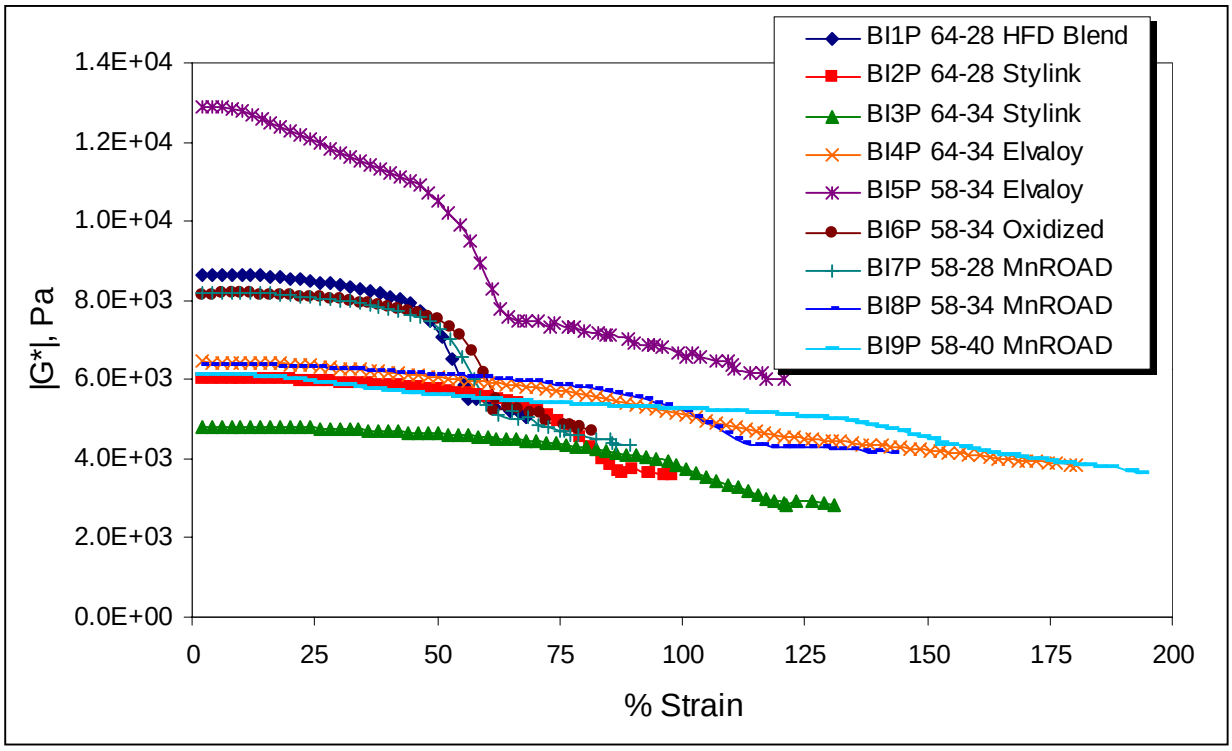

Figure 4.12 Strain Sweep Results (PAV, High Temperature)

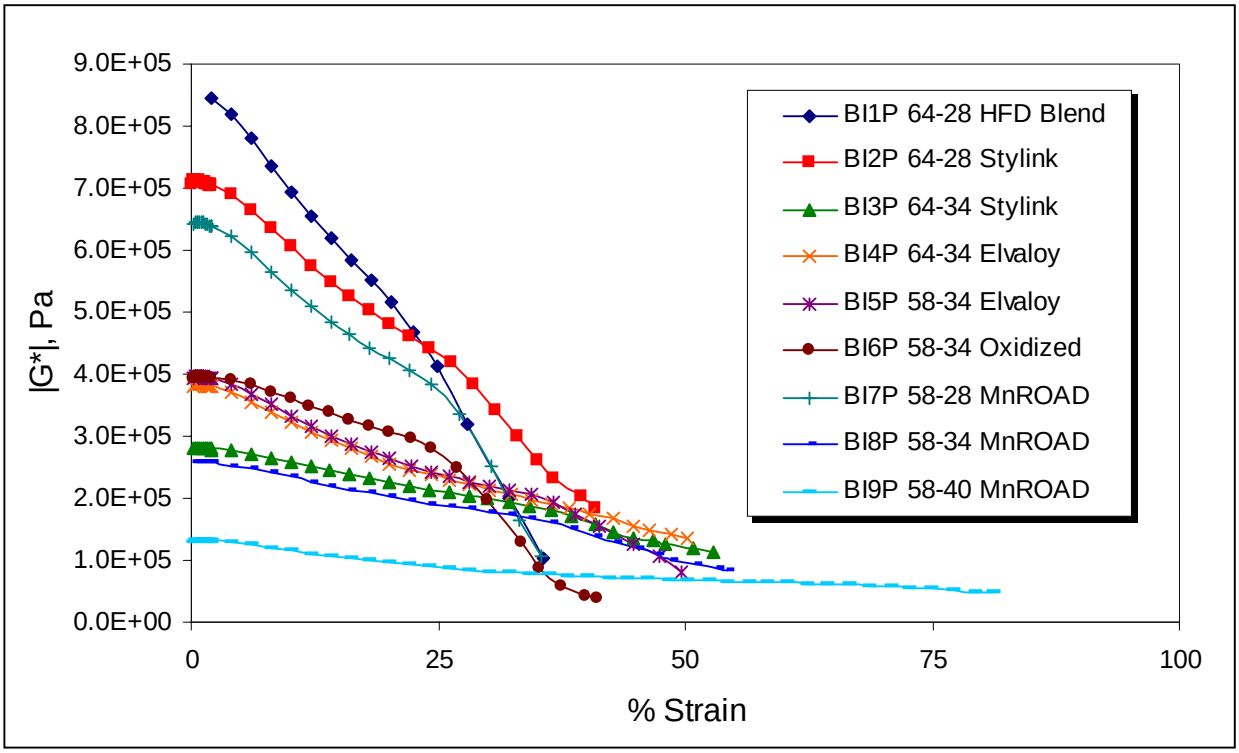

Figure 4.13 Strain Sweep Results (PAV, 34°C)

Fatigue

A qualification should be made before further discussion of the fatigue data. In many of the fatigue tests that were run it was observed after the test that the asphalt had debonded from the bottom plate in the DSR. This was especially true of the tests run at 750 kPa. Therefore it was likely the bond strength between the binder and the DSR plate or the compliance of the parallel plates that was being tested and not the true fatigue behavior of the asphalt. Care was taken to ensure a good bond before the test was started, but to no avail. Nevertheless, the analyses proceeded as if the binders failed under true fatigue.

The fatigue data was processed according to the method set forth by Bonnetti et al [18]. The dissipated energy ratio (DER) was calculated as a function of the number of loading cycles from the selected initial energy, loading rate, and temperature during the fatigue test. A model was fit to the DER up to the maximum value before it dropped off. The number of cycles to failure, N_p, was then determined for each binder. The N_{p10} and N_{p20} (numbers of loading cycles at which the DER deviated from the equality line R = N by 10% and 20%, respectively) were also determined. A typical plot of the DER is shown in Figure 4.14, along with the model parameters for that binder. The DER plots for each binder are shown in Appendix D.

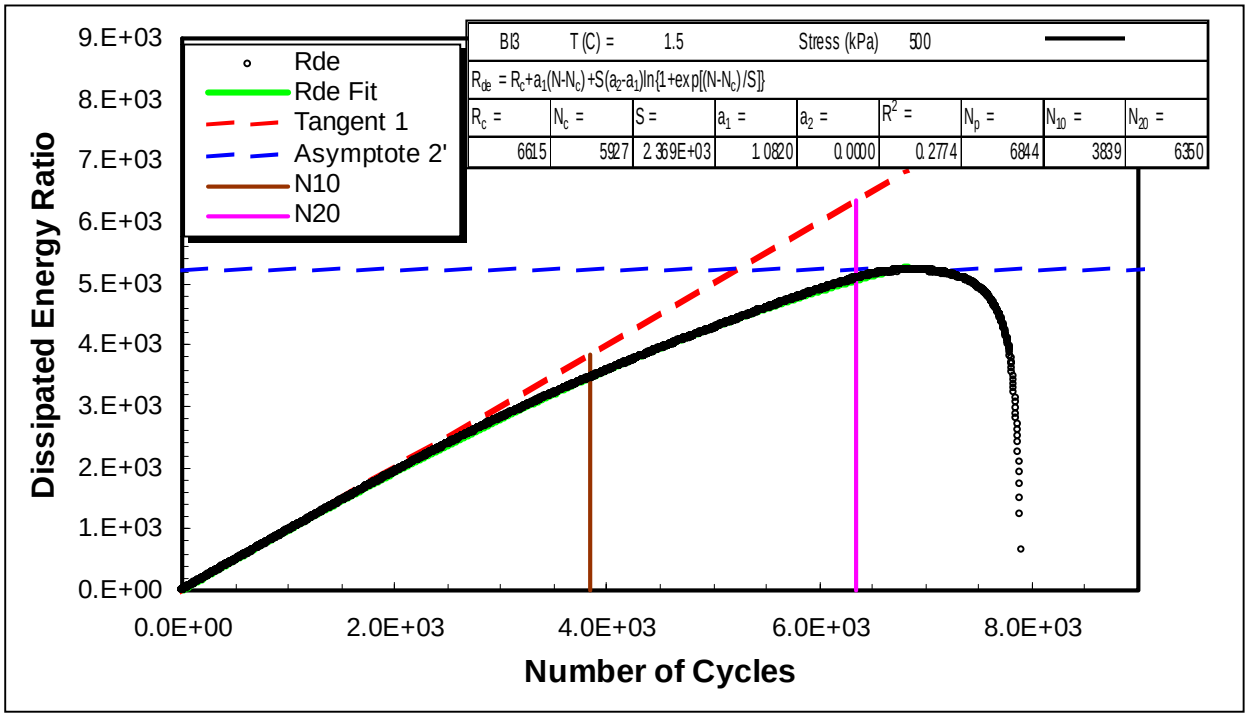

Figure 4.14 Typical Dissipated Energy Ratio (DER) Plot

The model fitting parameters for all of the binders are shown in Table 4.7. N_p or N_{p20} are commonly used to define the fatigue life of the asphalt binders. Binder 1 had the lowest fatigue life, while binders 4 and 6 also had low fatigue lives. Binders 3 and 5 performed the best in terms of fatigue. During the testing it was apparent that the stress level influenced the fatigue life of the binders. Some binders did not fail when they were tested at 500 kPa, but they failed quickly when the stress was raised to 750 kPa. There was also the problem of bond failure that was mentioned previously.

Table 4.7 DER Model Fitting Parameters

Asphalt ID	Temp, °C	σ_o, kPa	Rc	Nc	S	a1	a2	R2	Np	N10	N20	Np2
BI1	9.2	750	432.5	383.3	158.9	1.090	0	0.134	410	250	396	432
BI2	9.2	500	7853.8	6118.9	3509.6	1.175	0	0.416	5403	3935	5516	7854
BI3	1.5	500	6614.6	5926.8	2369.4	1.082	0	0.277	6844	3839	6350	6615
BI4	2.1	500	1281.8	1151.8	455.9	1.080	0	0.284	1465	843	1226	1282
BI5	1.8	750	5821.1	5059.2	2225.9	1.103	0	1.000	6161	2663	5442	5821
BI6	3.1	750	822.8	818.9	148.9	1.004	0	0.284	1210	829	934	823
BI7	8.8	500	10432.9	7464.1	5043.2	1.228	0	1.000	5107	4097	8439	10433
BI8	2.5	500	5299.0	4922.9	1711.1	1.056	0	1.000	5104	4055	4966	5299
BI9	-9.0	750	4527.6	2719.8	2437.2	1.328	0	1.000	5080	815	3565	4528

Critical Cracking Temperature

Bending Beam Rheometer and Direct Tension test results were summarized according to the AASHTO specifications mentioned in Chapter 3. The parameters measured include the stiffness (S) and m-value at 60 seconds (BBR) and the stress and strain at failure (DTT). Table 4.8 shows the summary data for BBR tests, and Table 4.9 shows the summary data for DTT tests. According to the AASHTO M 320 specification, all of these binders are verified at their low temperature PG grades.

Table 4.8 BBR Test Results

	Asphalt	Grade	Source	T, °C	S(60), MPa	m(60)
RTFOT	BI1	64-28 HFD Blend	Koch	-18	143.0	0.359
				-24	391.5	0.301
	BI2	64-28 Stylink	Koch	-18	164.0	0.377
				-24	364.5	0.295
	BI3	64-34 Stylink	Koch	-24	163.0	0.385
				-30	344.0	0.283
	BI4	64-34 Elvaloy	MIF	-24	162.0	0.374
				-30	367.0	0.298
	BI5	58-34 Elvaloy	Murphy	-24	174.5	0.404
				-30	461.0	0.310
	BI6	58-34 Oxidized	Husky	-24	193.0	0.376
				-30	464.0	0.284
	BI7	58-28 MnROAD	Koch	-18	155.0	0.392
				-24	358.0	0.299
	BI8	58-34 MnROAD	Koch	-24	190.5	0.372
				-30	437.5	0.275
	BI9	58-40 MnROAD	Koch	-30	94.0	0.388
				-36	265.5	0.322
PAV	BI1	64-28 HFD Blend	Koch	-18	194.0	0.322
				-24	458.5	0.252
	BI2	64-28 Stylink	Koch	-18	211.0	0.318
				-24	462.0	0.259
	BI3	64-34 Stylink	Koch	-24	186.0	0.349
				-30	409.0	0.272
	BI4	64-34 Elvaloy	MIF	-24	244.0	0.317
				-30	461.5	0.261
	BI5	58-34 Elvaloy	Murphy	-24	249.0	0.330
				-30	489.0	0.264
	BI6	58-34 Oxidized	Husky	-24	248.5	0.312
				-30	530.5	0.248
	BI7	58-28 MnROAD	Koch	-18	197.5	0.320
				-24	468.5	0.253
	BI8	58-34 MnROAD	Koch	-24	268.5	0.315
				-30	487.5	0.205
	BI9	58-40 MnROAD	Koch	-30	154.0	0.331
				-36	306.5	0.283

Table 4.9 DTT Test Results

	Asphalt	Grade	Source	T, °C	Failure Stress MPa	Failure Strain %
RTFOT	BI1	64-28 HFD Blend	Koch	-18	4.28	3.65
				-24		0.30
	BI2	64-28 Stylink	Koch	-18	3.79	2.09
				-24	2.18	0.51
	BI3	64-34 Stylink	Koch	-24	4.60	4.60
				-27	4.43	2.15
	BI4	64-34 Evaloy	MIF	-24	3.99	2.40
				-26.8	5.27	1.77
	BI5	58-34 Evaloy	Murphy	-24	3.79	2.46
				-28.5	4.45	1.00
	BI6	58-34 Oxidized	Husky	-24	2.64	1.57
				-28.5	3.09	0.66
	BI7	58-28 MnROAD	Koch	-18		
				-24		
	BI8	58-34 MnROAD	Koch	-24		
				-30		
	BI9	58-40 MnROAD	Koch	-30		
				-36		
PAV	BI1	64-28 HFD Blend	Koch	-18	3.22	1.28
				-24	5.43	1.02
	BI2	64-28 Stylink	Koch	-18	4.41	1.82
				-24	4.21	0.72
	BI3	64-34 Stylink	Koch	-24	4.89	4.02
				-28.9	4.09	1.37
	BI4	64-34 Evaloy	MIF	-24	5.02	2.14
				-28.8	4.42	0.95
	BI5	58-34 Evaloy	Murphy	-24	4.71	1.98
				-28.9	3.52	0.65
	BI6	58-34 Oxidized	Husky	-24	3.76	1.15
				-28.5	3.65	0.87
	BI7	58-28 MnROAD	Koch	-18	2.85	0.82
				-24	3.13	0.43
	BI8	58-34 MnROAD	Koch	-24	4.03	1.11
				-30	3.83	0.44
	BI9	58-40 MnROAD	Koch	-30	4.70	3.21
				-36	6.43	1.33

The BBR and DTT test results were analyzed to calculate the critical cracking temperature (T_{cr}) according to the procedure explained in Chapter 2. The thermal stress for each binder was calculated using BBR data in a sophisticated spreadsheet. The tensile strength data from the DTT test was plotted on the same graph. The point of intersection is defined as the

critical cracking temperature. A typical graph showing thermal stress and strength curves is shown in Figure 4.15. The pavement constants (PC = 18 and PC = 24) are factors by which the binder thermal stresses are multiplied to empirically arrive at the mixture thermal stresses.

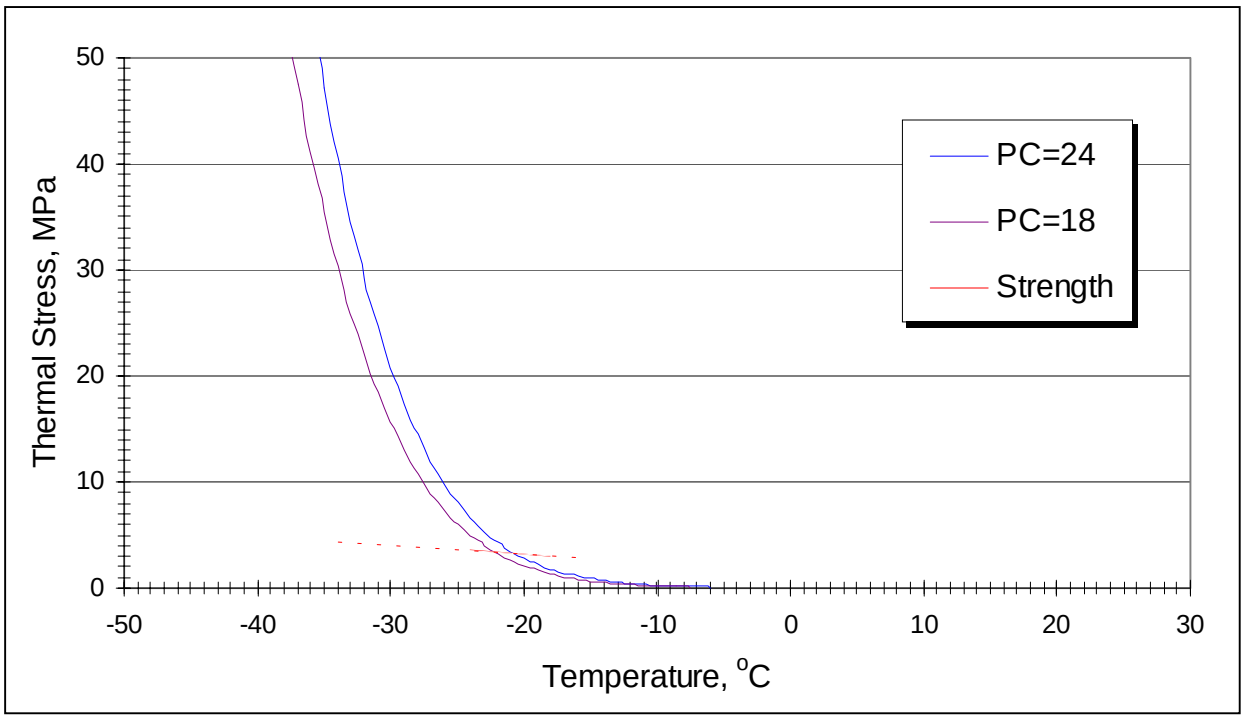

Figure 4.15 Typical Critical Cracking Temperature Plot

Table 4.10 shows the limiting low temperature for each binder from a number of different methods. The first two are limiting conditions from the Bending Beam Rheometer: 10°C below the temperature at which the stiffness at 60 seconds equals 300 MPa and at which the m-value equals 0.300. The next limit is 10°C below the temperature at which the Direct Tension failure strain is 1.0%. The final two limits are the critical cracking temperatures using both BBR and DTT data and pavement constants of 18 and 24. The five methods to determine critical cracking temperature yield similar results for most binders. The variation of T_{cr} values for a given binder is typically within 15 percent.

Table 4.10 Critical Cracking Temperatures

	Asphalt	S=300 MPa	*m*=0.300	ε_f=1%	PC=24	PC=18
RTFOT	BI1	-32.4	-34.1	-31.1	-31.0	-32.5
	BI2	-32.5	-33.6	-31.1	-26.9	-27.5
	BI3	-38.9	-39.0	-40.0	-37.5	-38.9
	BI4	-38.5	-39.8	-42.1	-38.5	-40.1
	BI5	-37.3	-40.6	-38.5	-38.9	-40.0
	BI6	-37.0	-39.0	-36.3	-34.9	-36.8
	BI7	-32.7	-33.9			
	BI8	-37.3	-38.4			
	BI9	-46.7	-48.0			
PAV	BI1	-31.0	-29.9	-34.5	-32.2	-34.9
	BI2	-30.7	-29.8	-31.9	-29.8	-27.9
	BI3	-37.6	-37.8	-40.3	-34.2	-35.5
	BI4	-35.9	-35.8	-38.5	-35.8	-34.1
	BI5	-35.7	-36.7	-37.0	-33.2	-32.2
	BI6	-35.5	-35.1	-36.3	-34.7	-32.0
	BI7	-30.9	-29.8	-26.2	-28.1	-26.5
	BI8	-35.1	-34.8	-34.7	-36.8	-35.0
	BI9	-45.8	-43.8	-48.0	-39.7	

Rutting Potential of the Three MnROAD Asphalt Binders

A recent survey performed at MnROAD facility showed that for the three Superpave cells 33, 34, and 35, the rutting behavior was different although the binders in these cells had the same PG high temperature limit of 58°C. The PG 58-40 showed higher rutting than the 58-34 and 58-28. The results obtained in the current research effort show that most likely the three binders mentioned above have different rutting resistance.

First, a visual inspection of figures 4.16 and 4.17 that show the |G*| at 10 rad/s versus temperature master curves, for both the RTFOT residue and the PAV residue, indicates that the temperature susceptibility of the three binders is quite different: the PG -40 is less temperature susceptible than the other two and as a consequence remains “softer” than the -34 and -28 in the temperature range corresponding to rutting accumulation (from 58°C down to the twenties). Taking into consideration that rutting occurs over a range of temperatures rather than at one particular temperature it becomes apparent that the -40 binder will rut more than the other two binders. The same trend is observed in Figure 4.18 which shows the zero shear viscosity versus temperature for the RTFOT residue of the three asphalt binders.

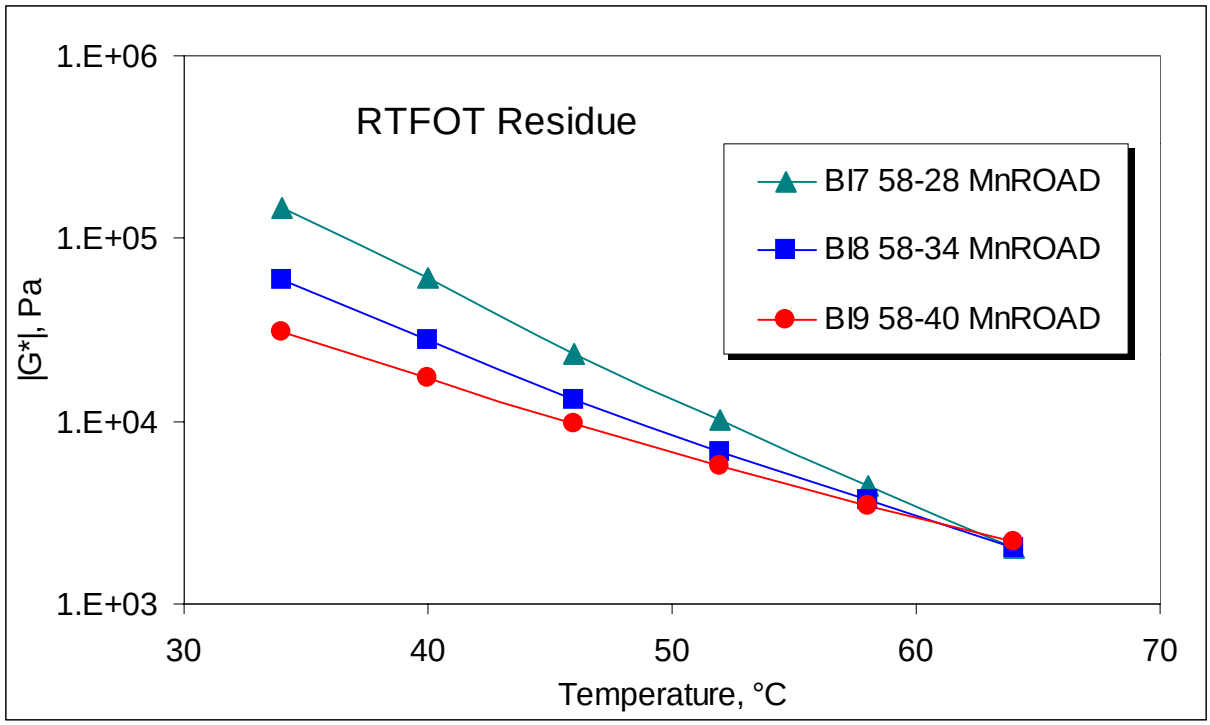

Figure 4.16 |G*| vs. Temperature @ 10 rad/s – MnROAD Binders (RTFOT)

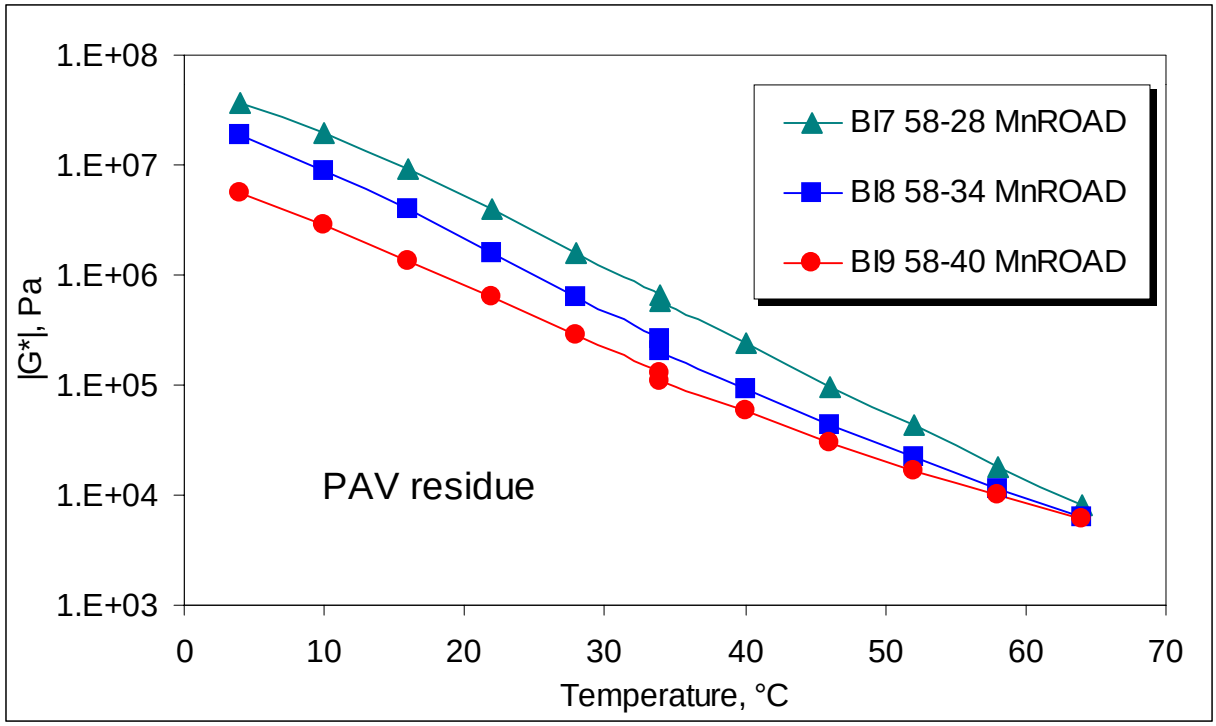

Figure 4.17 |G*| vs. Temperature @ 10 rad/s – MnROAD Binders (PAV)

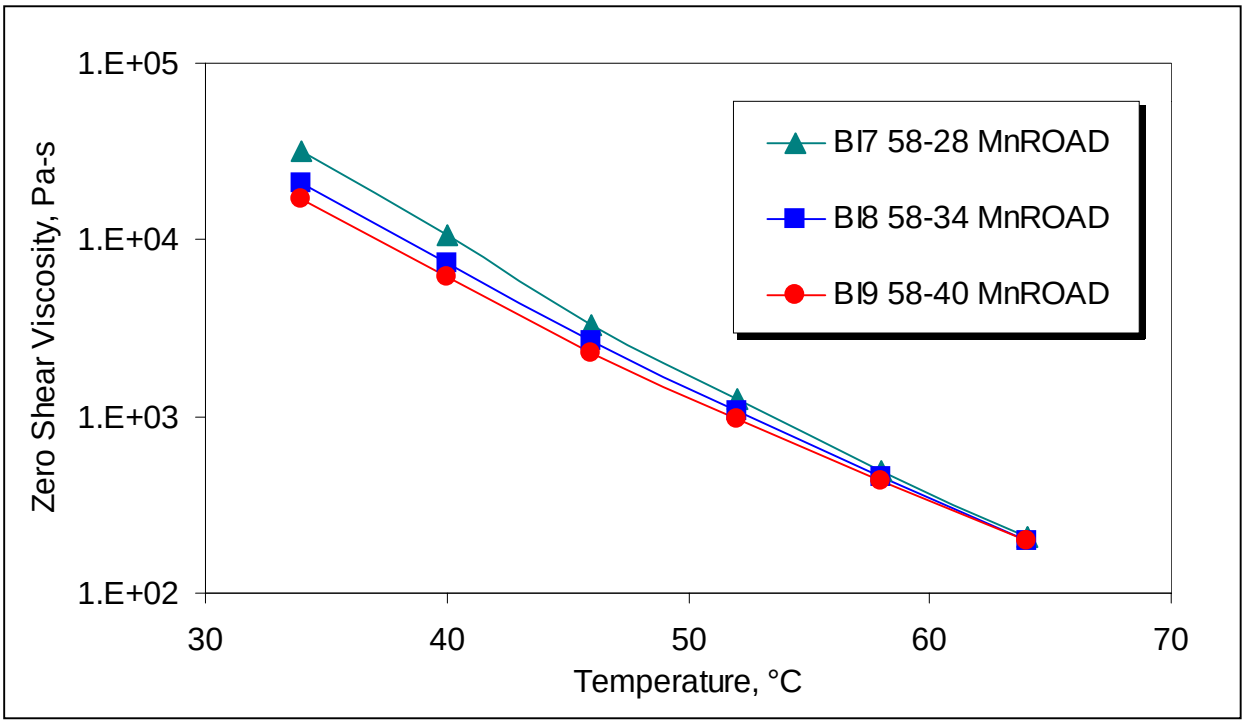

Figure 4.18 Zero Shear Viscosity vs. Temperature – MnROAD Binders (RTFOT)

Second, the plots of |G*| at 10 rad/s versus strain at 64°C, as shown in Figure 4.19, indicate that the PG -40 binder is more strain susceptible than the other two binders. This means that at higher strains this binder performs worse than the other two. At this time it is not clear if the strains observed in the binder film in the pavement are similar to the strains used in laboratory experiments that obey linear viscoelastic conditions. Previous studies by Bahia indicated that the strain levels in the binder film can exceed a few hundred percent at warmer temperatures. It appears that this limited result also indicates that the PG 58-40 will perform worse in rutting than the other two binders.

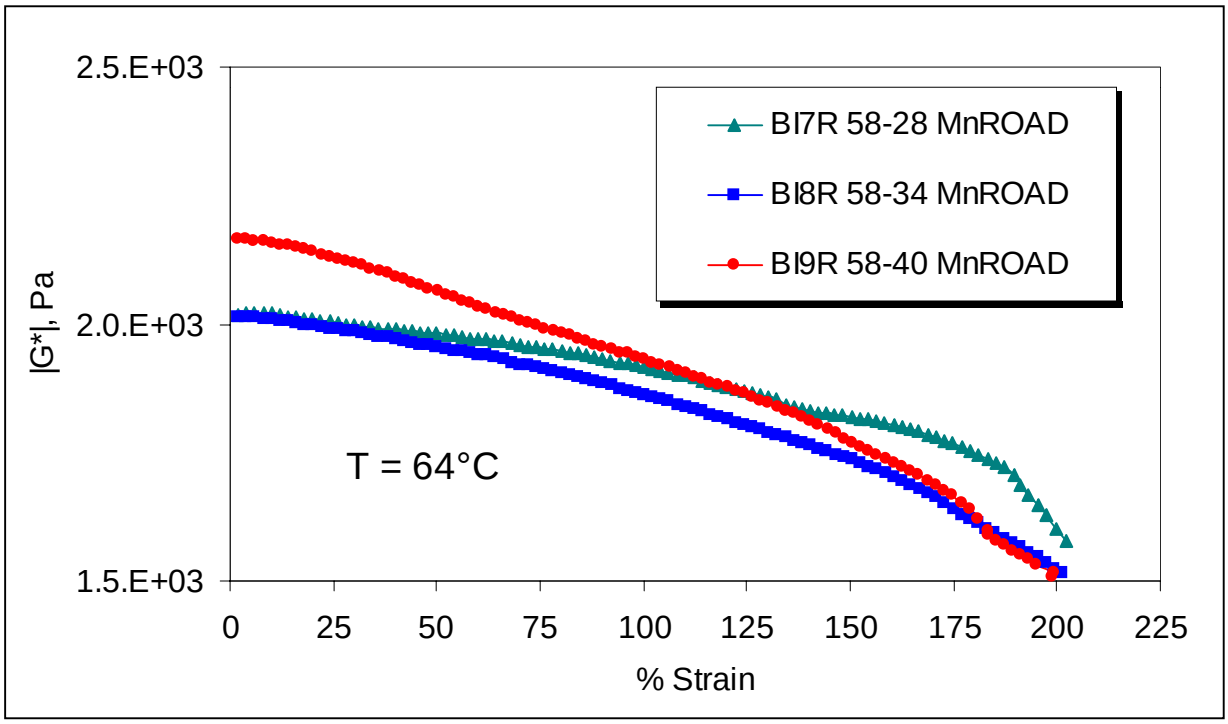

Figure 4.19 Strain Sweeps – MnROAD Binders (RTFOT)

Summary

A number of laboratory tests have been performed on the nine asphalt binders used in this project in various aging conditions. These tests are an indication of specification tests that may be proposed in the future. The aim of this project was not so much to exhaustively analyze the binders in terms of their relative performance to one another, but to simply understand how to perform the tests and then catalogue the data in a database for future reference.

CHAPTER 5:
DATABASE DESCRIPTION

Introduction

A simple database was constructed to store all of the test data from this project. The database was constructed in Microsoft Access®, which is easy to use and readily available to most users.

Database Structure

Information from each binder test was imported into an Access® table. Every table contained the asphalt ID, a description including the PG grade, and the aging condition when tested. The tables were first created in Microsoft Excel® and then imported into Access®. The only drawback to this system was that the tables were manually input into the database, and the data files needed some processing before their entry. However, the data that was obtained in this project was easily imported into the database without much trouble.

This database is quite flexible. It is possible to add more tables to the database if additional tests are performed on the binders in the future. It is also possible to append data at the end of each table if tests are performed on additional binders. Table 5.1 lists the tables that are contained in the Access® database. Tables 5.2 through 5.13 contain the column labels in each of the Access® tables.

Table 5.1 List of Tables in Database

- BBR Header
- BBR Test Results
- CAM Model Parameters
- Fatigue
- Fatigue Model
- Frequency Sweeps – Original
- Frequency Sweeps – PAV
- Frequency Sweeps – RTFOT
- Repeated Creep
- Repeated Creep Model
- Strain Sweeps
- Zero Shear Viscosity

Table 5.2 BBR Header Columns

• asphalt_ID	• BBR_test_ID	• force_const_mN/bit
• description	• target_temp_C	• defl_const_micrometer/bit
• condition	• min_temp_C	• cmpl_micrometer/N
• operator	• max_temp_C	• cal_date
• specimen	• soak_time_min	• a
• time	• conf_test_Gpa	• b
• date	• conf_test_date	• c

Table 5.2 gives basic information about the sample being tested, testing parameters, and calibration data. The terms a, b, and c are fit in the BBR software to the stiffness vs. time data.

Table 5.3 BBR Test Results Columns

• asphalt_ID	• time_s	• estimated_S_Mpa
• description	• force_mN	• %_Difference
• condition	• deflection_mm	• m
• BBR_test_ID	• measured_S_Mpa	

Table 5.3 gives the BBR test data at selected time intervals.

Table 5.4 CAM Model Parameters Columns

• asphalt_ID	• a4	• a46
• description	• a10	• a52
• condition	• a16	• a58
• crossover_frequency_rad/s	• a22	• a64
• q	• a28	• a70
• v	• a34	
• w	• a40	

Table 5.4 shows the parameters fit with the CAM model to DSR frequency sweep data (see the discussion of rheological master curves in Chapter 2). The parameter q is simply the log of the crossover frequency, ω_c. The shift factors (a4, a10, a16, etc.) shift the frequency at each temperature to a reduced frequency at the reference temperature.

Table 5.5 Fatigue Columns

• asphalt_ID	• freq_Hz	• torque_microN_m
• description	• G'_Pa	• strain_%
• condition	• G"_Pa	• temp_C
• operator	• |G*|_Pa	• time_sec
• test_date	• gap_micrometers	• cycle_N
• freq_rad/s	• |n*|_Pa-s	• dissipated_energy_WN
• delta_degrees	• stress_Pa	• dissipated_energy_ratio_DER

Table 5.5 shows the fatigue test data obtained during time sweep tests for each binder. The dissipated energy ratio is explained in Chapters 2 and 4.

Table 5.6 Fatigue Model Columns

• asphalt_ID	• Rc	• R2
• description	• Nc	• Np
• condition	• S	• N10
• temp_C	• a1	• N20
• sigma_0_kPa	• a2	• Np2

Table 5.6 contains the parameters for the model fit to fatigue test data. Sigma_0 is the constant stress applied during the test, Rc is the constant dissipated energy ratio, Nc is the constant number of loading cycles, S is the shape parameter, a1 is the slope of the lower asymptote of R vs. N, a2 is the slope of the upper asymptote of R vs. N, and R2 (R^2) is the goodness of fit between the model and the actual data. Np, N10, N20, and Np2 are different measures of the number of cycles to failure in fatigue. For a more in-depth description of the fatigue model, see Bonnetti et al [18].

Table 5.7 Frequency Sweeps - Original Columns

• asphalt_ID	• G'_Pa	• torque_microN-m
• description	• G"_Pa	• strain_%
• condition	• |G*|_Pa	• temp_C
• operator	• |G*|sin(delta)_kPa	• time_sec
• test_date	• |G*|/sin(delta)_kPa	• diameter_mm
• freq_rad/s	• gap_micrometers	
• delta_degrees	• |n*|_Pa-s	

Tables 5.7 through 5.9 show the raw data from frequency sweep tests performed on original, PAV, and RTFOT binders, respectively.

Table 5.8 Frequency Sweeps - PAV Columns

• asphalt_ID	• G'_Pa	• torque_microN-m
• description	• G"_Pa	• strain_%
• condition	• |G*|_Pa	• temp_C
• operator	• |G*|sin(delta)_kPa	• time_sec
• test_date	• |G*|/sin(delta)_kPa	• diameter_mm
• freq_rad/s	• gap_micrometers	
• delta_degrees	• |n*|_Pa-s	

Table 5.9 Frequency Sweeps - RTFOT Columns

• asphalt_ID	• G'_Pa	• torque_microN-m
• description	• G"_Pa	• strain_%
• condition	• |G*|_Pa	• temp_C
• operator	• |G*|sin(delta)_kPa	• time_sec
• test_date	• |G*|/sin(delta)_kPa	• diameter_mm
• freq_rad/s	• gap_micrometers	
• delta_degrees	• |n*|_Pa-s	

Table 5.10 Repeated Creep Columns

• asphalt_ID	• compliance_m^2/N	• temp_C
• description	• gap_micrometers	• torque_microN-m
• condition	• time_sec	• viscosity_Pa-s
• operator	• shear_stress_Pa	• diameter_mm
• test_date	• strain_%	

Table 5.10 includes the raw data collected from repeated creep tests.

Table 5.11 Repeated Creep Model Columns

• asphalt_ID	• G_0	• R-squared
• description	• eta_0	• max_strain_test
• condition	• G_1	• max_strain_fit
• temp_C	• eta_1	• max_strain_Shenoy

Table 5.11 contains the parameters from models fit to repeated creep test data. The parameters G_0, eta_0, G_1, and eta_1 come from the Burgers model described by Bahia et al [16]. The R-squared is the goodness of fit between the Burgers model and the test data. Shenoy's model to predict the total accumulated strain is described in [25]. The last three inputs in the table are the maximum strains obtained from the test, Burgers model, and Shenoy's model.

Table 5.12 Strain Sweeps Columns

• asphalt_ID	• G'_Pa	• torque_microN-m
• description	• G"_Pa	• strain_%
• condition	• |G*|_Pa	• temp_C
• operator	• |G*|sin(delta)_kPa	• time_sec
• test_date	• |G*|/sin(delta)_kPa	• diameter_mm
• freq_rad/s	• gap_micrometers	
• delta_degrees	• |n*|_Pa-s	

Table 5.12 shows the data obtained from strain sweep tests on the binders.

Table 5.13 Zero Shear Viscosity Columns

• asphalt_ID	• temp_C	• zsv_Pa-s_G"/freq
• description	• zsv_Pa-s_CAM	• zsv_Pa-s_slope
• condition	• zsv_Pa-s_G*/freq	

Table 5.13 includes zero shear viscosity obtained by four different methods using frequency sweep test data on the RTFOT aged binders at various temperatures. These methods are described in Chapter 4.

CHAPTER 6:
CONCLUSIONS AND RECOMMENDATIONS

Conclusions

The goal of this project was not so much to exhaustively analyze the binders in terms of their relative performance to one another, but to simply understand how to perform the tests and then catalogue the data in a database for future reference. This was accomplished successfully.

The Bending Beam Rheometer (BBR) and Direct Tension Tester (DTT) were used together to determine the critical cracking temperature of the binders at low temperatures. A majority of the laboratory work in this project involved testing with the Dynamic Shear Rheometer (DSR). Frequency sweeps were performed over a range of temperatures. This data was used to generate master curves and to calculate zero shear viscosity, the latter of which is being proposed as a new high temperature performance specification. Strain sweeps verified that frequency sweep testing was performed in the linear viscoelastic range. Repeated creep tests measured the permanent strain accumulated after 100 cycles, which is also being proposed as a specification test indicative of rut resistance in asphalt pavements. Fatigue tests were performed at intermediate temperatures. The data from this test gave an indication of the fatigue cracking performance of asphalt pavements in the field.

A database was created in Microsoft Access®, which is easy to use and readily available to most users. Test results, along with some model parameters, were stored in tables inside the database. As more test results become available, the can easily be imported to the database.

Recommendations

There is always the opportunity for future research in the area of asphalt binder material characterization. Future work may include refinement of the laboratory testing and analysis methods, additional binders being tested, and newly developed tests being added to the existing database. It would also be desirable to correlate the binder tests in the laboratory with mixture performance in the field. Finally, this project intended to simply perform the laboratory tests and collect all of the results in a database. It may be worthwhile to take a closer look at the data and analyze the differences between the asphalt binders.

REFERENCES

1. Anderson, D. A., M. O. Marasteanu, C. E. Antle, and T. Ruscetti, *Relationship of SHRP Asphalt Binder Properties to Performance*, Final Report Submitted to Western Research Institute, FHWA Contract DTFH-61-92-C-00170, Nittany Engineers and Management Consultants, Inc., 1997.
2. A. Basu, *An Evaluation of the Time-Temperature Equivalence Factor and of the Physical Hardening Effects on Low-Temperature Asphalt Binder Specifications*, M.S. Thesis, University of Minnesota, 2002.
3. "Standard Practice for Determination of Low-Temperature Performance Grade (PG) of Asphalt Binders," American Association of State Highway and Transportation Officials (AASHTO) Designation PP42-01, *AASHTO Provisional Standards*, May 2002 Edition.
4. Marasteanu, M. O., and D. A. Anderson, "Establishing Linear Viscoelastic Conditions for Asphalt Binders," *Transportation Research Record 1728*, 2000, pp. 1-6.
5. Marasteanu, M. O., and D. A. Anderson, "Techniques for Determining Errors in Asphalt Binder Rheological Data," *Transportation Research Record 1766*, 2001, pp. 32-39.
6. Marasteanu, M. O., and D. Anderson, "Time-Temperature Dependency of Asphalt Binders – An Improved Model," *Journal of the Association of Asphalt Paving Technologists*, vol. 65, 1996, pp. 408-435.
7. Soleymani, H. R., H. U. Bahia, and A. T. Bergan, "Time-Temperature Dependency of Blended and Rejuvenated Asphalt Binders," *Journal of the Association of Asphalt Paving Technologists*, vol. 68, 1999, pp. 129-152.
8. Rowe, G. M., M. J. Sharrock, M. G. Bouldin, and R. N. Dongre, "Advanced Techniques to Develop Asphalt Master Curves from the Bending Beam Rheometer."
9. Rowe, G. M. and M. J. Sharrock, "Development of Standard Techniques for the Calculation of Master Curves for Linear Viscoelastic Materials," *Journal of Applied Asphalt Binder Technology*, April 2001, pp. 72-81.
10. Marasteanu, M. O., and D. A. Anderson, *Improved Model for Bitumen Rheological Characterization*, Eurobitume Workshop on Performance Related Properties for Bituminous Binders, Luxembourg, May 1999, paper no. 133.

11. Marasteanu, M. O., and D. A. Anderson, *Determination of Asphalt Binders Viscosity from Other Rheological Parameters*, Proceedings of the International Society of Asphalt Pavements, Copenhagen, Denmark, 2002.
12. Rowe, G. M., J. A. D'Angelo, and M. J. Sharrock, *Use of the Zero Shear Viscosity as a Parameter for the High Temperature Binder Specification Parameter,* 2nd International Symposium on Binder Rheology and Pavement Performance, 2002.
13. D. Sybilski, "Zero-Shear Viscosity of Bituminous Binder and Its Relation to Bituminous Mixture's Rutting Resistance," *Transportation Research Record 1535*, 1996, pp. 15-21.
14. Anderson, D. A., Y. M. Le Hir, J. P. Planche, and D. Martin, "Zero Shear Viscosity of Asphalt Binders," *Transportation Research Record 1810*, 2002, pp. 54-62.
15. Bouldin, M. G., R. Dongre, and J. D'Angelo, "Proposed Refinement of Superpave High-Temperature Specification Parameter for Performance-Graded Binders," *Transportation Research Record 1766*, 2001, pp. 40-47.
16. Bahia, H. U., H. Zhai, M. Zeng, Y. Hu, and P. Turner, "Development of Binder Specification Parameters Based on Characterization of Damage Behavior," *Journal of the Association of Asphalt Paving Technologists*, vol. 70, 2001.
17. Anderson, D. A., Y. M. Le Hir, M. O. Marasteanu, J. P. Planche, D. Martin, and G. Gauthier, "Evaluation of Fatigue Criteria for Asphalt Binders," *Transportation Research Record 1766*, 2001, pp. 48-56.
18. Bonnetti, K. S., K. Nam, and H. U. Bahia, "Measuring and Defining Fatigue Behavior of Asphalt Binders," *Transportation Research Record 1810*, 2002, pp. 33-43.
19. Hoare, T. R., and S. A. M. Hesp, "Low-Temperature Fracture Testing of Asphalt Binders: Regular and Modified Systems," *Transportation Research Record 1728*, 2000, pp. 36-42.
20. Anderson, D. A., L. Lapalu, M. O. Marasteanu, Y. M. Le Hir, J. P. Planche, and D. Martin, "Low-Temperature Thermal Cracking of Asphalt Binders as Ranked by Strength and Fracture Properties," *Transportation Research Record 1766*, 2001, pp. 1-6.
21. Lee, N. K., G. R. Morrison, and S. A. M. Hesp, "Low Temperature Fracture of Polyethylene-Modified Asphalt Binders and Asphalt Concrete Mixes," *Journal of the Association of Asphalt Paving Technologists*, vol. 64, 1995, pp. 534-574.

22. Roy, S. D., and S. A. M. Hesp, "Low-Temperature Binder Specification Development: Thermal Stress Restrained Specimen Testing of Asphalt Binders and Mixtures," *Transportation Research Record 1766*, 2001, pp. 7-14.
23. Reinke, G. H., and S. L. Engber, "Impact of Factors Affecting Determination of Glass Transition Temperature Using a Dynamic Shear Rheometer," *Journal of the Association of Asphalt Paving Technologists*, vol. 70, 2001.
24. Anderson, D. A., and M. O. Marasteanu, "Physical Hardening of Asphalt Binders Relative to Their Glass Transition Temperatures," *Transportation Research Record 1661*, 1999, pp. 27-34.
25. Shenoy, A., "Refinement of the Superpave Specification Parameter for Performance Grading of Asphalt," *Journal of Transportation Engineering*, September/October 2001, pp. 357-362.

Appendix A:

Master Curves

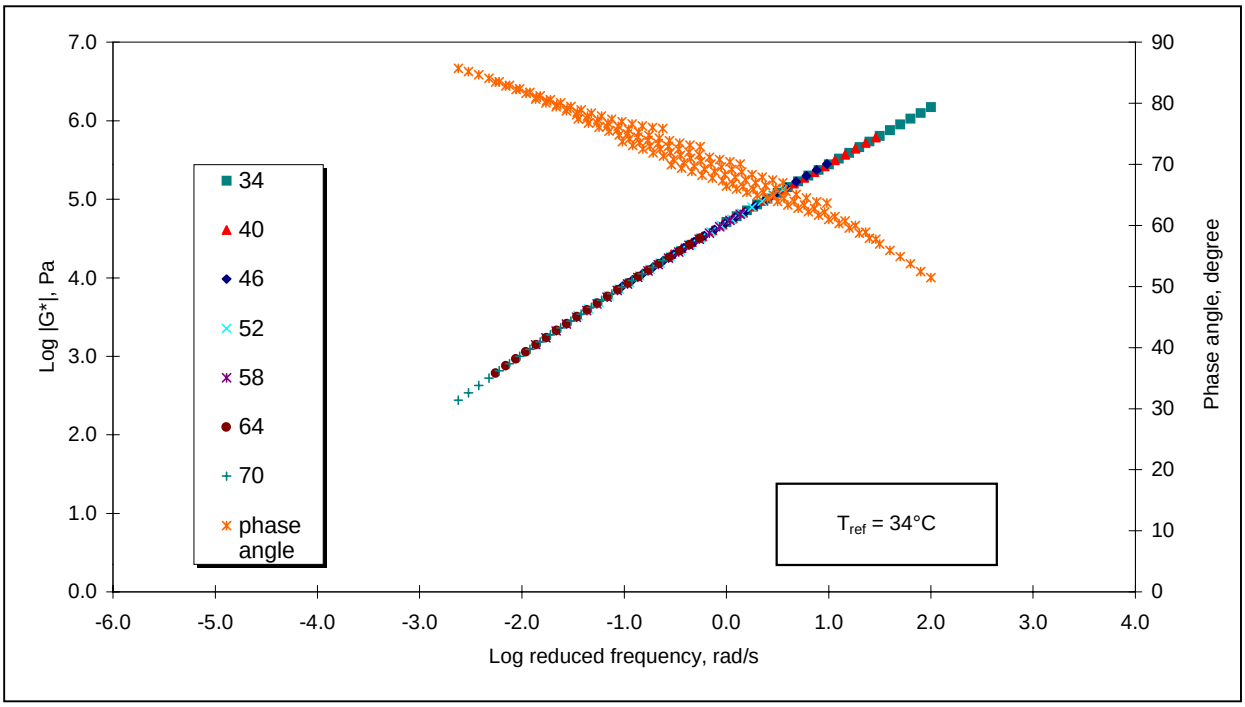

Figure A.1 Master Curve – Binder 1, RTFOT

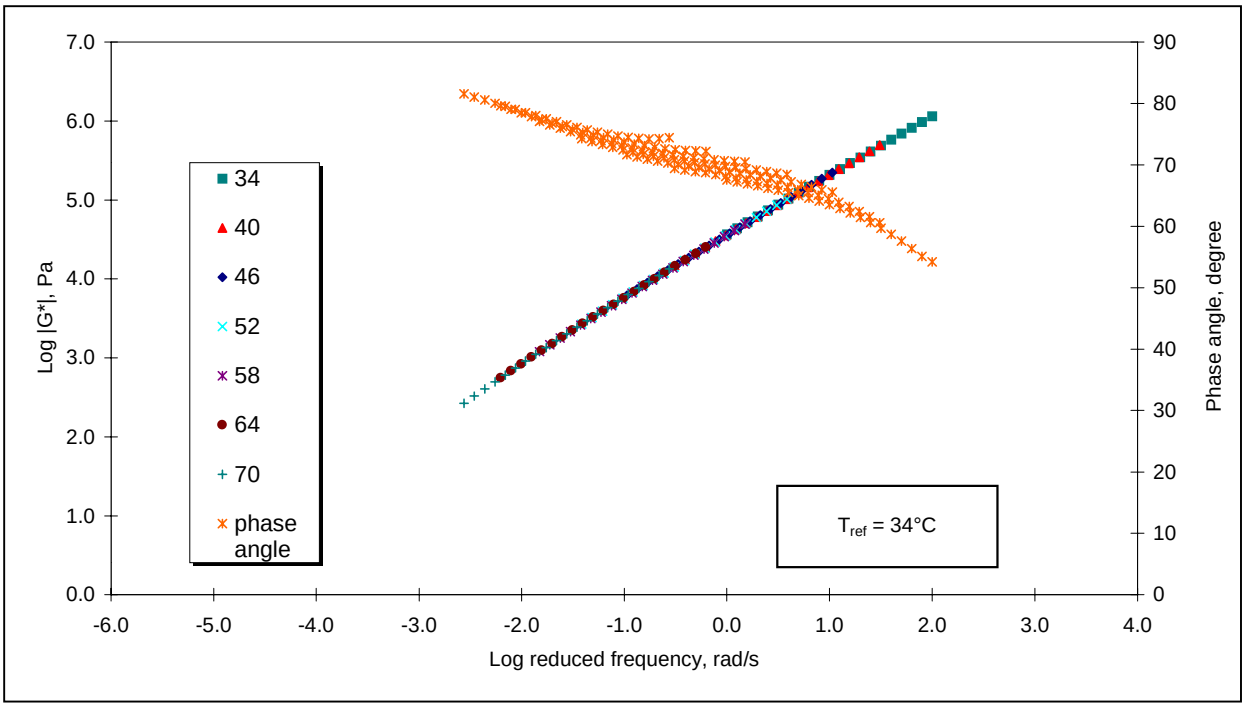

Figure A.2 Master Curve – Binder 2, RTFOT

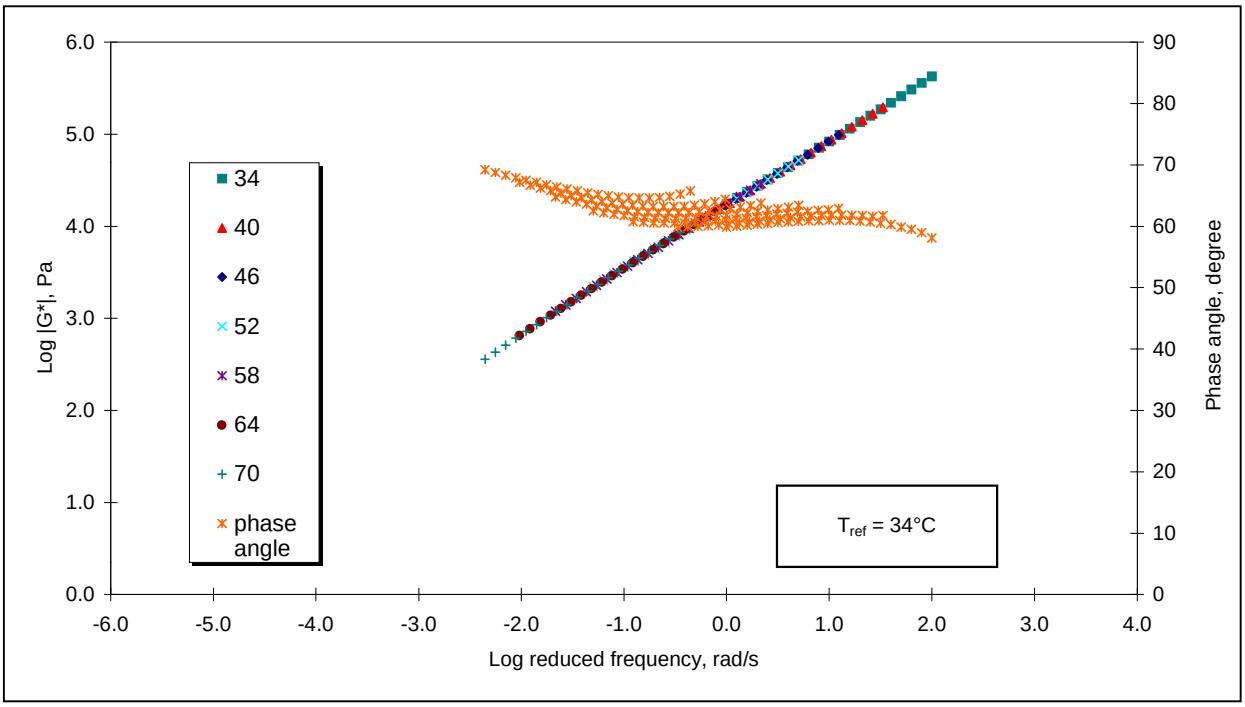

Figure A.3 Master Curve – Binder 3, RTFOT

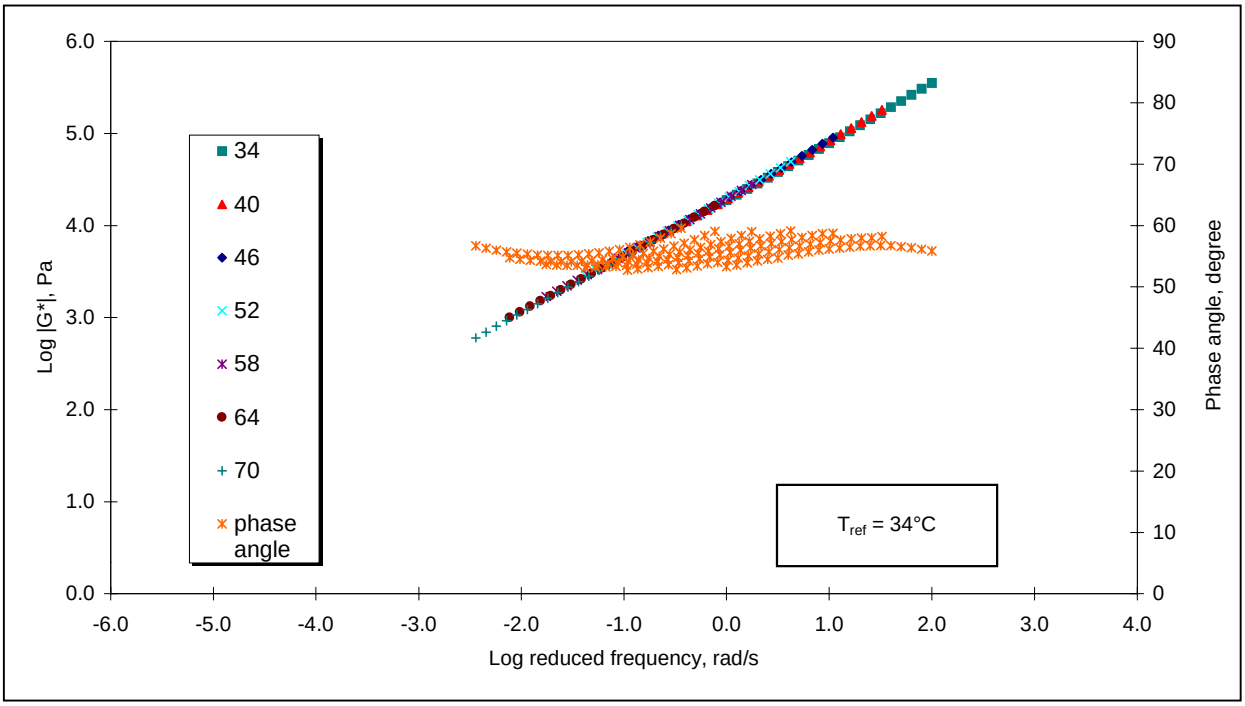

Figure A.4 Master Curve – Binder 4, RTFOT

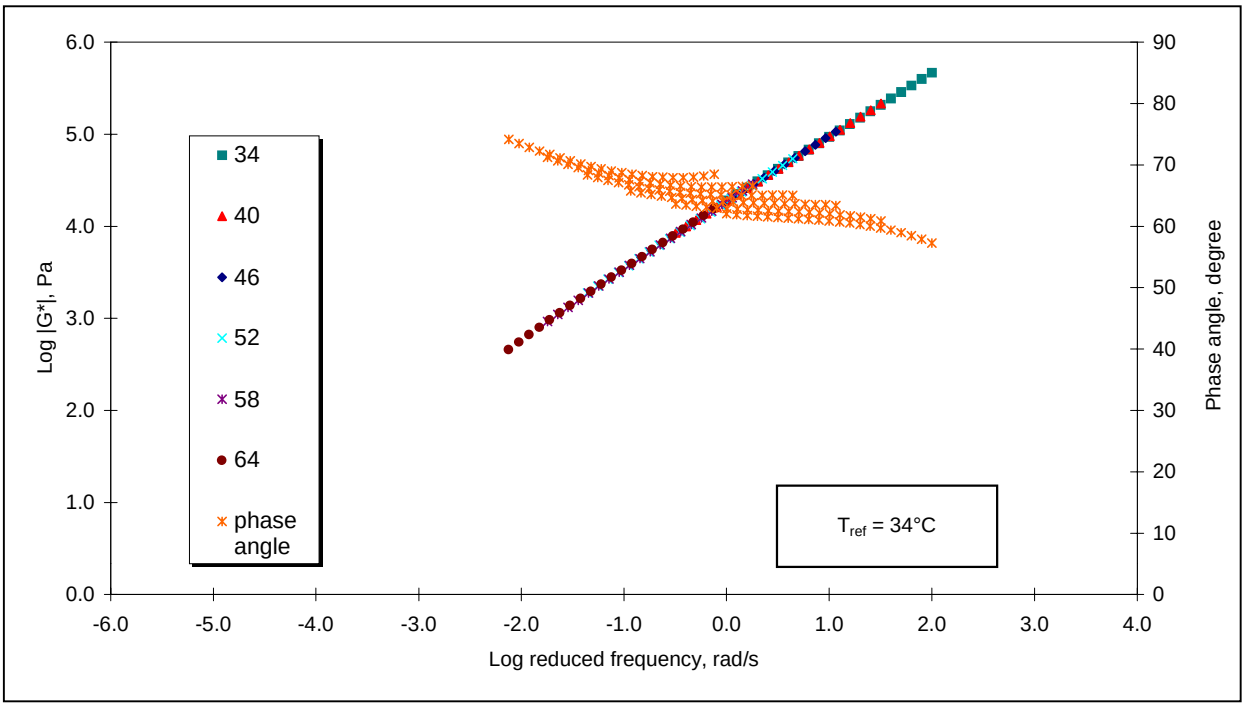

Figure A.5 Master Curve – Binder 5, RTFOT

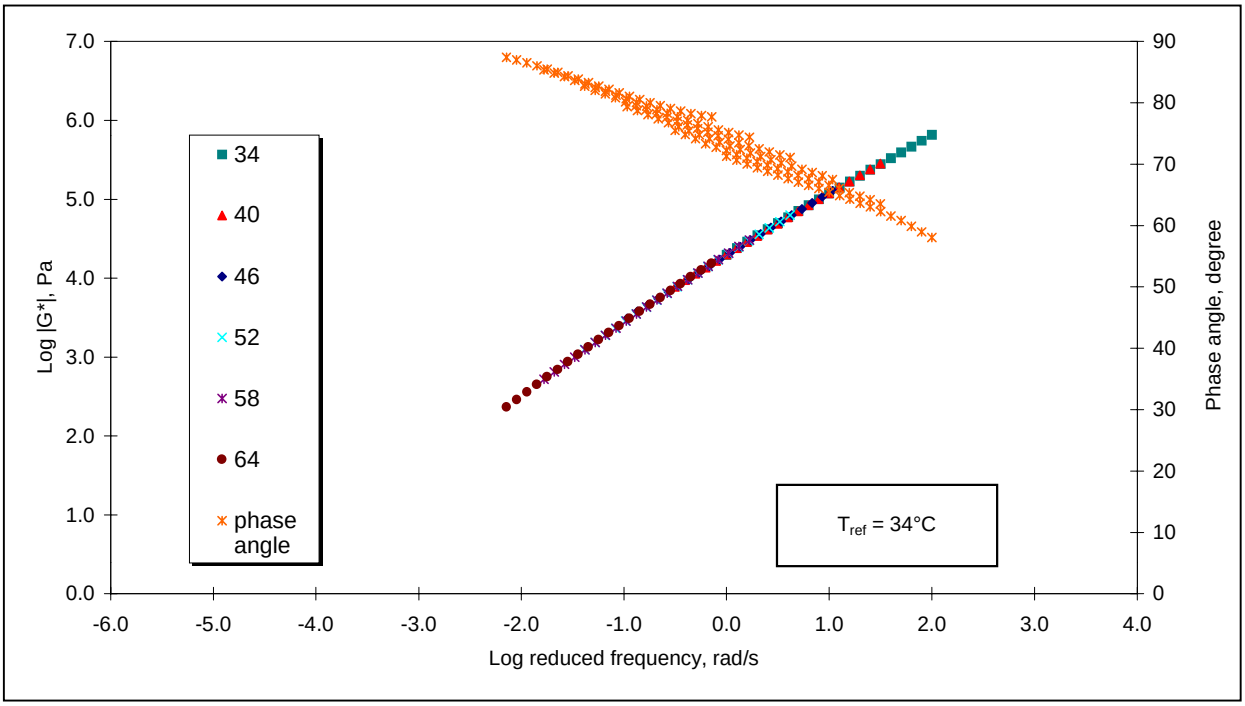

Figure A.6 Master Curve – Binder 6, RTFOT

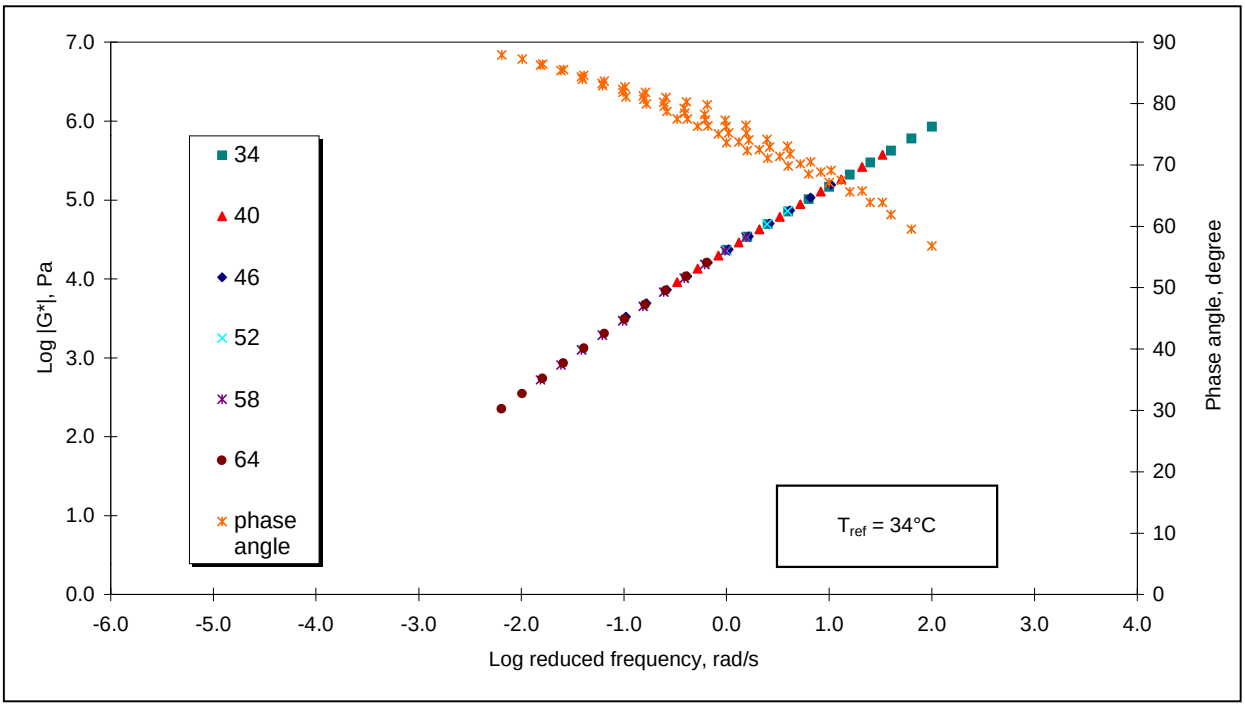

Figure A.7 Master Curve – Binder 7, RTFOT

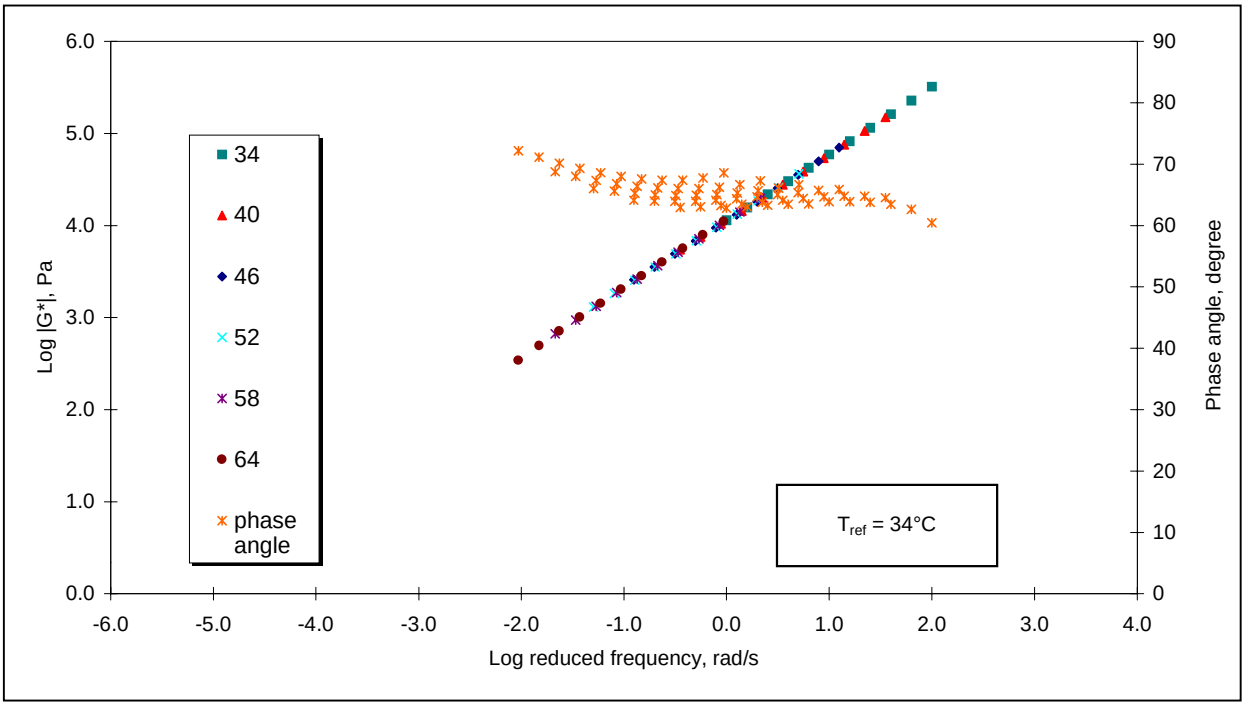

Figure A.8 Master Curve – Binder 8, RTFOT

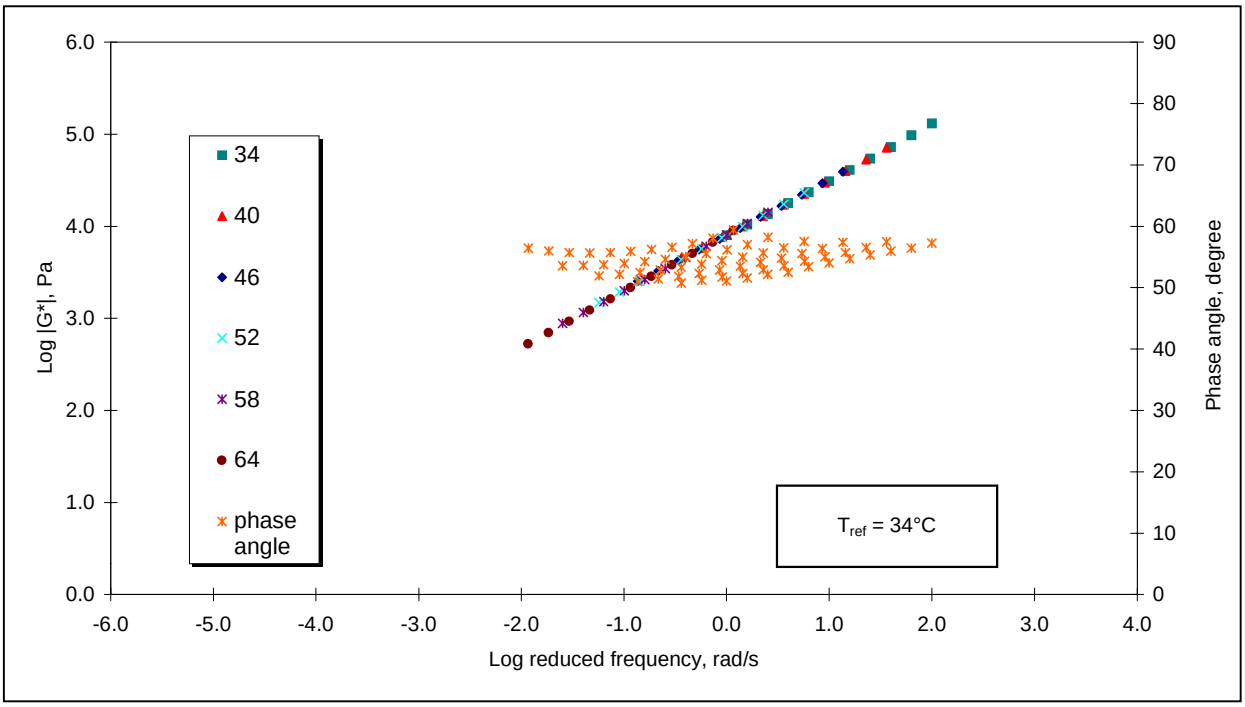

Figure A.9 Master Curve – Binder 9, RTFOT

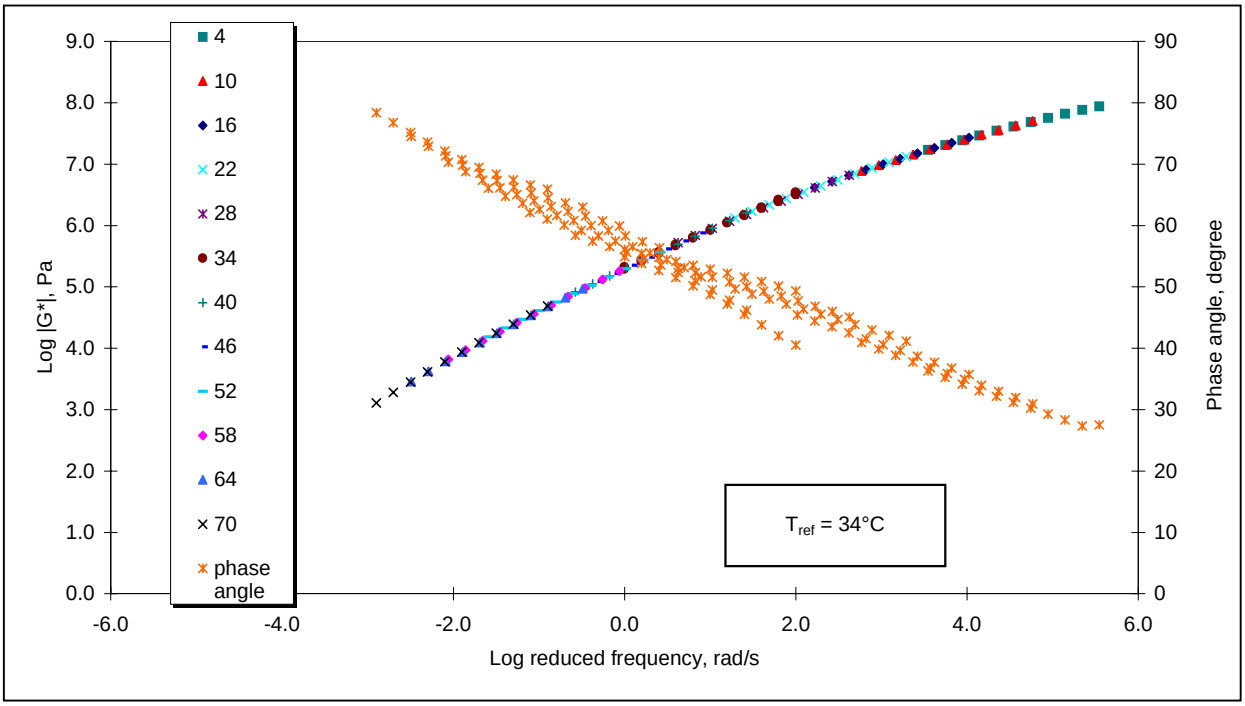

Figure A.10 Master Curve – Binder 1, PAV

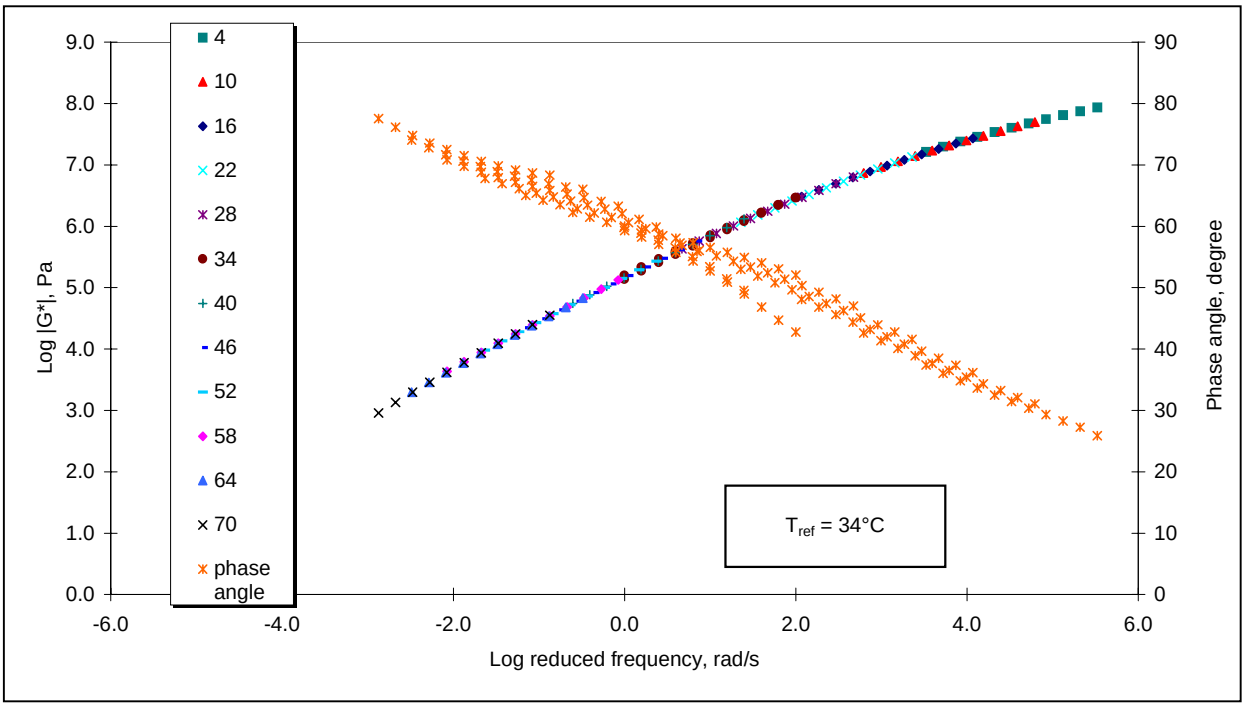

Figure A.11 Master Curve – Binder 2, PAV

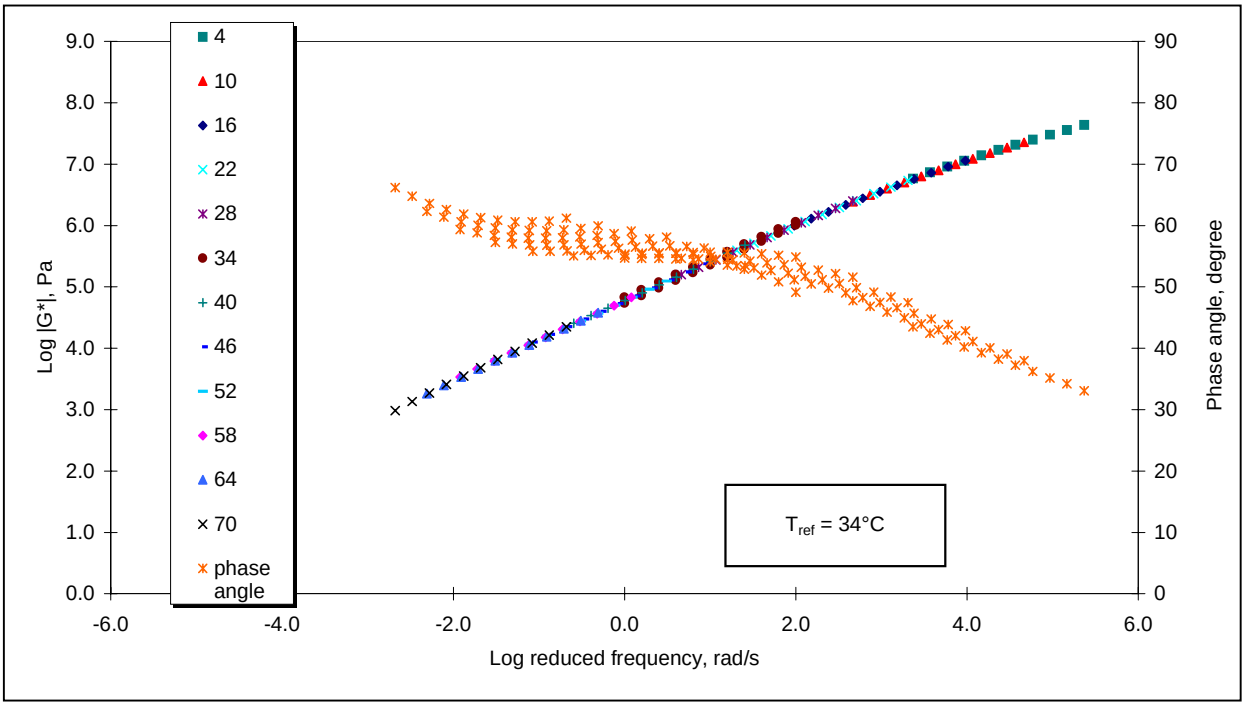

Figure A.12 Master Curve – Binder 3, PAV

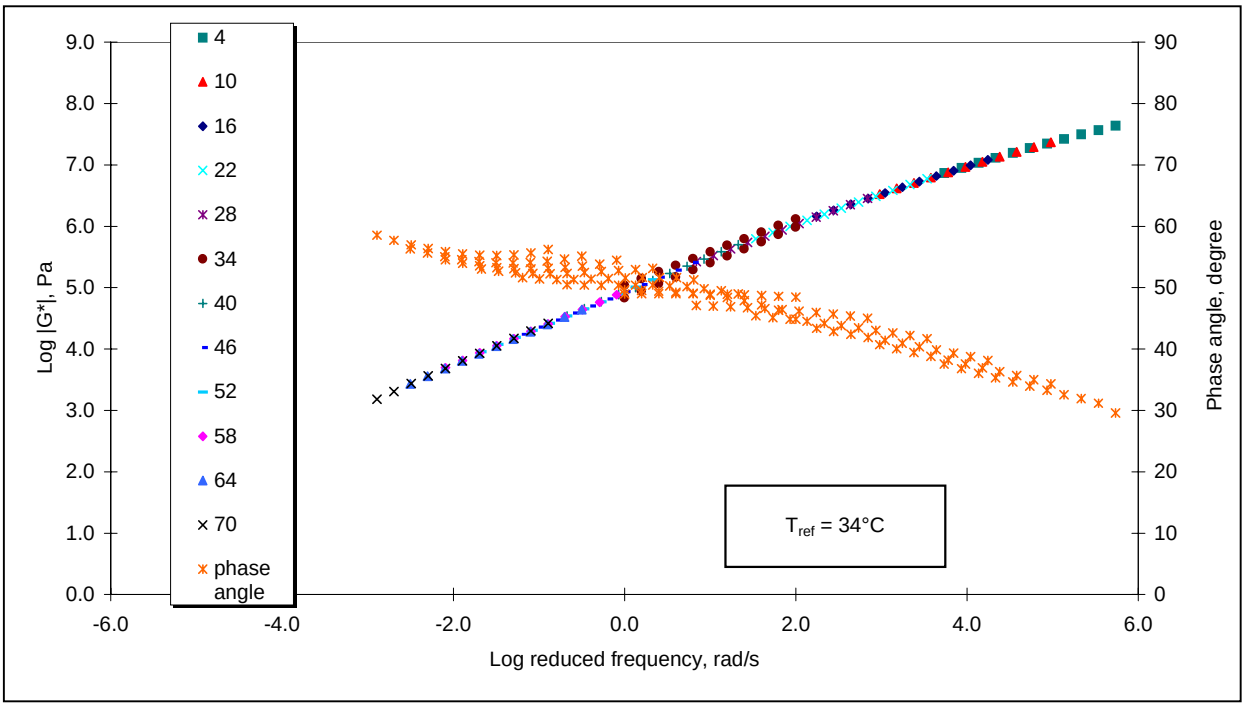

Figure A.13 Master Curve – Binder 4, PAV

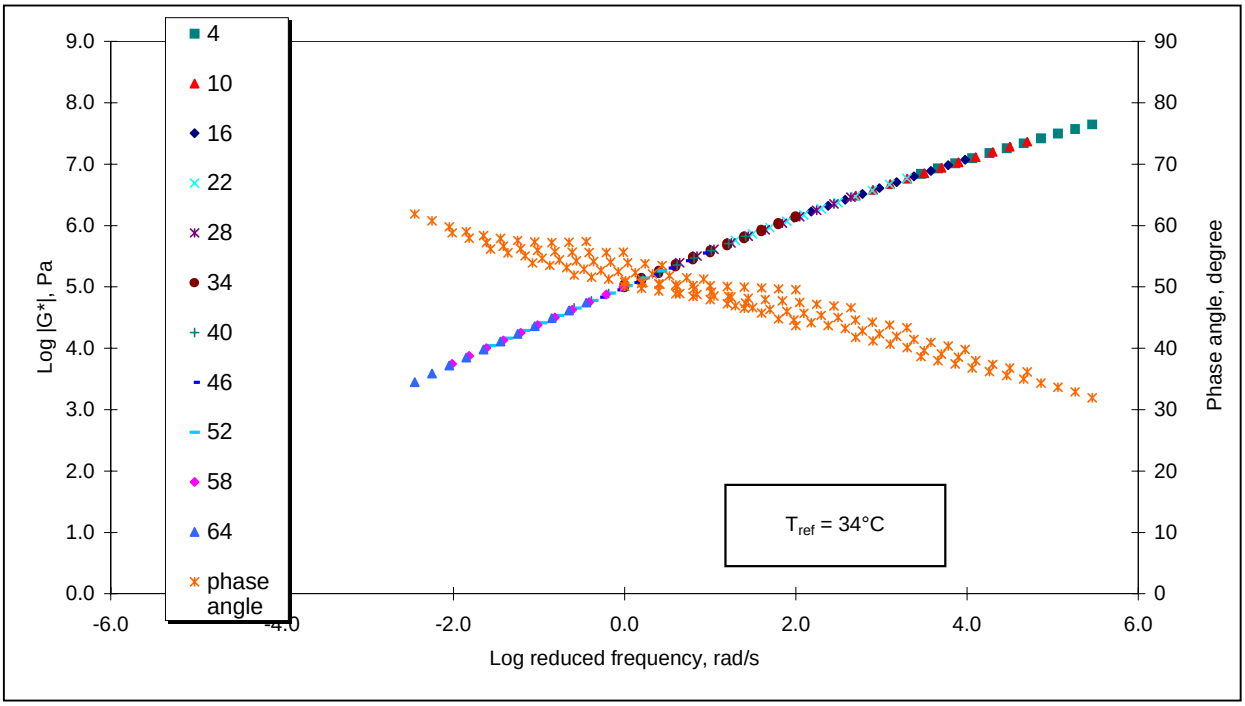

Figure A.14 Master Curve – Binder 5, PAV

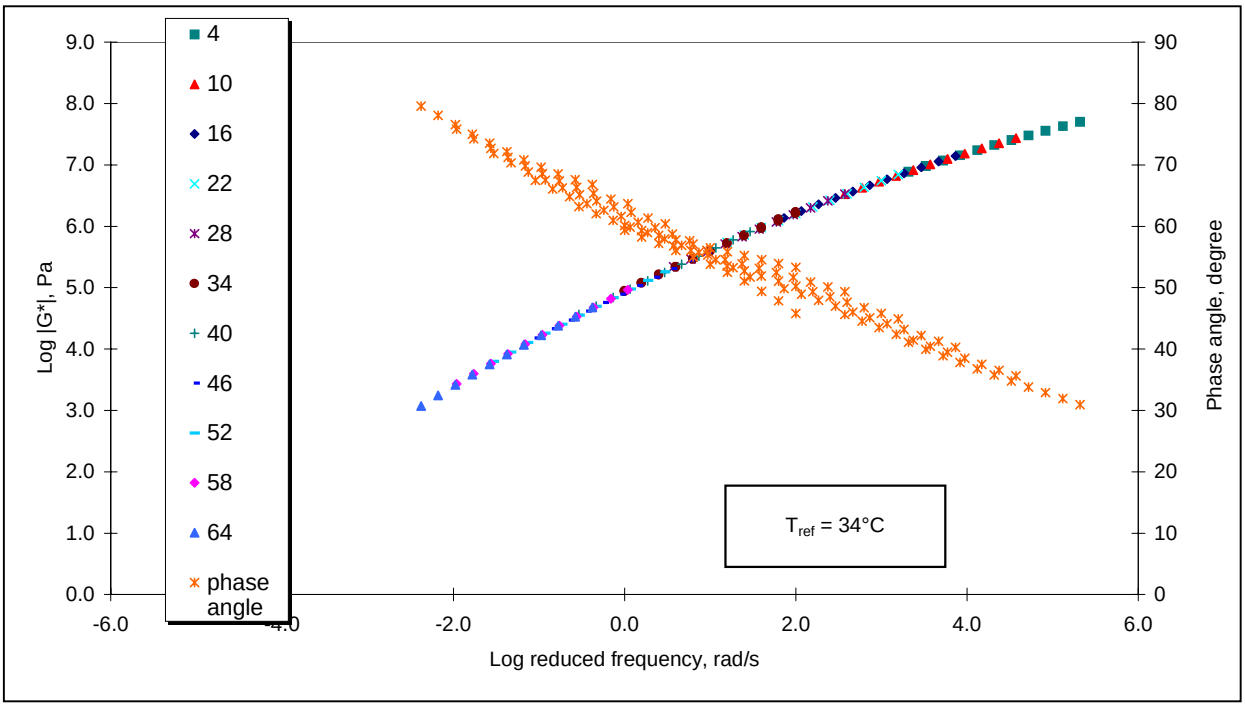

Figure A.15 Master Curve – Binder 6, PAV

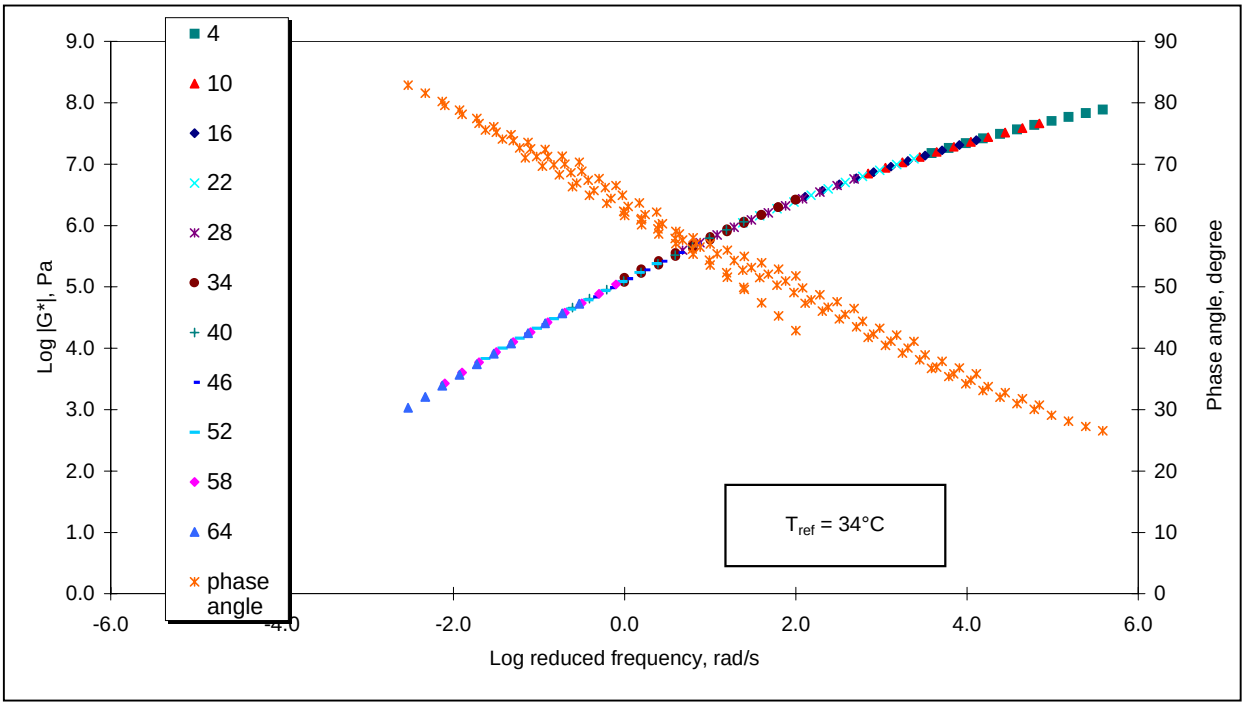

Figure A.16 Master Curve – Binder 7, PAV

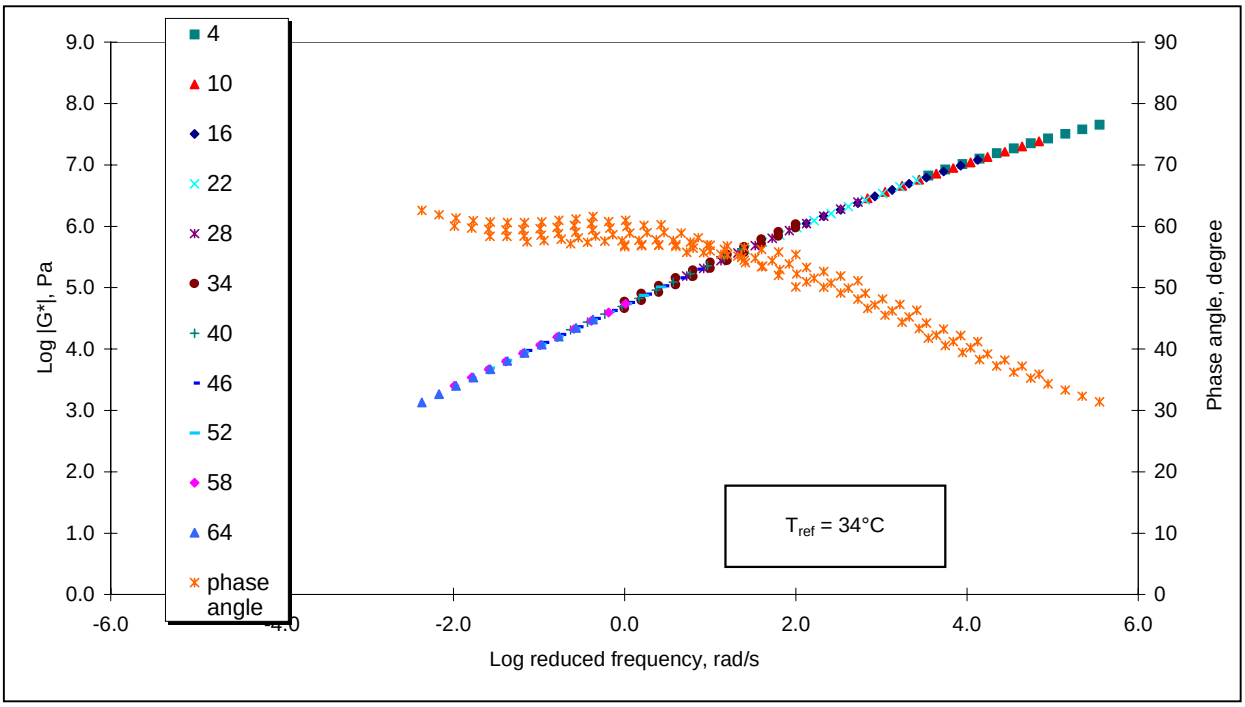

Figure A.17 Master Curve – Binder 8, PAV

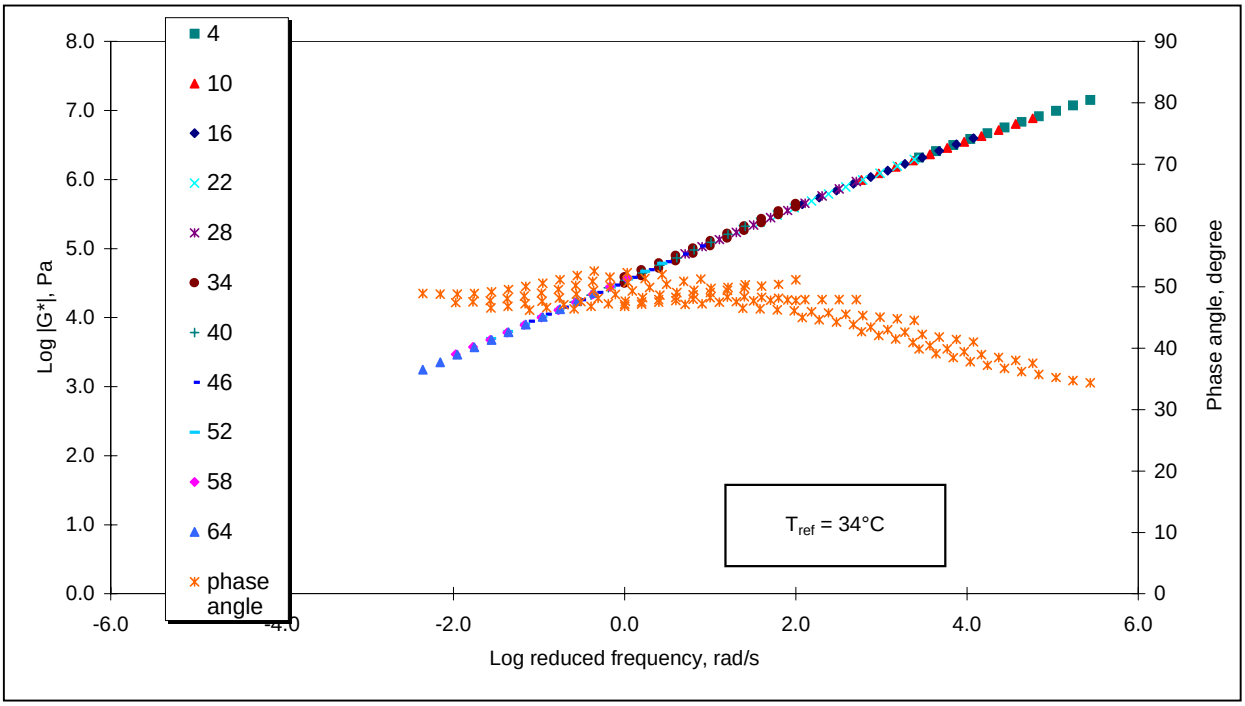

Figure A.18 Master Curve – Binder 9, PAV

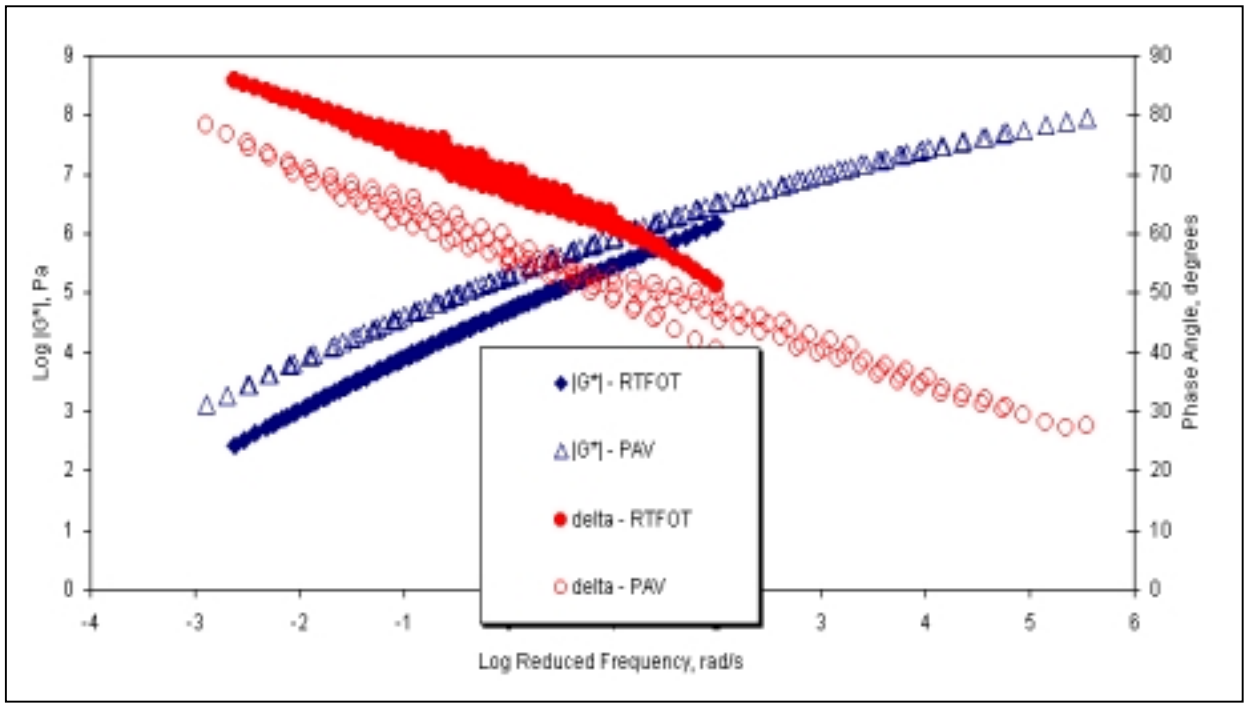

Figure A.19 Master Curves – Binder 1, PAV and RTFOT

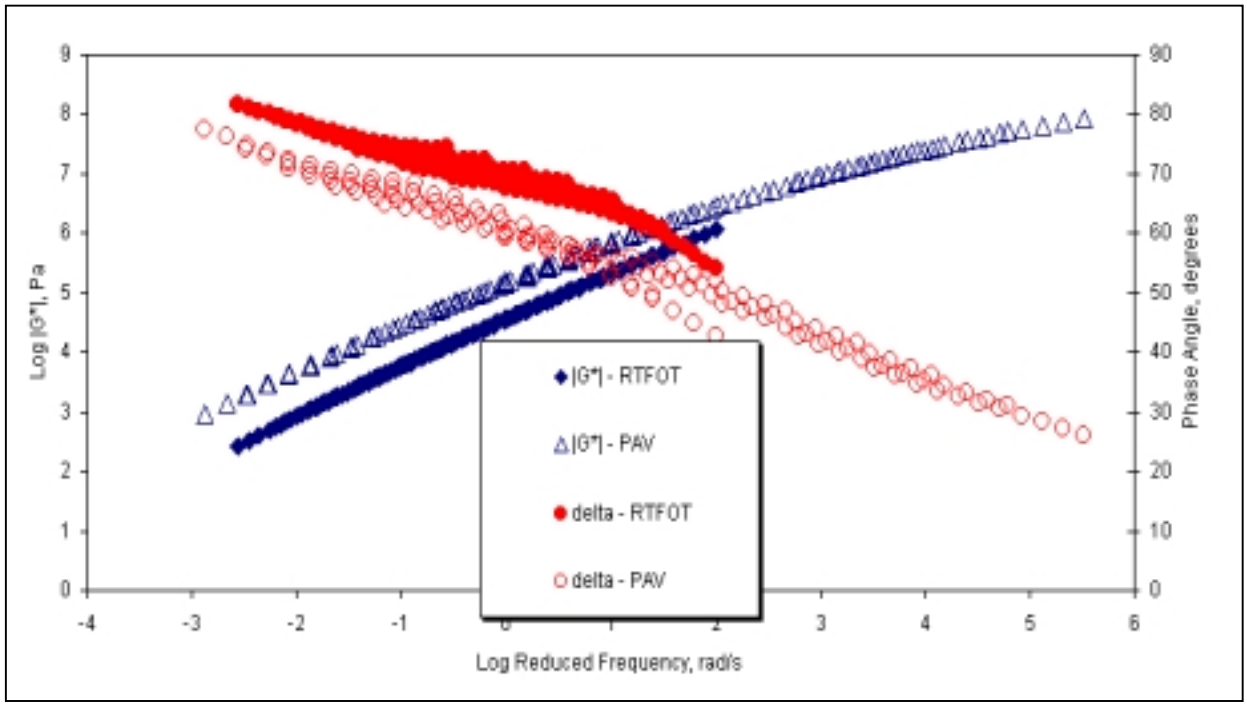

Figure A.20 Master Curves – Binder 2, PAV and RTFOT

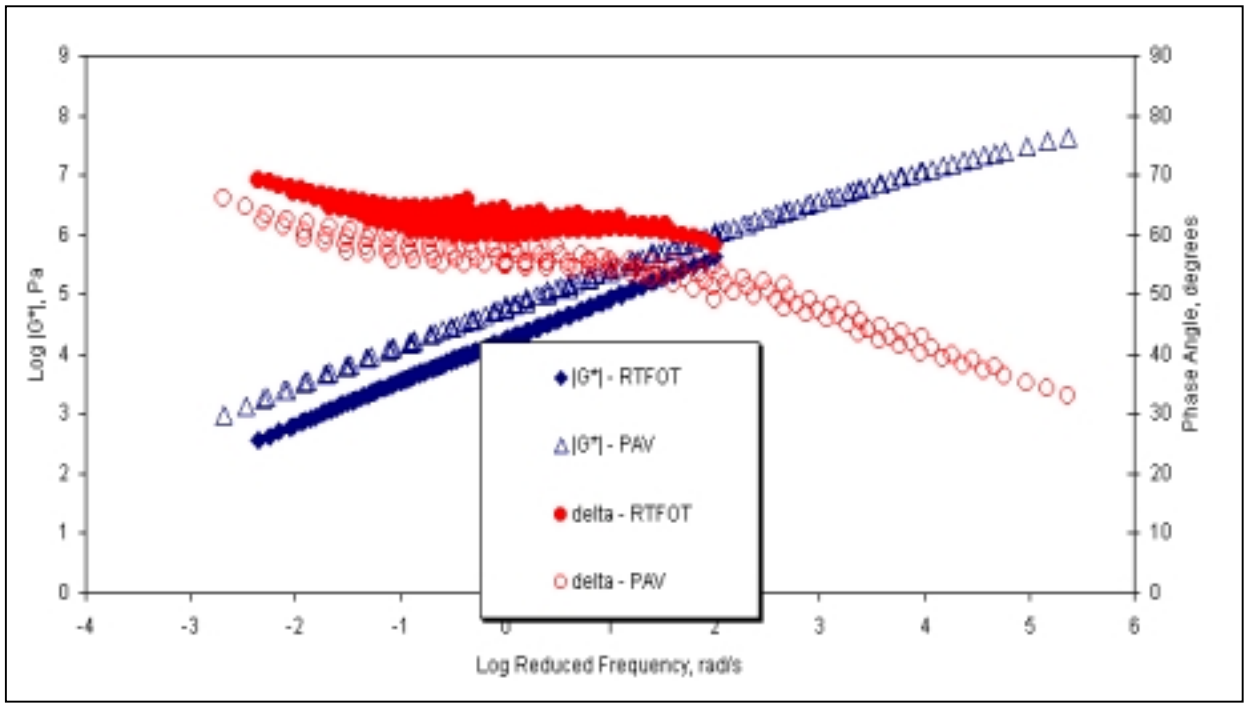

Figure A.21 Master Curves – Binder 3, PAV and RTFOT

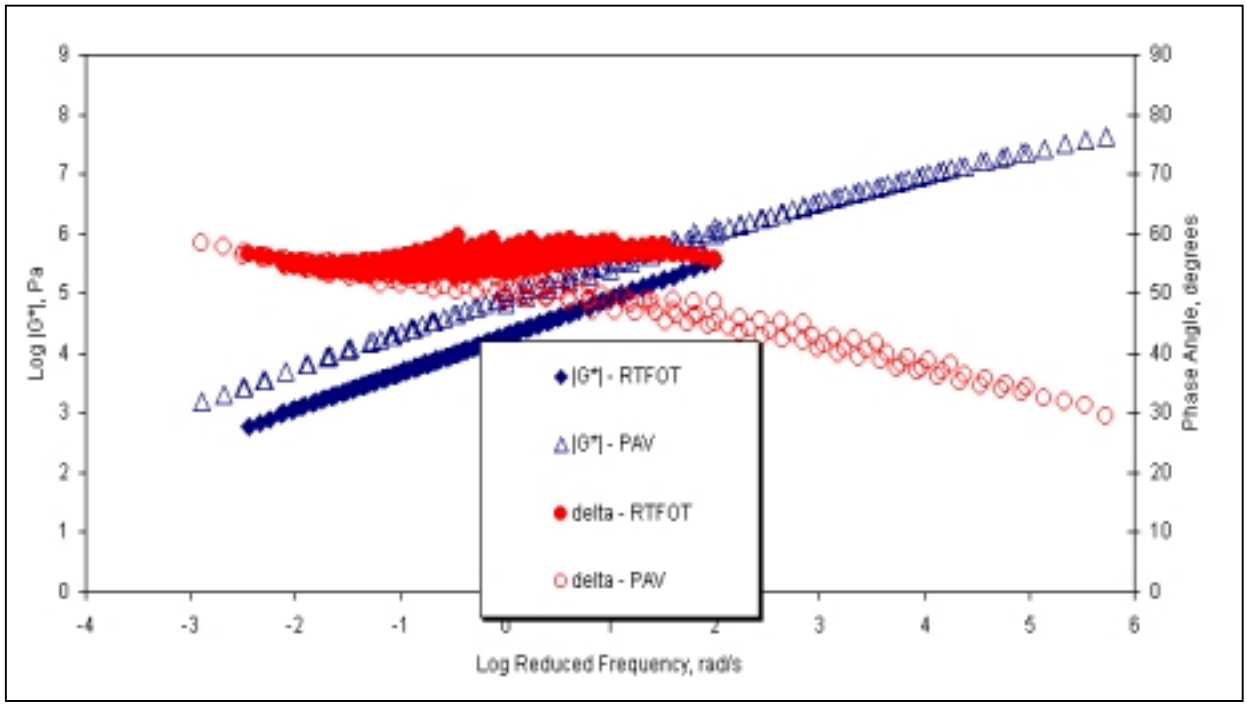

Figure A.22 Master Curves – Binder 4, PAV and RTFOT

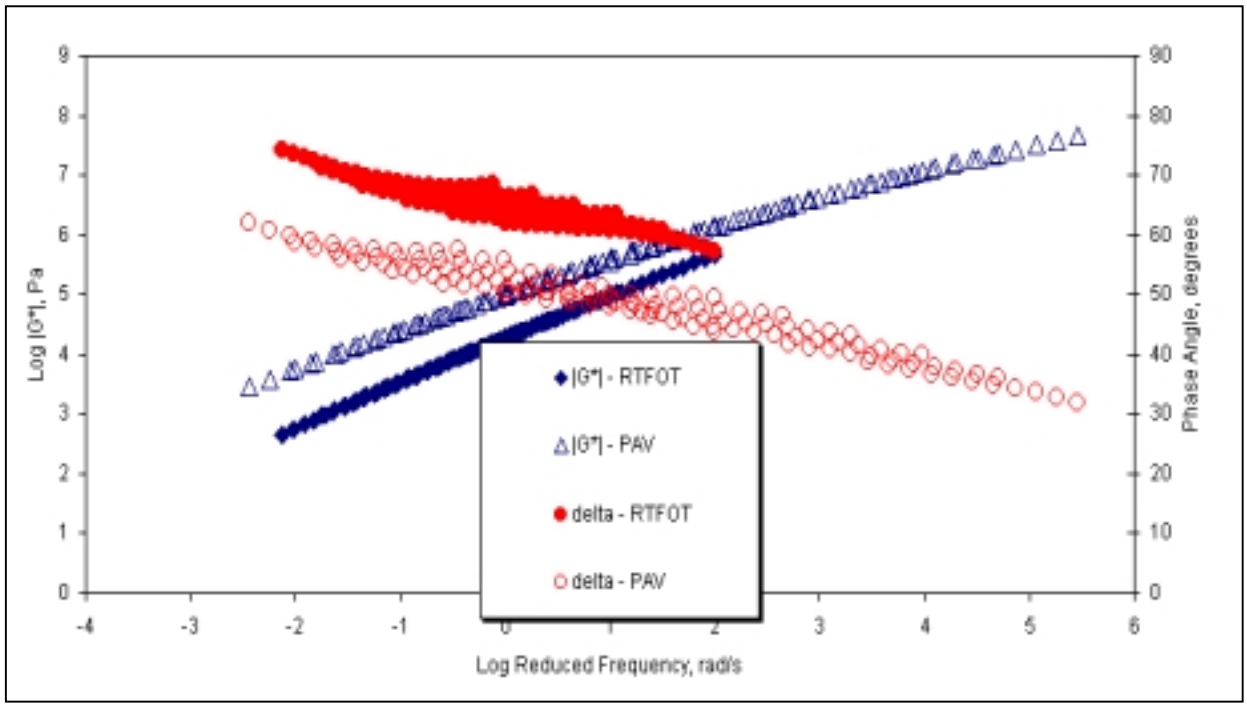

Figure A.23 Master Curves – Binder 5, PAV and RTFOT

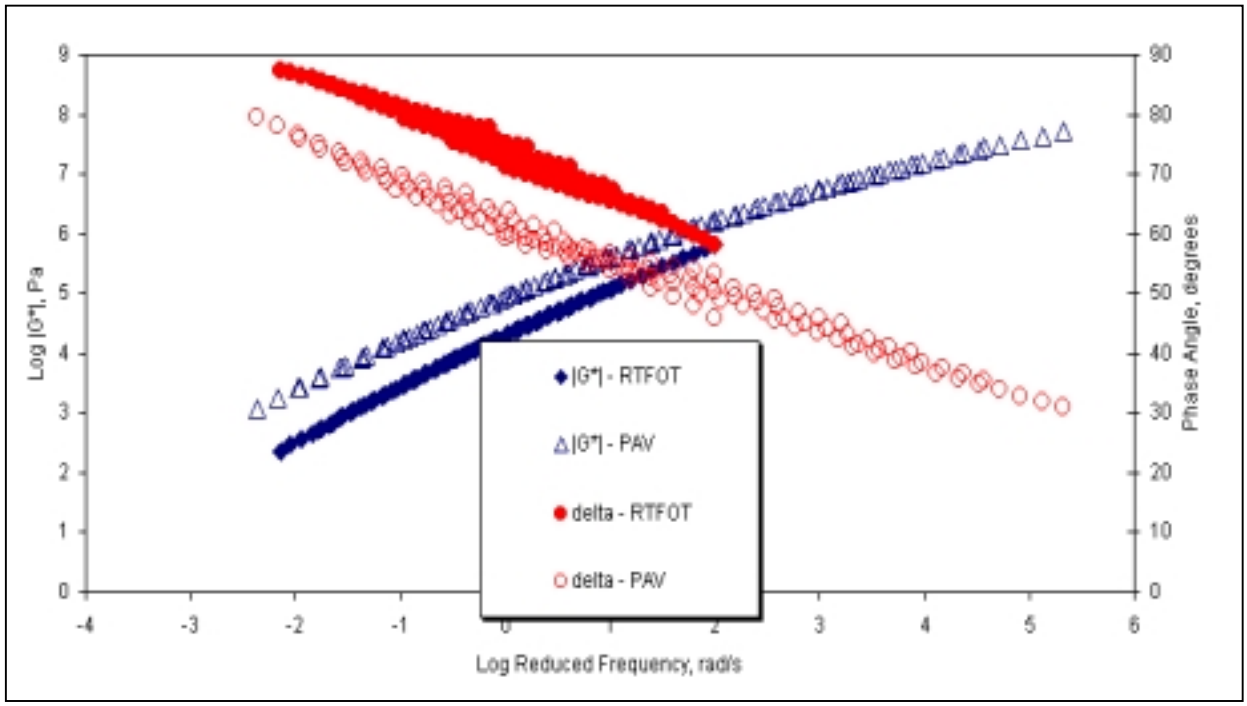

Figure A.24 Master Curves – Binder 6, PAV and RTFOT

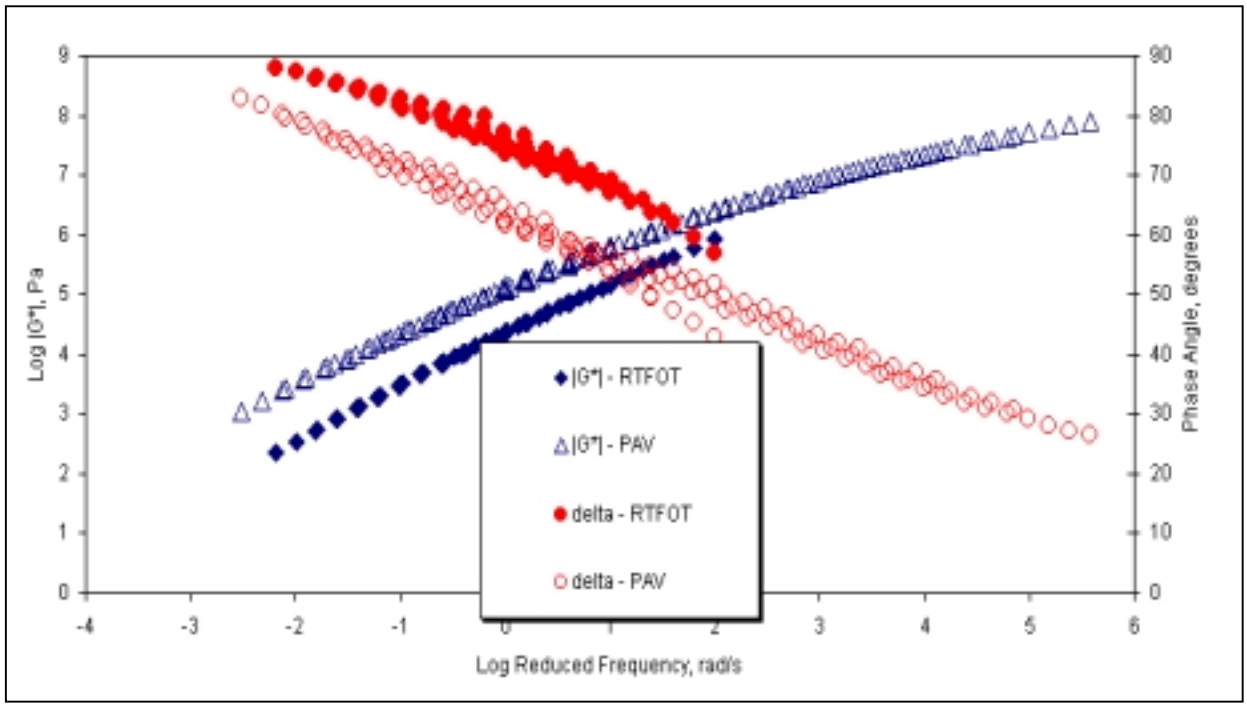

Figure A.25 Master Curves – Binder 7, PAV and RTFOT

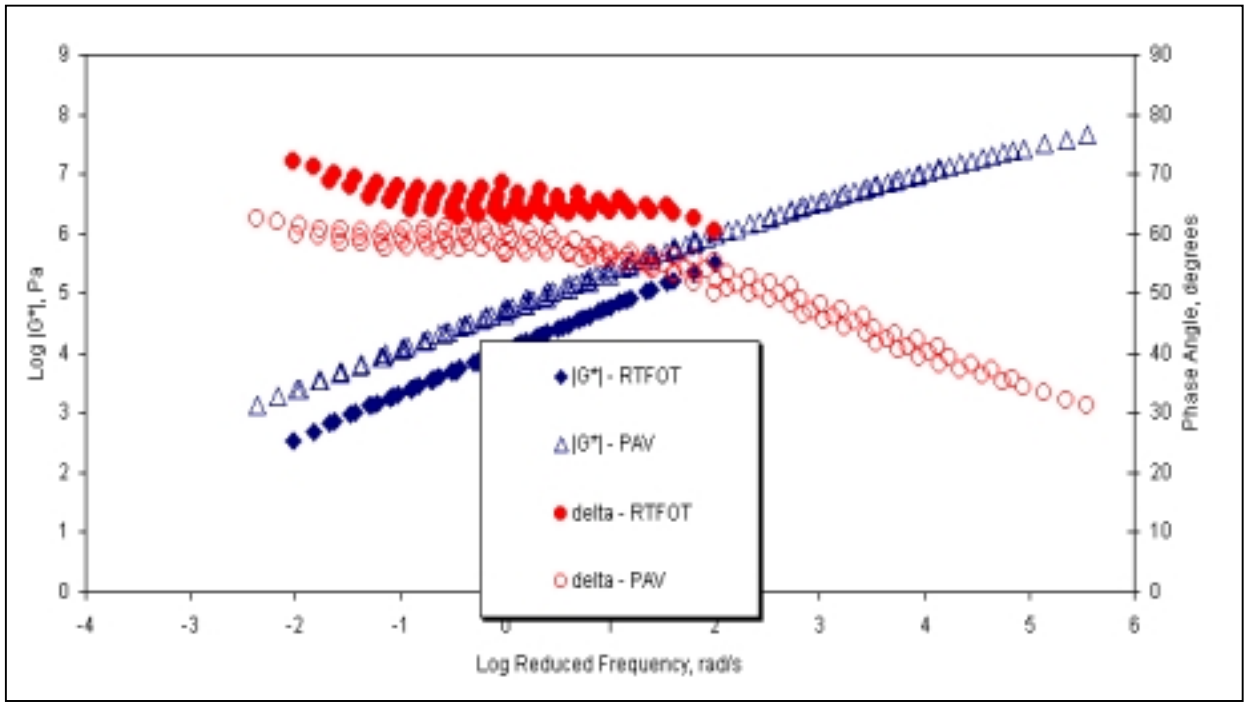

Figure A.26 Master Curves – Binder 8, PAV and RTFOT

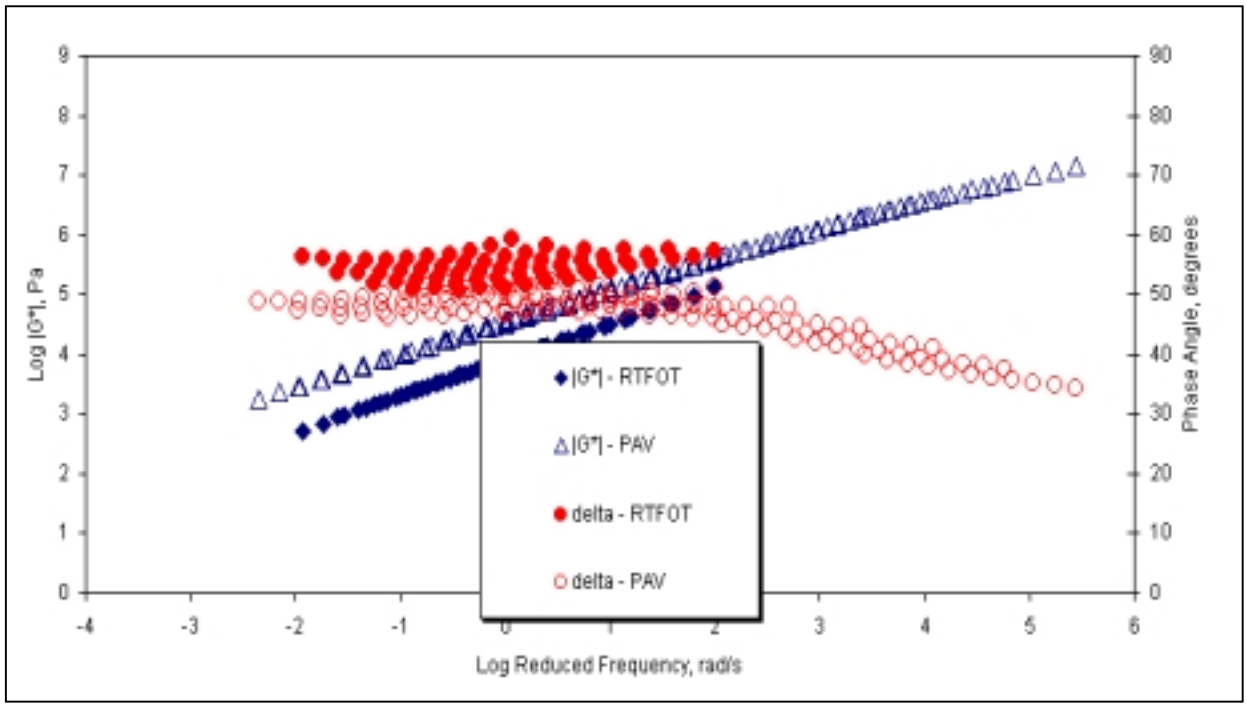

Figure A.27 Master Curves – Binder 9, PAV and RTFOT

Appendix B:

Zero Shear Viscosity Plots

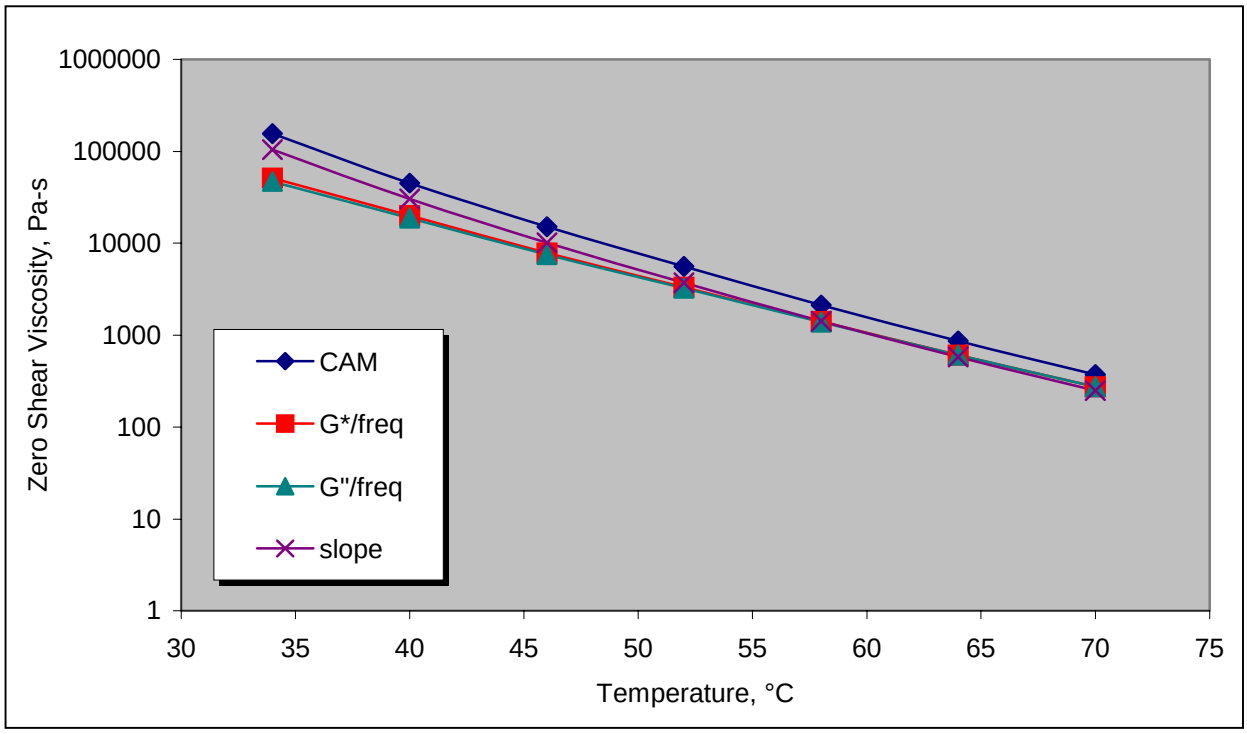

Figure B.1 Zero Shear Viscosity – Binder 1

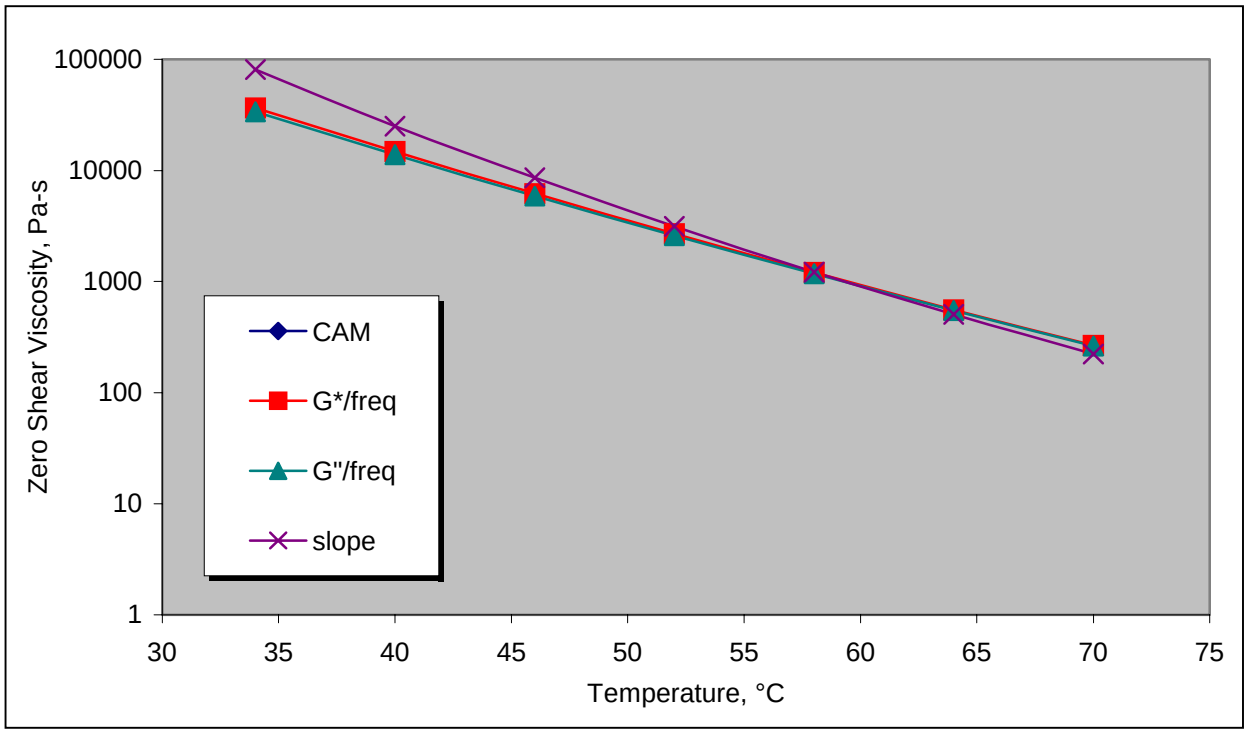

Figure B.2 Zero Shear Viscosity – Binder 2

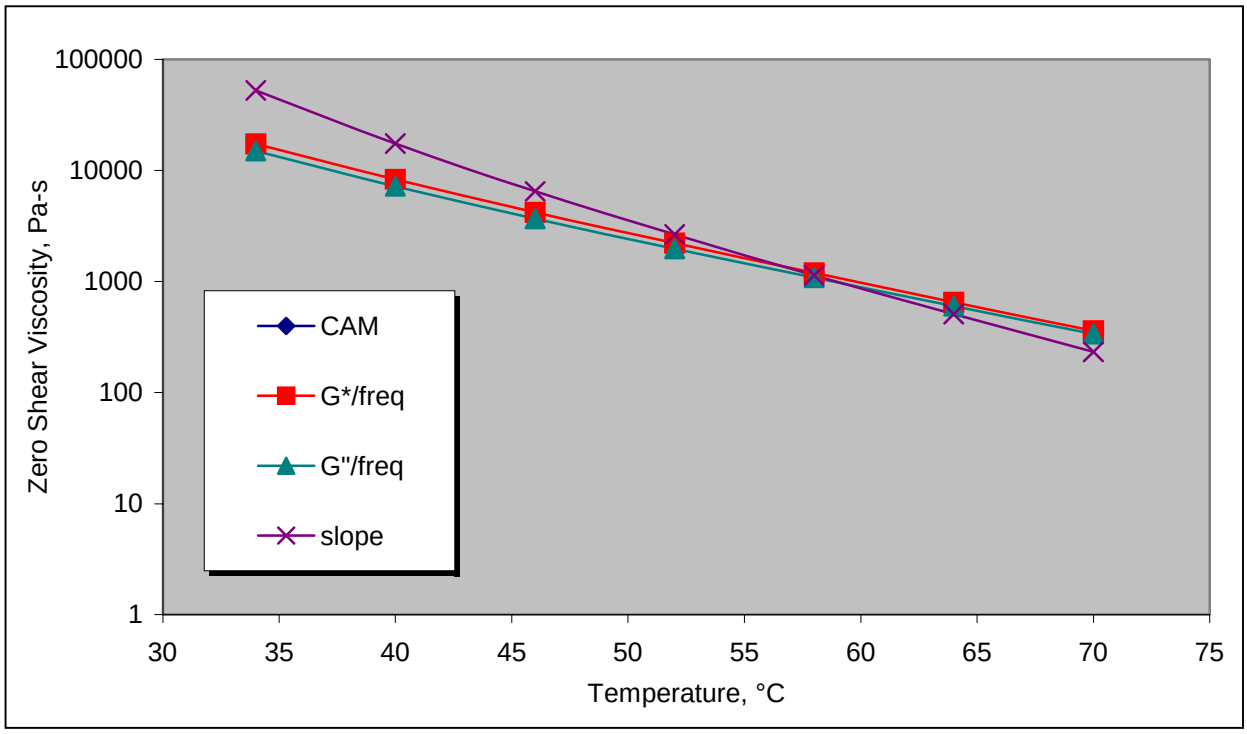

Figure B.3 Zero Shear Viscosity – Binder 3

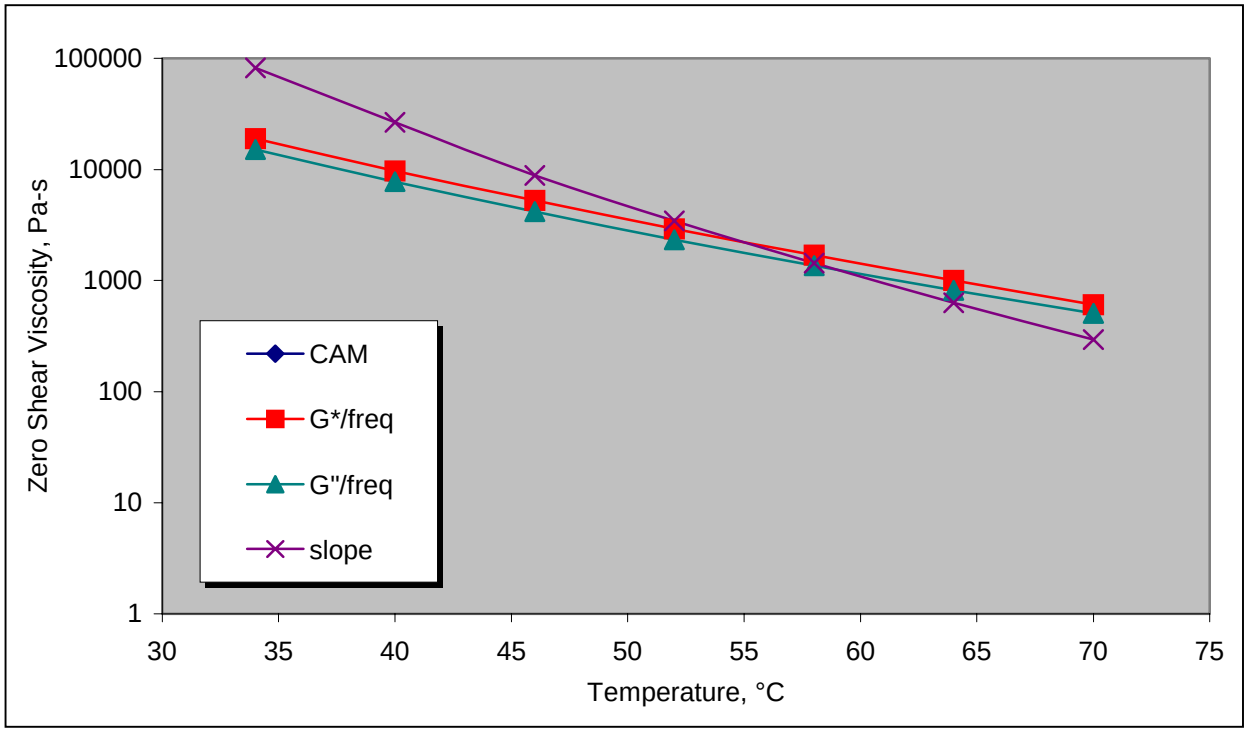

Figure B.4 Zero Shear Viscosity – Binder 4

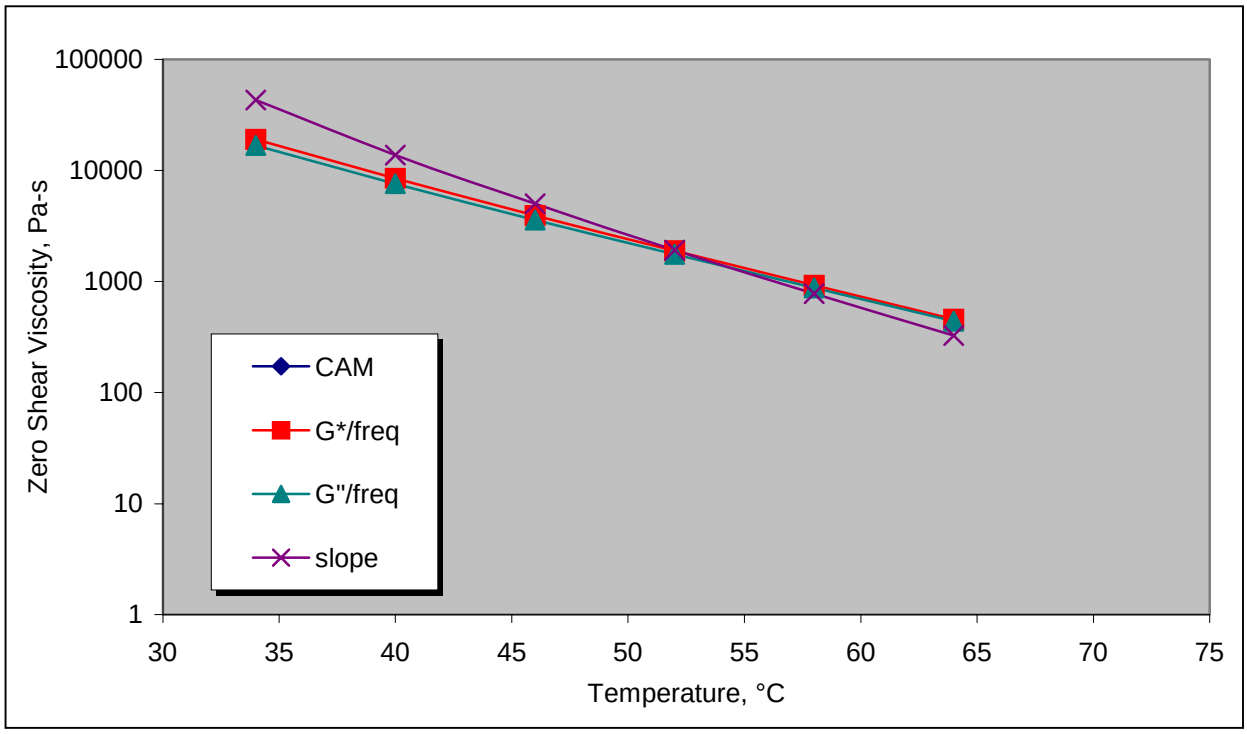

Figure B.5 Zero Shear Viscosity – Binder 5

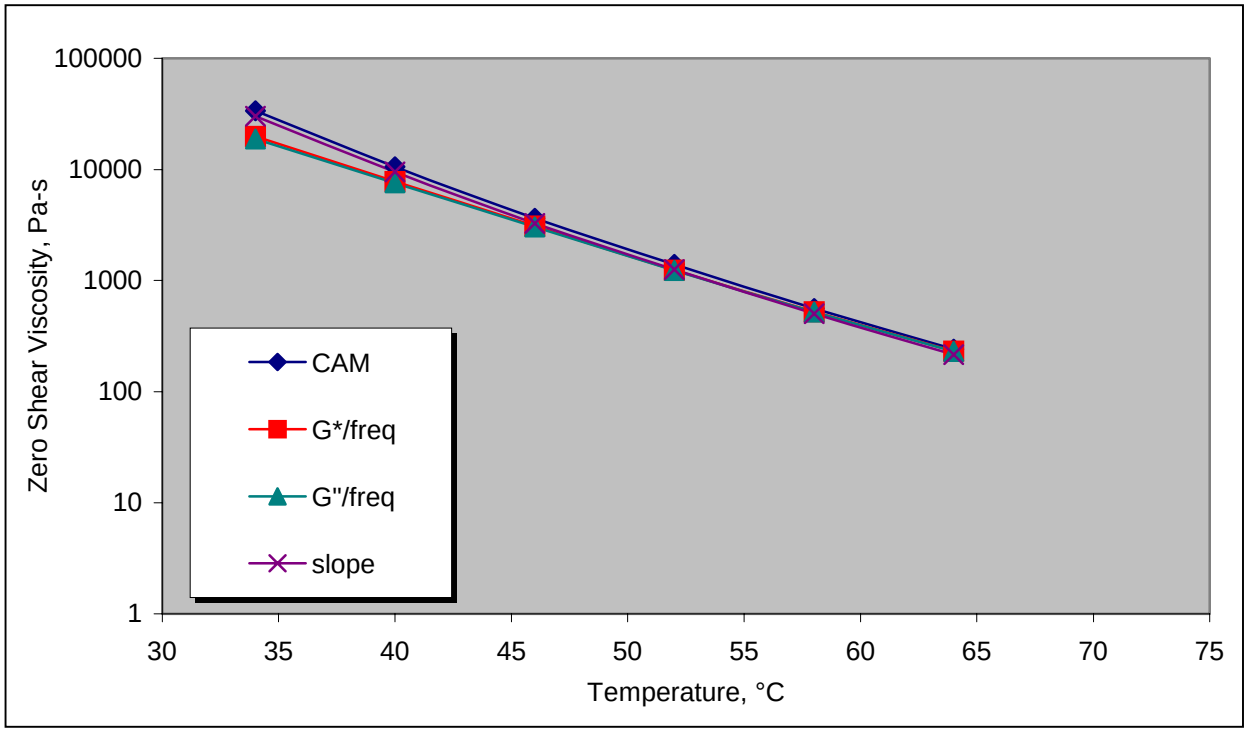

Figure B.6 Zero Shear Viscosity – Binder 6

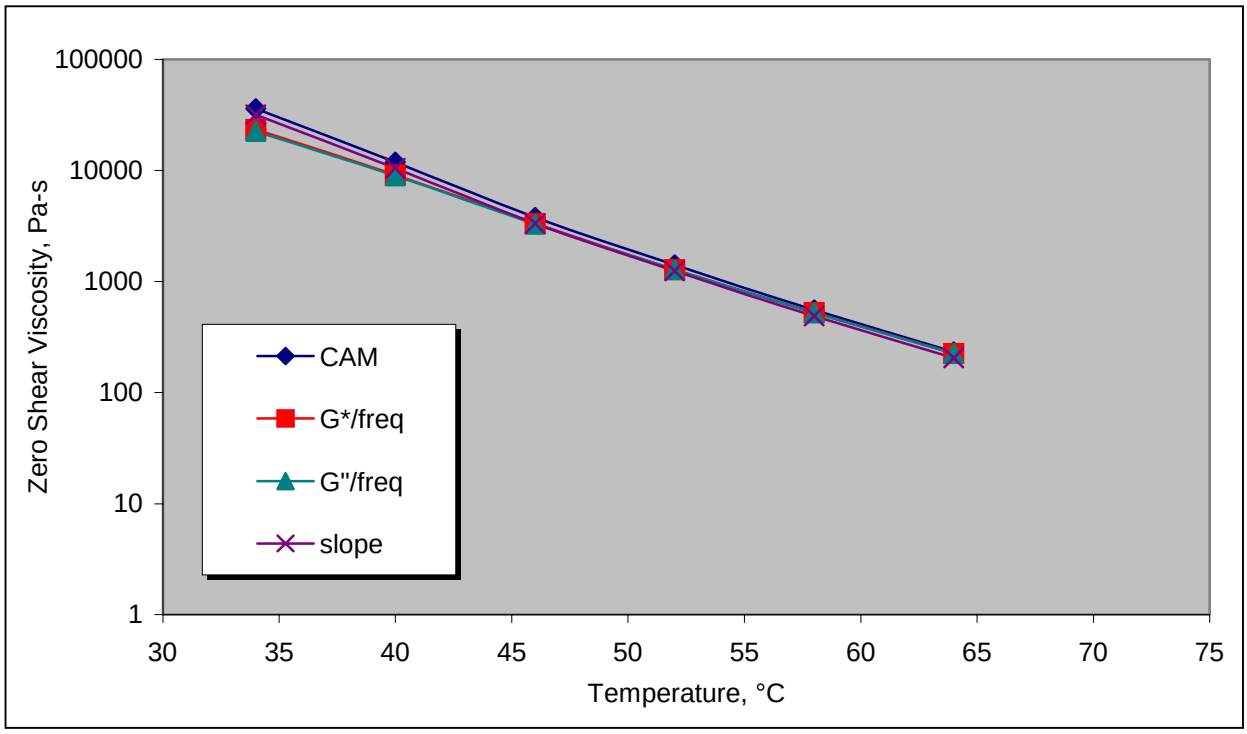

Figure B.7 Zero Shear Viscosity – Binder 7

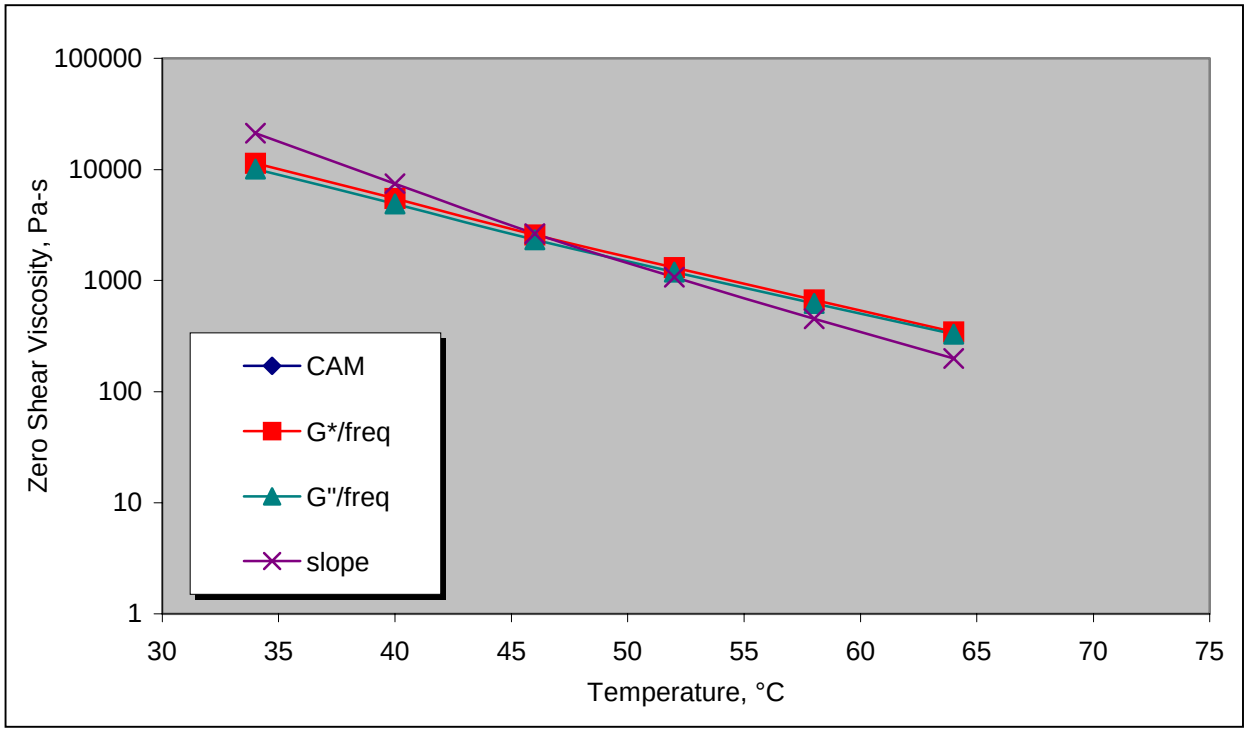

Figure B.8 Zero Shear Viscosity – Binder 8

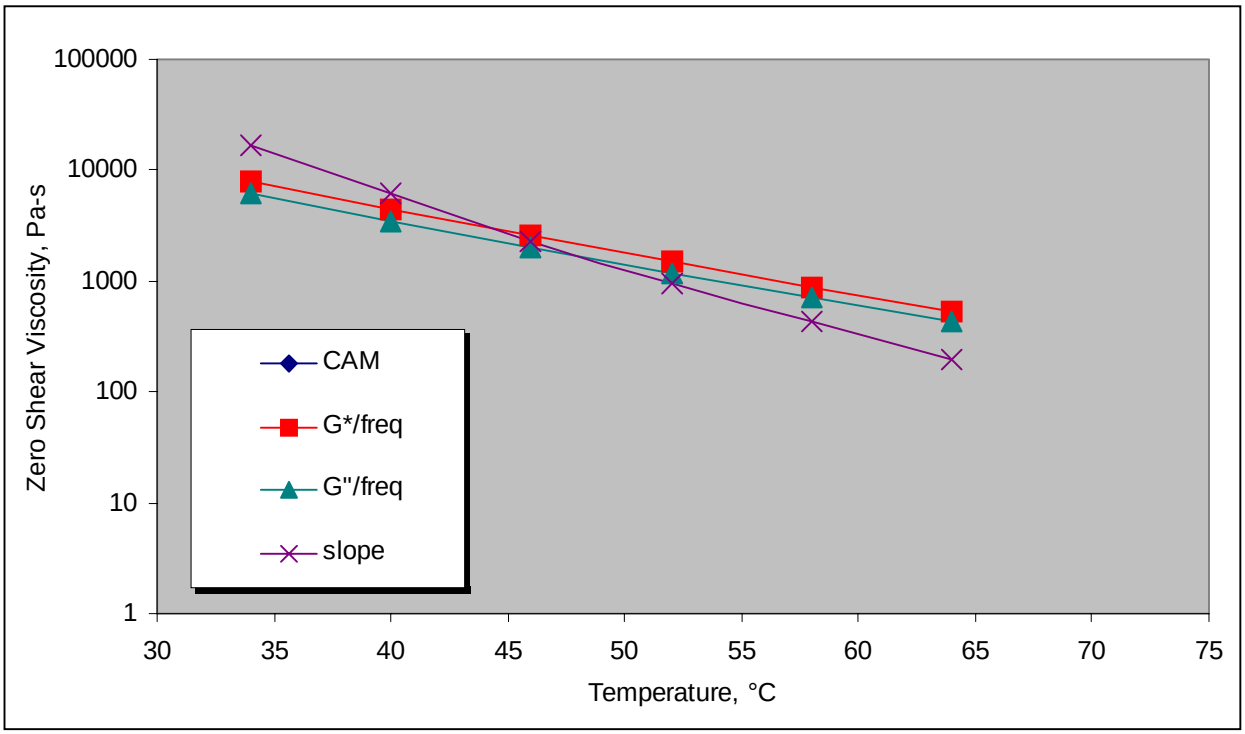

Figure B.9 Zero Shear Viscosity – Binder 9

Appendix C:

Repeated Creep Figures

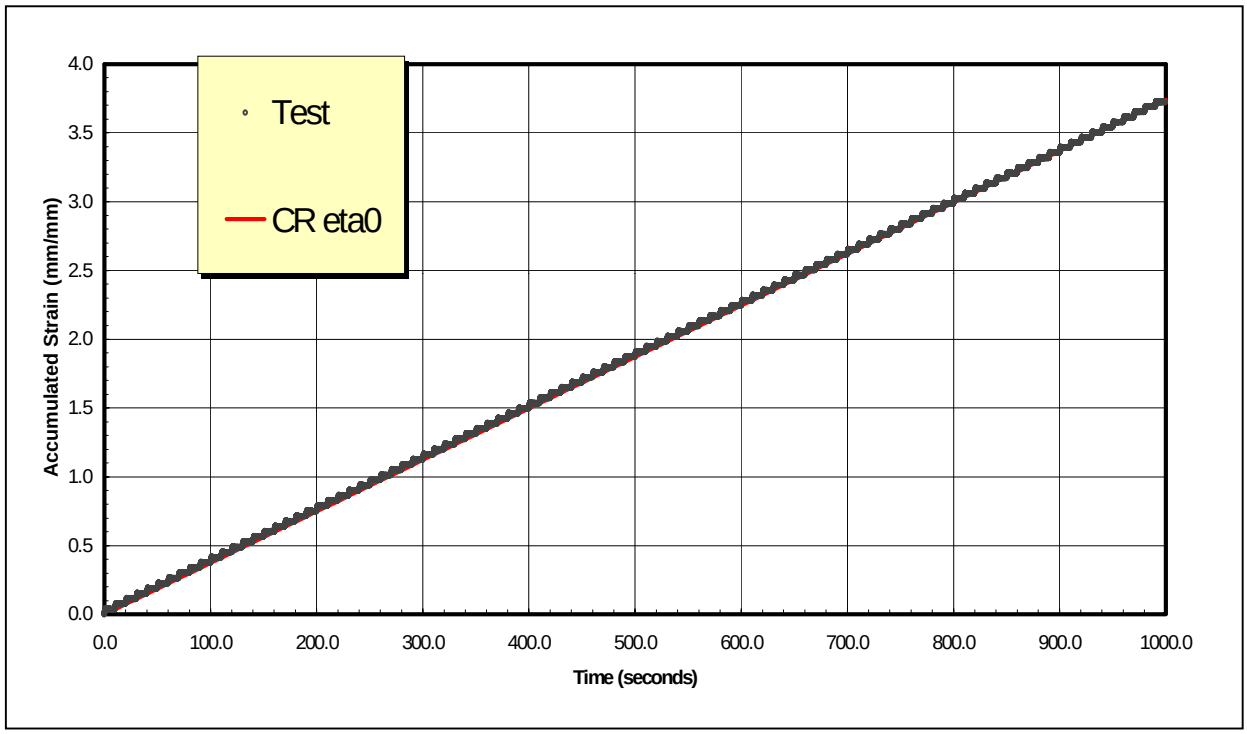

Figure C.1 Repeated Creep Graph – Binder 1

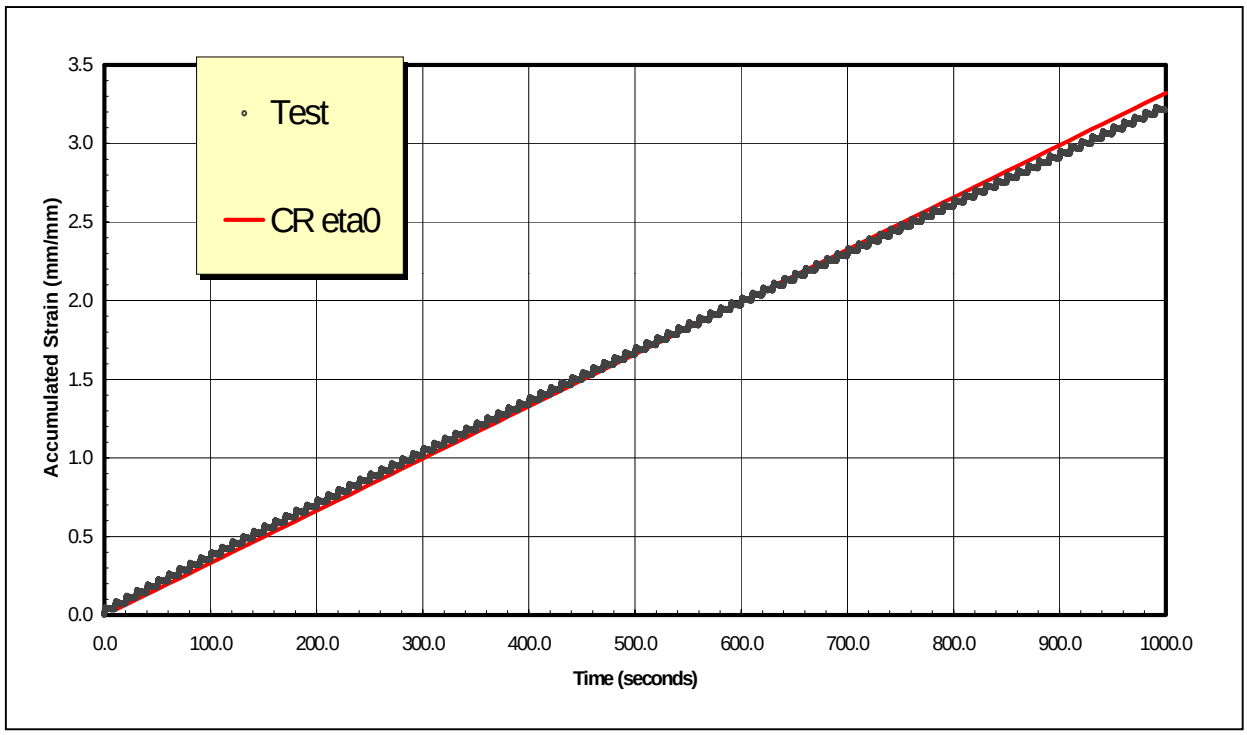

Figure C.2 Repeated Creep Graph – Binder 2

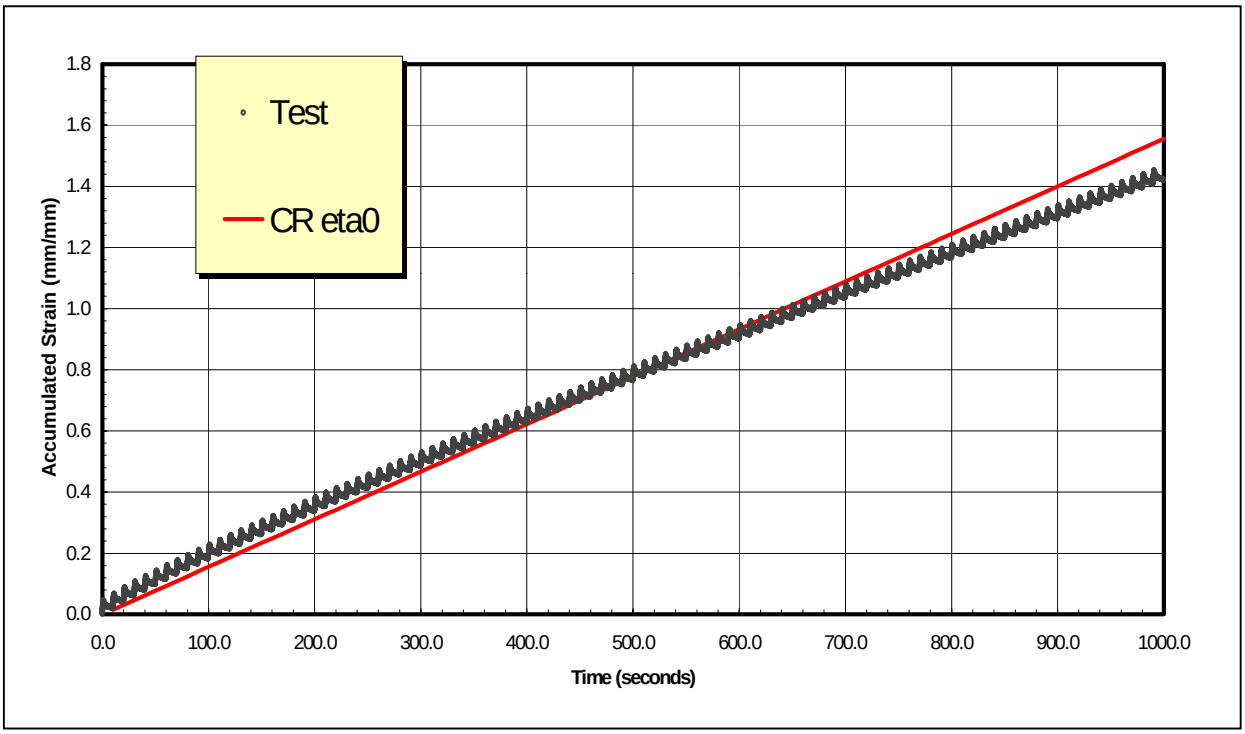

Figure C.3 Repeated Creep Graph – Binder 3

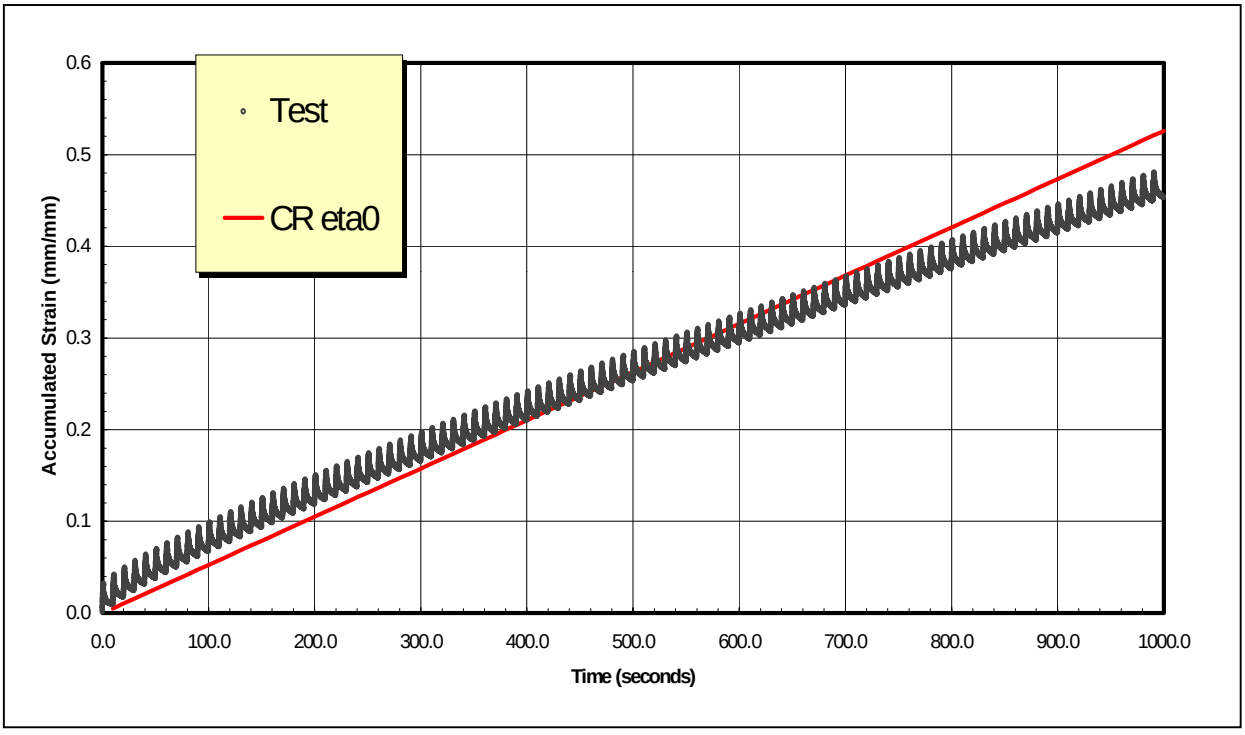

Figure C.4 Repeated Creep Graph – Binder 4

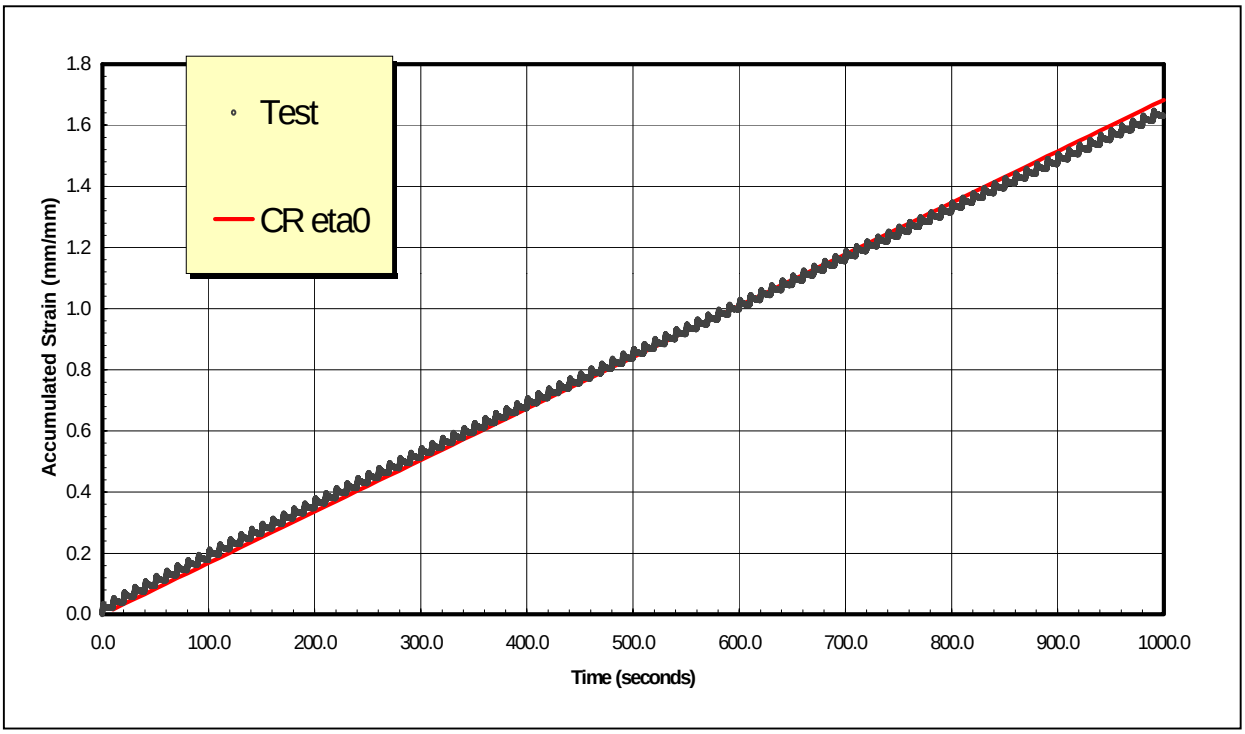

Figure C.5 Repeated Creep Graph – Binder 5

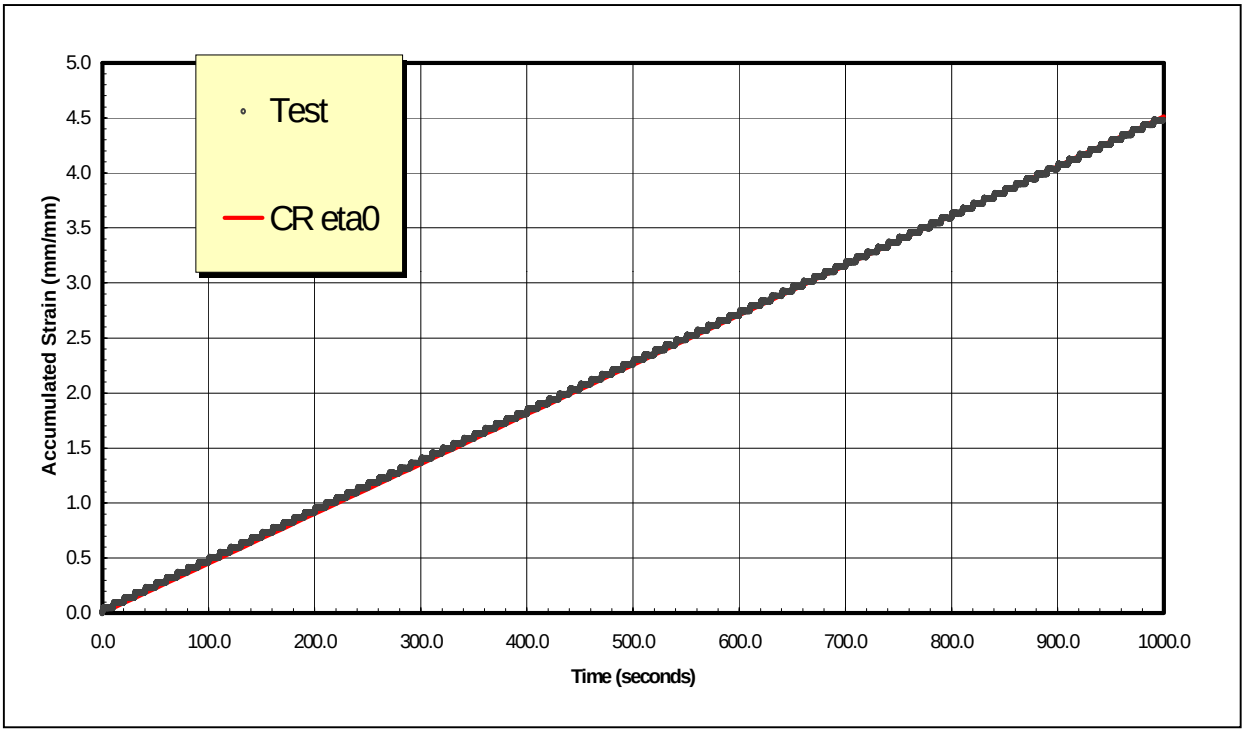

Figure C.6 Repeated Creep Graph – Binder 6

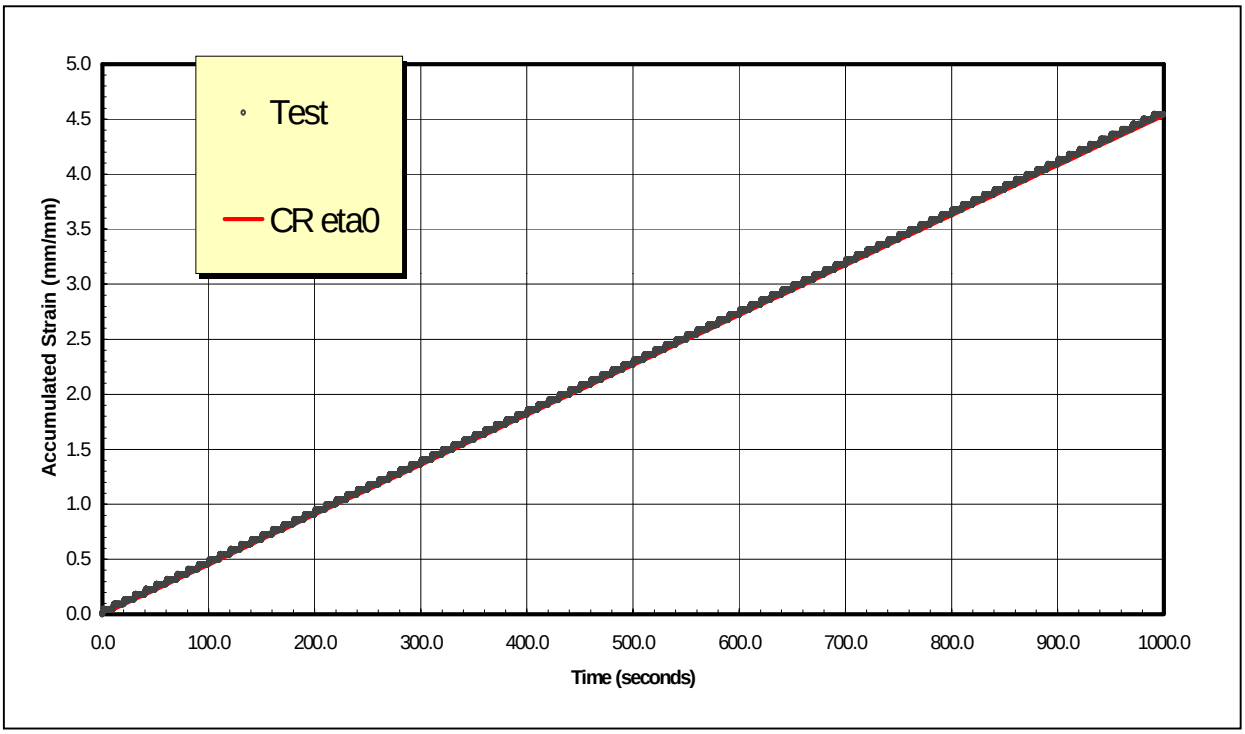

Figure C.7 Repeated Creep Graph – Binder 7

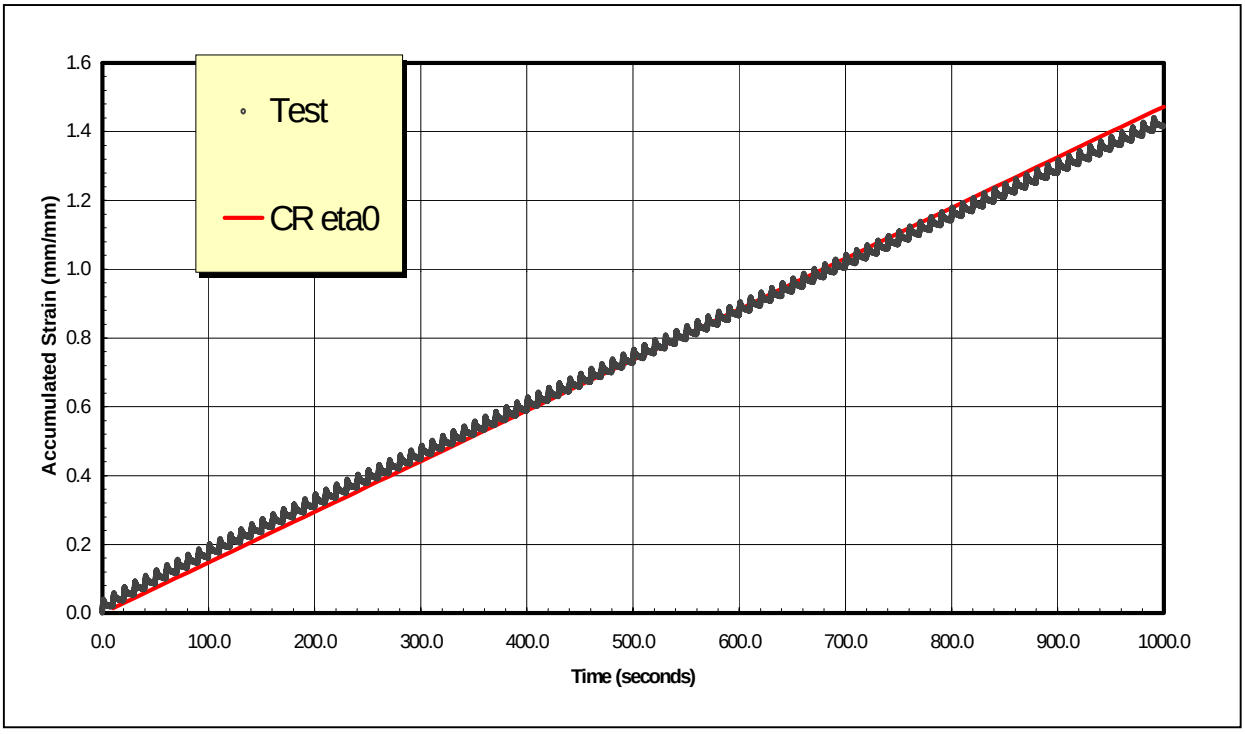

Figure C.8 Repeated Creep Graph – Binder 8

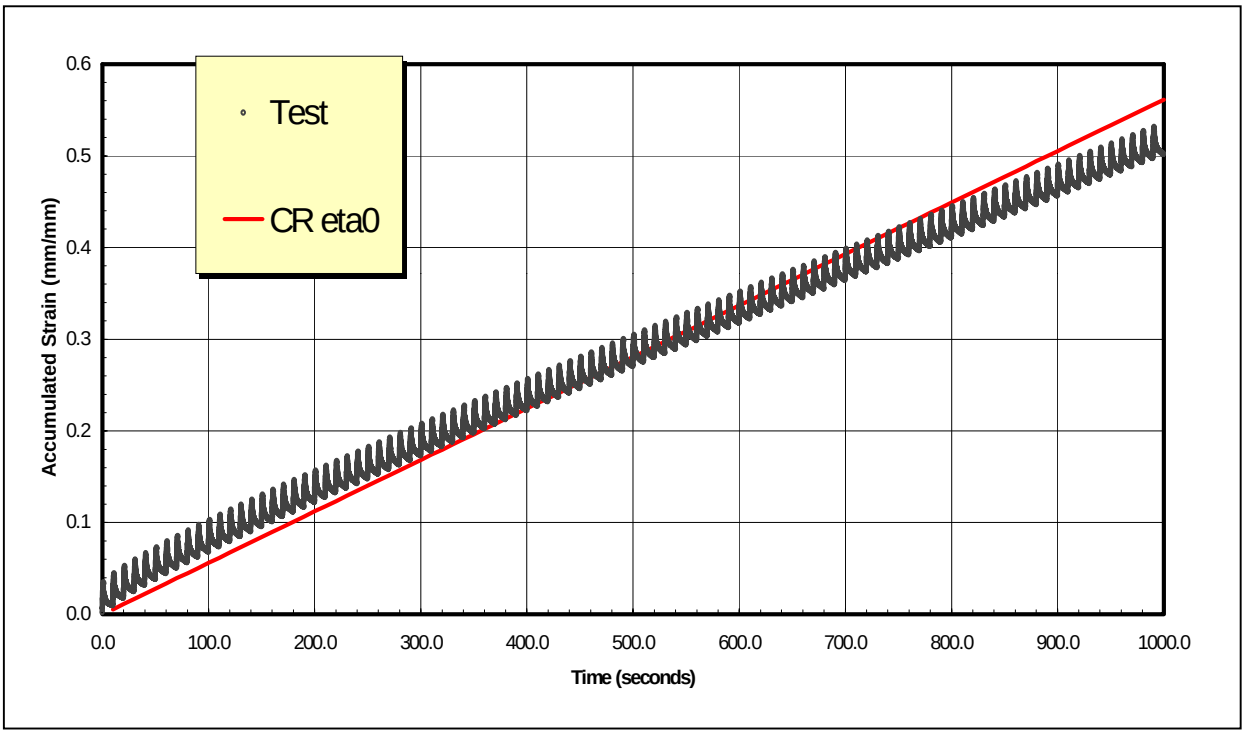

Figure C.9 Repeated Creep Graph – Binder 9

Appendix D:

Fatigue Test Results

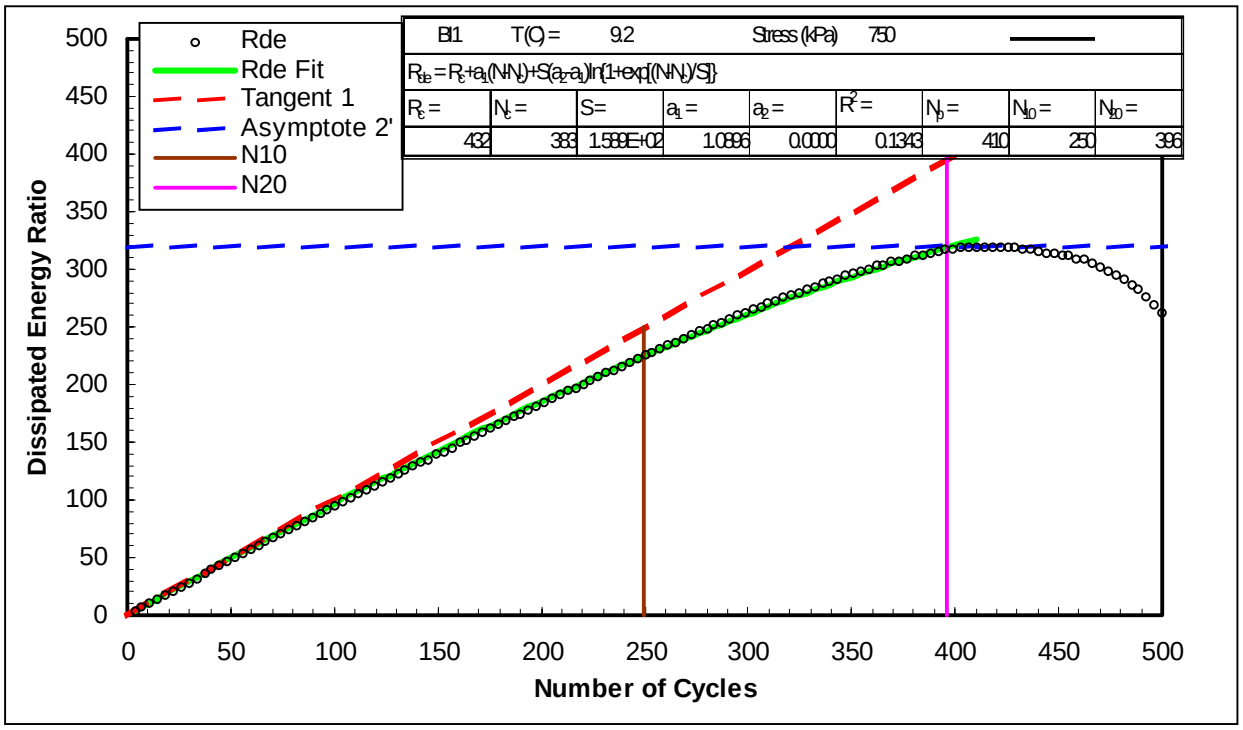

Figure D.1 Dissipated Energy Ratio Plot – Binder 1

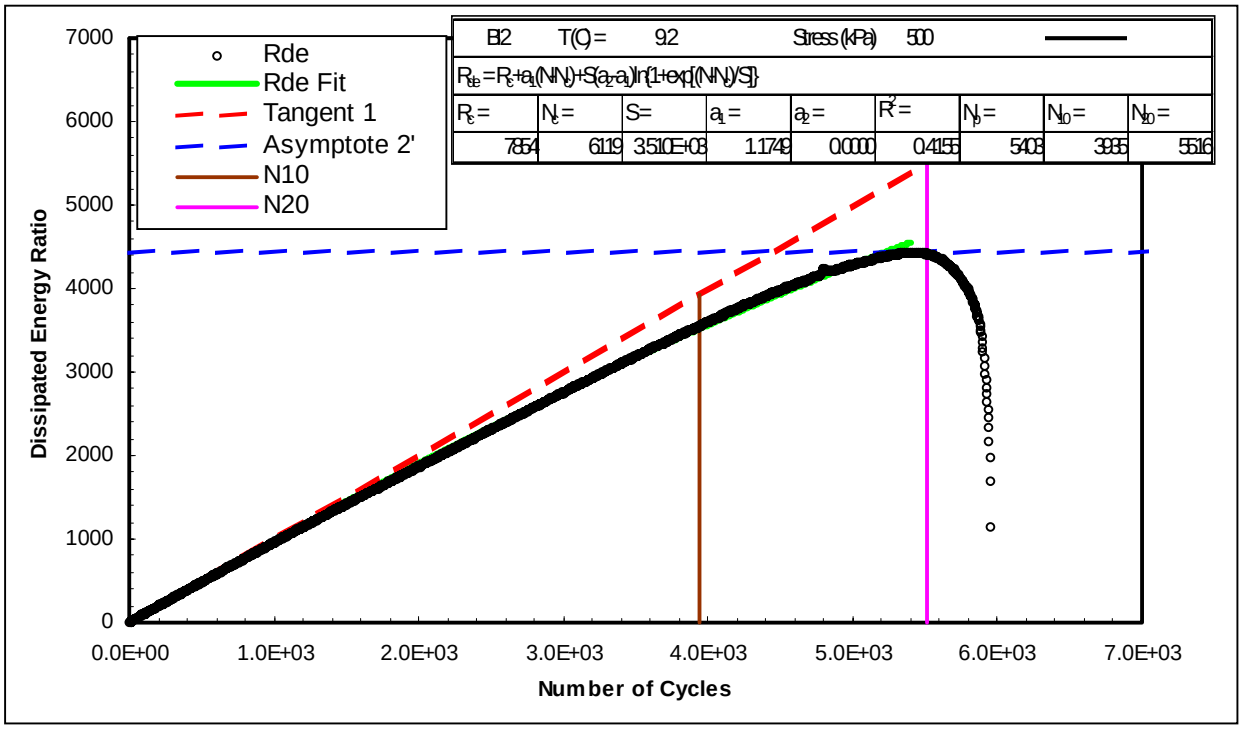

Figure D.2 Dissipated Energy Ratio Plot – Binder 2

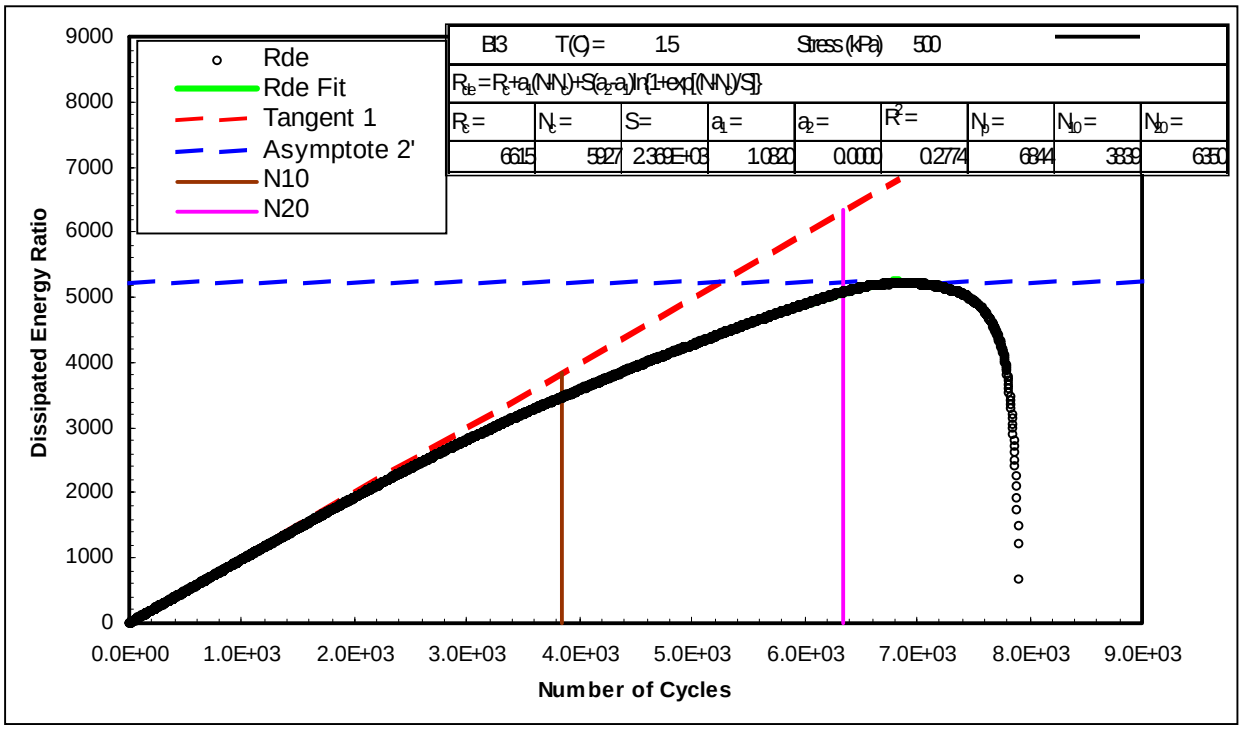

Figure D.3 Dissipated Energy Ratio Plot – Binder 3

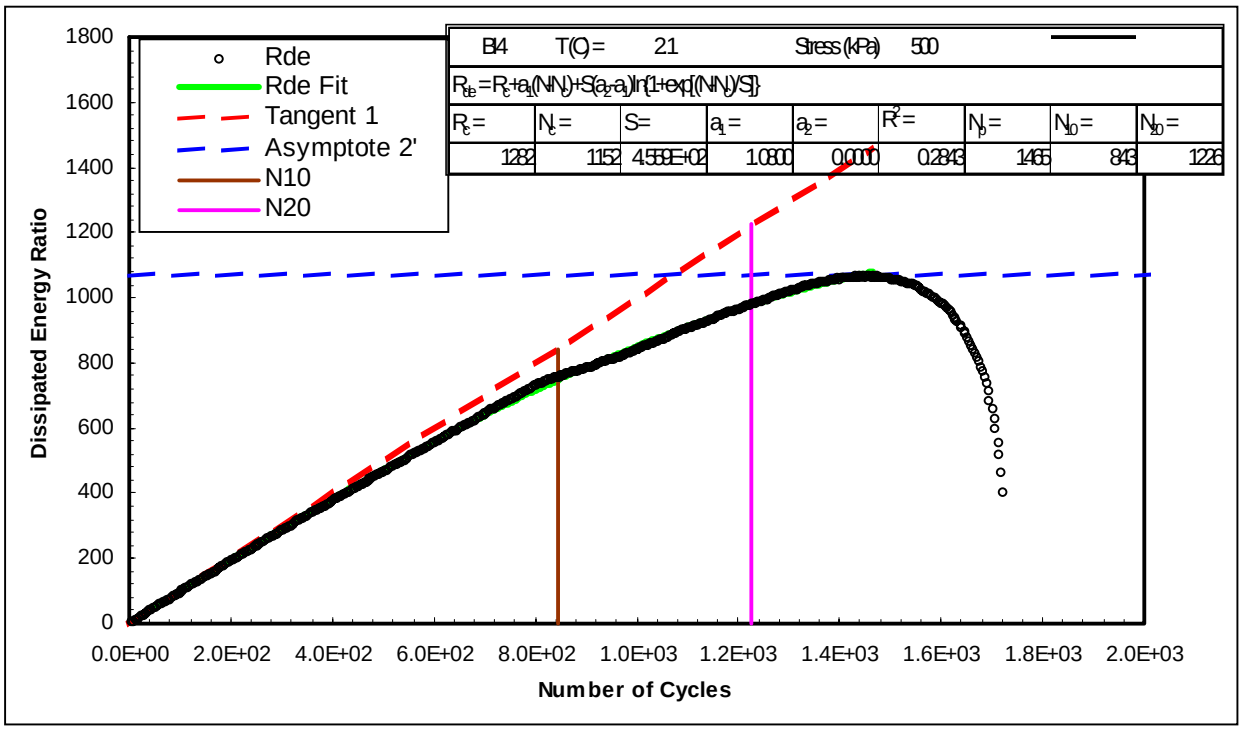

Figure D.4 Dissipated Energy Ratio Plot – Binder 4

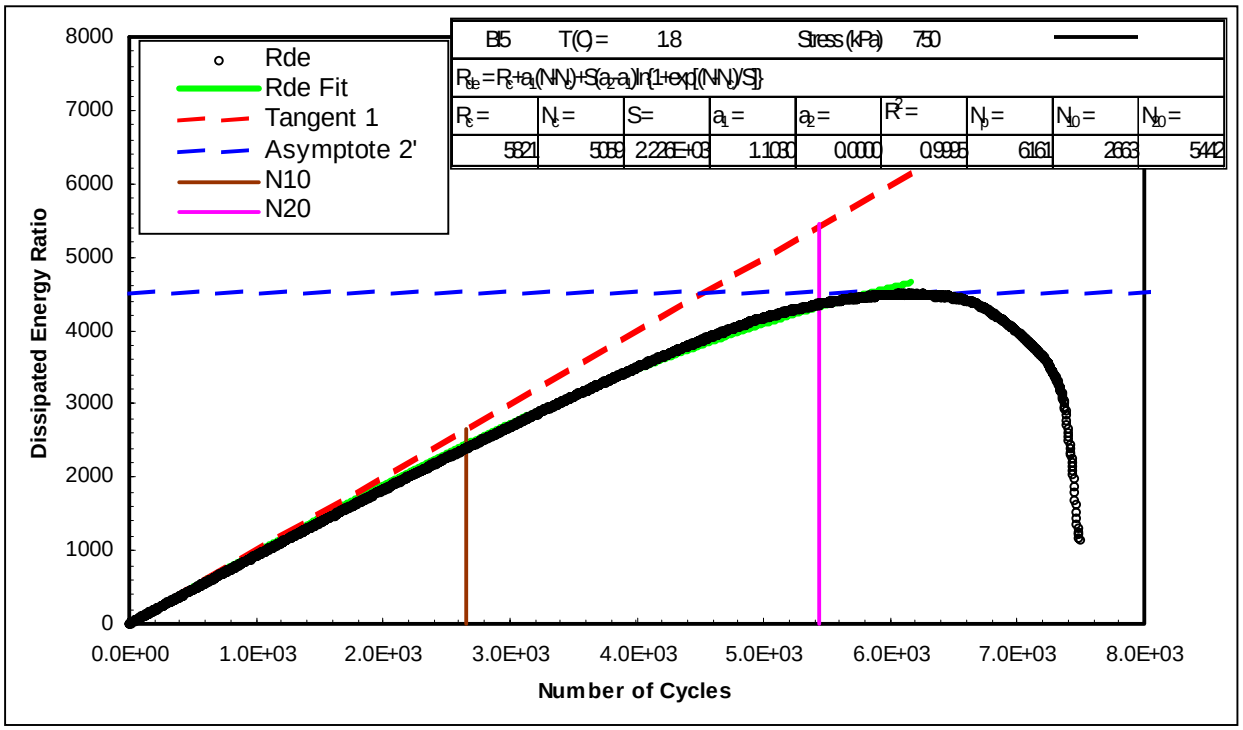

Figure D.5 Dissipated Energy Ratio Plot – Binder 5

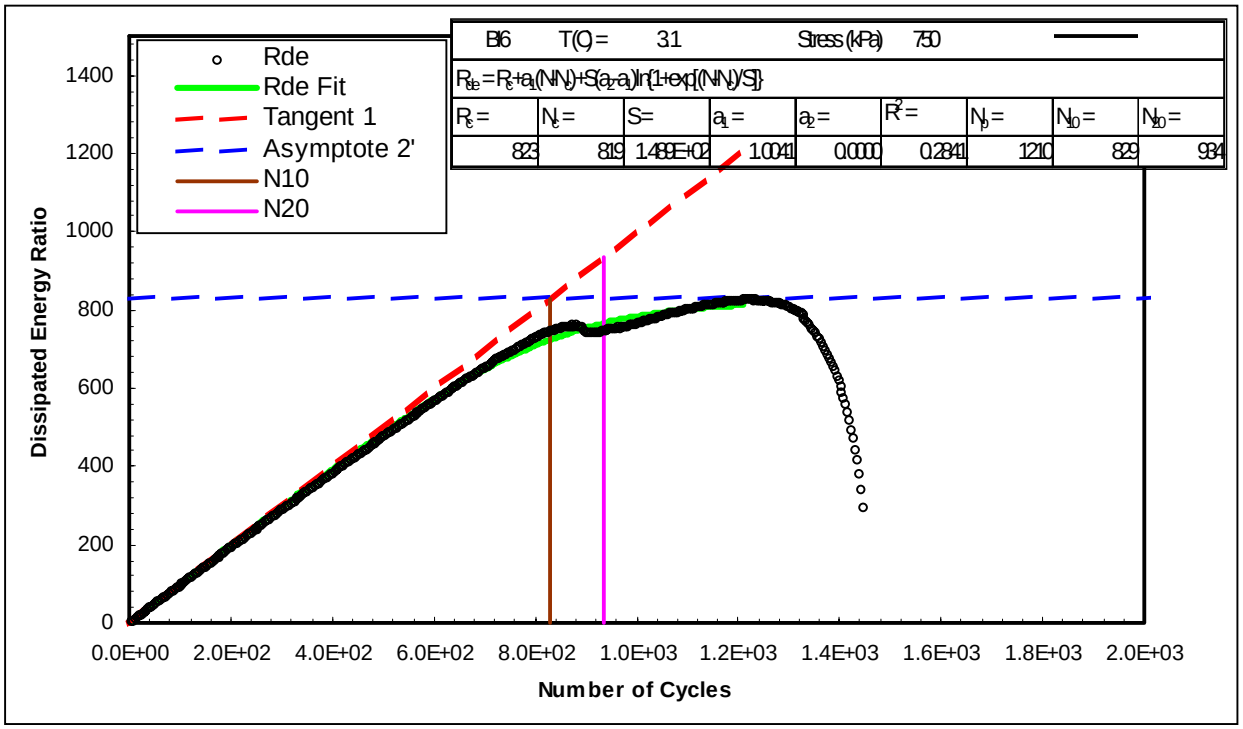

Figure D.6 Dissipated Energy Ratio Plot – Binder 6

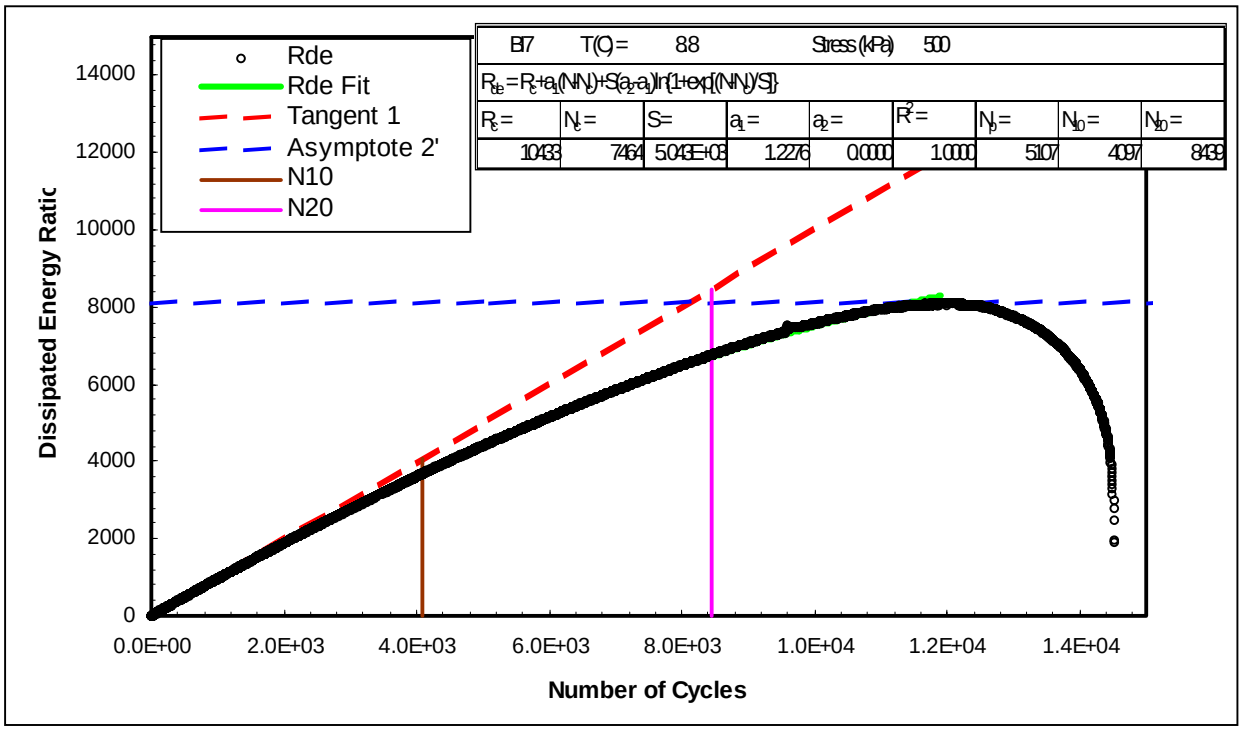

Figure D.7 Dissipated Energy Ratio Plot – Binder 7

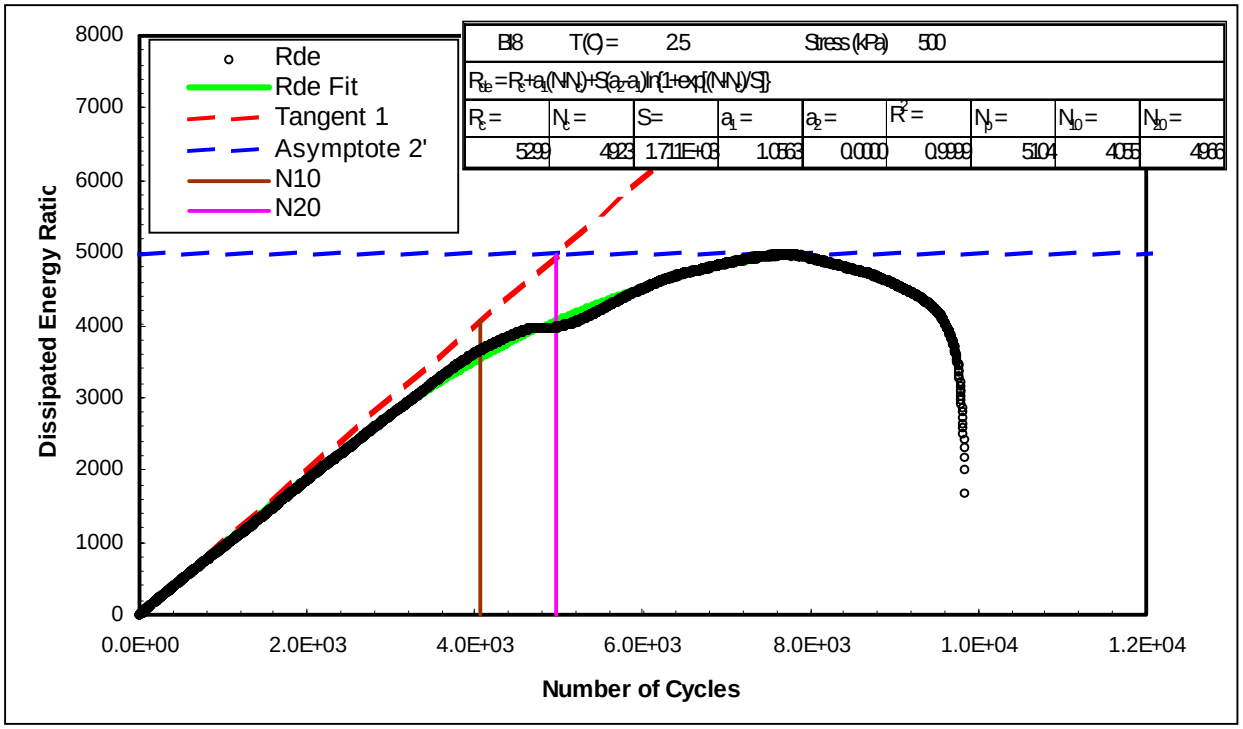

Figure D.8 Dissipated Energy Ratio Plot – Binder 8

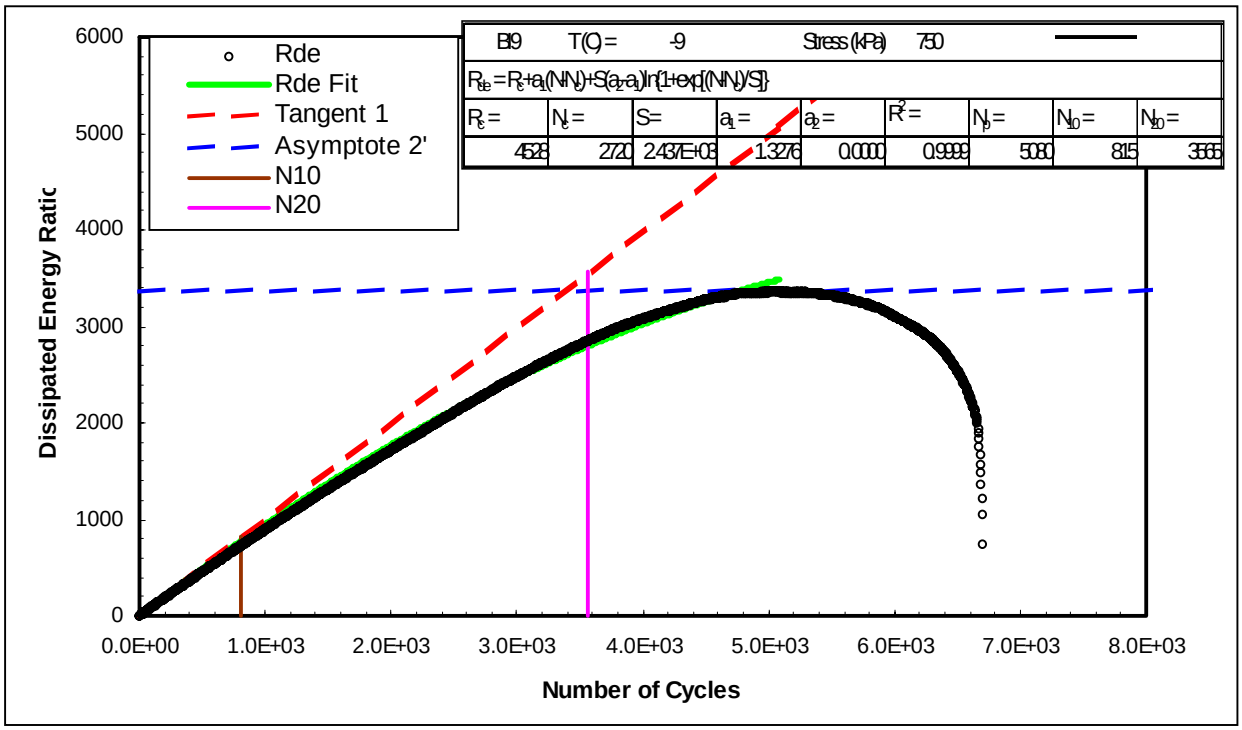

Figure D.9 Dissipated Energy Ratio Plot – Binder 9